Neutrally stable vibration energy harvesting

MSc Thesis

Sergio de Paula Pellegrini
June 2012

Delft University of Technology

Report title	Neutrally stable vibration energy harvesting
Report type	MSc. thesis
Author	Sergio de Paula Pellegrini
Date	June 2012
Institute	Delft University of Technology Faculty of Mechanical, Maritime and Materials Engineering
Exam committee	prof. dr. F. C. T. van der Helm prof. dr. ir. J. L. Herder dr. ir. M. Schenk

Cover Distributed energy generation and islamic patterns both have Unity and multiplicity at their core. Own design.

"Pero no olvides, que de acuerdo a la semilla
Así serán, los frutos que recogerás.
Siembra..."

Siembra, Rubén Blades

Preface

This volume summarizes ten months of work, in which my previously obtained expertise in bond graph modeling and in numerical methods is combined with newly acquired knowledge in the fields of energy harvesting, compliant mechanisms and static balancing.

Although the effort and ideas are mostly mine, results are never achieved individually. I have much to thank to Just Herder, my adviser, and to Nima Tolou, my daily supervisor, for giving me the freedom to come up with these innovative ideas. Also, to Simon Guest, for the three-month internship at the Cambridge University Engineering Department. Still on the same level, I should thank Mark Schenk and Juan Gallego for the long hours of fruitful discussions. Mark's stepwise approach is evident in chapters 3 and 4 and Juan's view on static balancing is reflected in chapter 5.

I should also thank Toon Lamers, Gerard Dunning, Pieter Pluimers and Jos Lassooij for the many discussions that helped me solidify concepts and have a more clear view on static balancing.

I am very grateful for the essential support from Rakshith, Nadeem, Nakul, Anupam & Revathi and from Aswin & Nishant, hosting me often on my short stays in Delft spread throughout the last four months.

Last – and far from least, I should thank my parents for their love, patience and trust in providing all the needed support for this crazy adventure of studying abroad, because of love towards engineering, academy and a woman.

Sergio de Paula Pellegrini
Frankfurt, June 3rd 2012

Summary

This thesis brings together, for the first time, the fields of energy harvesting and static balancing.

The proposal of two new architectures for the design of mechanical oscillators is supported by an extensive review on the existing energy harvesters. For the first one, a statically balanced oscillator, an analytical study proved it to be ineffective. This pushed for the development of a statically balanced frequency up-converter, that can integrate an energy harvester capable of coping with low frequencies vibrations of broadband nature.

On the static balancing ground, a new mechanism is proposed, with the balancing of the folded suspension, a traditional mechanism of precision engineering. Numerical analysis suggests that high quality balancing is achieved for a large amplitude of motion.

A preliminary study is also executed, introducing bond graph modeling to the field of energy harvesting. Bond graphs are a natural representation for the cross-domain nature of energy harvesters, allowing an integrative view.

Contents

Preface **vii**

Summary **ix**

1 Introduction **1**
1.1 Energy generation 1
1.2 Energy harvesting 1
1.3 Objectives 2
1.4 Outline 2

2 Preliminaries on energy harvesting – Application of Bond Graph Modeling to Energy Harvesters **5**
2.1 Introduction 5
2.2 Bond graph modeling 6
2.3 Mechanical oscillators 8
2.4 Conversion methods 9
2.5 Partial conclusions 12

3 Existing mechanical oscillators **15**
3.1 Resonant oscillator 15
3.2 Resonance-based oscillators 22
3.3 Duffing monostable oscillators 25
3.4 Bistable oscillators 26

4 Statically balanced energy harvester **39**
4.1 Panorama on static balancing 39
4.2 Dynamic behavior of a statically balanced damped system 40
4.3 Discussion and conclusion 45

5 Statically balanced frequency up-conversion energy harvester **49**
5.1 Design paradigm 49
5.2 Dynamic behavior 50
5.3 Statically balanced suspension conceptual design 56
5.4 Conclusion 63

6 Conclusions **65**

Bibliography **67**

A Electromechanical materials **73**
A.1 Energy conversion phenomena 73
A.2 Material properties 75
A.3 Common practices 80

B Comparison among conversion methods **83**

C ANSYS code for analysis of statically balanced folded suspension **85**

Chapter 1

Introduction

1.1 Energy generation

One of the most important current technological challenges is the generation of energy in different scales. In fact, data on primary energy consumption of the United States of America, for instance, [U.S. Energy Information Administration, 2011] show a 150-fold increase in the last 200 years. Even though primary energy consumption stabilized in the United States, Europe and Eurasia [British Petroleum, 2011], the overall consumption is still rising, as there are countries developing their industries and increasing their own energetic needs.

Moreover, as a fruit of the history of our technological development, 88% of all the energy used in the world in 2010 was extracted from fossil fuels. Regardless of the discussion on global warming [Intergovernmental panel on climate change, Onça, 2011], it is a fact that we do not know the extent of the impacts of our technologies. In opposition, we do know, with Thermodynamic's Second Law, that it is impossible to obtain work – useful energy – without some sort of impact. Given our ignorance on the extent of the impact of our actions, diversifying the sources of primary energy is advised, in order to assure that we meet "the needs of the present without compromising the ability of future generations to meet their own needs" [United Nations, 11 December 1987].

One ongoing research approach is to increase the efficiency of electrical and electronic systems. If on one hand improving the energy efficiency is a legitimate engineering goal, on the other hand this increase in performance leads to a greater energy consumption, phenomenon known as the rebound effect. Indeed, there are cases in which a higher efficiency leads to an overall increase in energy consumption that exceeds the energy savings generated with the efficiency improvement. This phenomenon was first understood and described in 1865, being known as the Jevons paradox, and applied for energy consumption in the 1980s, being known as the Khazzoom-Brookes postulate. Although the extent of the "rebound" for energy consumption is still not clear, the existence of a "rebound" cannot be ignored [Herring and Cleveland].

Alternatively, one can aim at pursuing technological improvements for the supply counterpart. One possibility is to provide the generation of small amounts of power close to the consumer. Indeed, a decentralized power generation grid avoids the intrinsic power losses associated with energy transmission.

In this context, this thesis will address local power generation at low amounts and small scale. This is an expanding research field, known as energy harvesting.

1.2 Energy harvesting

Currently, several applications that need low amounts of energy are powered with batteries. Even though batteries allow mobility, they can only supply a limited amount of power, after which they need to be recharged. Batteries, thus, do not lower the dependence on the centralized power generation. Moreover, there are environmental problems associated with the disposal of the batteries, as they rely on the use of heavy metals. Energy harvesting can push for the replacement of batteries, decreasing the need of toxic metals.

Also, emerging technologies can benefit from a continuous and long-term supply of energy. Wireless Sensor Networks (WSN), for instance, can become an effective alternative for industrial and structural monitoring, avoiding the costs related to wiring and battery replacements.

Different sources of energy are considered for energy harvesting. Sunlight, thermal gradients and mechanical vibrations are commonly available in nature and are the most explored in the energy harvesting literature. For environments without direct sunlight, mechanical vibrations are considered to be the best energy source, as thermal energy availability is highly dependent on the temperature difference [Roundy et al., 2003, Mathúna et al., 2008, Kim et al., 2009]. Thus, the scope of this thesis is further specified as focusing on vibration energy harvesters.

1.3 Objectives

The main goal of this text is to bring together the fields of vibration energy harvesting and static balancing. An extensive discussion on energy harvesting will allow the proposition and conceptual evaluation of innovative design paradigms for energy harvesting using statically balanced oscillators as a solution for harvesting broadband, low frequency and large amplitude vibration inputs, a current technological challenge.

1.4 Outline

For that purpose, chapter 2 introduces for the first time bond graph models for energy harvesting, reinforcing the intrinsic cross-domain nature of the field. Next, chapter 3 presents an extensive review of the mechanical oscillators used in energy harvesters, from the classic ones until the most recent advances. Then, chapter 4 proposes a statically balanced energy harvester, with an analytical analysis that eventually proves it not to be advantageous. Finally, chapter 5 presents a new paradigm for energy harvesting, named statically balanced frequency up-conversion. A model of concentrated parameters is numerically analyzed, proving exciting results. Additionally, embodiments for the statically balanced suspension are discussed, culminating in the numerical analysis of a newly proposed statically balanced folded suspension.

Bibliography

British Petroleum. BP statistical review of world energy June 2011. Available at bp.com/statisticalreview, 2011.

Horace Herring and Cutler Cleveland. Rebound effect. In Cutler J. Cleveland, editor, *Encyclopedia of Earth*. [First published in the Encyclopedia of Earth November 18, 2008; Last revised Date November 18, 2008; Retrieved May 8, 2012], http://www.eoearth.org/article/Rebound_effect.

Intergovernmental panel on climate change. Available at http://www.ipcc.ch.

Hyunuk Kim, Yonas Tadesse, and Shashank Priya. *Energy Harvesting Technologies*, chapter Piezoelectric Energy Harvesting, pages 3–40. Springer, 2009.

Cian Ó Mathúna, Terence O'Donnell, Rafael V. Martinez-Catala, James Rohan, and Brendan O'Flynn. Energy scavenging for long-term deployable wireless sensor networks. *Talanta*, 75(3):613 – 623, 2008. ISSN 0039-9140. Special Section: Remote Sensing.

D. de S. Onça. *"When the sun shines, they slip into the shade...": global warming ideology*. PhD thesis, Faculdade de Filosofia, Letras e Ciências Humanas da Universidade de São Paulo, 2011.

Shad Roundy, Paul K. Wright, and Jan Rabaey. A study of low level vibrations as a power source for wireless sensor nodes. *Computer Communications*, 26(11):1131 – 1144, 2003. ISSN 0140-3664. Ubiquitous Computing.

United Nations. "Report of the World Commission on Environment and Development." General Assembly Resolution 42/187, 11 December 1987.

U.S. Energy Information Administration. History of energy consumption in the United States, 1775-2009. Available at http://www.eia.gov, 2011.

Chapter 2

Preliminaries on energy harvesting – Application of Bond Graph Modeling to Energy Harvesters

2.1 Introduction

Vibration energy harvesting is a research field that exists for over 15 years, having as pioneers the works of [Lundgren et al., 1993, Williams and Yates, 1996], for instance. An extensive amount of studies focus on specific aspects of the field. Nevertheless, energy harvesting is an intrinsic cross-field application.

The main subsystems of those energy converters can be naturally grouped as: a) a mechanical oscillator, that seizes energy from the vibrations and stores it dynamically; b) a conversion method, that transforms the mechanical energy into electromagnetic field and c) a power conditioning circuit which processes and stores this energy electrically, making it available for usage. Those three blocks are inter-dependent, as the conversion of energy reflects as damping into the oscillator, or as the optimal topology of the power conditioning circuit depends to a great extent on the nature of the implemented conversion method. Moreover, the characteristics of the power conditioning circuit feedback into the mechanical part of the harvester, such that the oscillator's fundamental frequency is not mandatorily the same in the open loop and the closed loop configurations [Cammarano et al., 2010]. It results that vibration energy harvesters should be designed holistically, with an integrative view of those three subsystems [Kaźmierski and Beeby, 2011].

Aiming at providing an integral model, this paper shall introduce the use of bond graphs for the modeling of vibration energy harvesting. Bond graph modeling is the most suited method for dealing with complex systems of different physical domains. First because the object oriented modeling proportioned by bond graphs allows an interchangeability of the subparts of the harvester [Borutzky, 2004]. Then, the fact that different energetic domains are represented with the same basic elements allows the implementation of complete models. Examples include an electroacoustic transducer [Shoureshi and Carey, 1987], multi-phase systems [Greifeneder and Cellier, 2001], fluid flow [Baliño et al., 2006, Baliño, 2009], traffic flow [Chera et al., 2010] and an electrically controlled actuator [Alabakhshizadeh et al., 2011].

This incomplete study presents bond graph models for subsystems of vibration energy harvesting, aiming at making those building blocks available. This should facilitate the conceptual and numerical exploration of different topologies, both for the conditioning circuit and for the mechanical oscillator, offering an integrative graphical approach to the modeling of vibration energy harvesters.

For this purpose, first an introduction to bond graph modeling is accomplished. This is followed by the derivation of models for mechanical oscillators and for the different conversion methods. Finally, partial conclusions are presented.

2.2 Bond graph modeling

Bond graphs are a simple - yet complete - graphical modeling method, from which the governing differential equations can be obtained with a stepwise procedure. Several texts, such as [Karnopp et al., 2000, Breedveld, 2003, Gawthrop and Bevan, 2007, Borutzky, 2009, Cellier, 2011], provide a more complete introduction to bond graph modeling, that is out of the scope of this text. Nevertheless, the fundamentals are presented in this section, based mostly on [Karnopp et al., 2000, Cellier, 2011].

For every energetic domain, power is defined as a product between an intensive variable (independent of the amount) and an extensive variable (proportional to the amount). In bond graph methodology, those variables are defined as generalized effort, e, and generalized flow, f. Their integrals in time are also defined, as generalized momentum, p, and generalized displacement, q. Some examples in different energetic domains are presented in tab. 2.1.

Table 2.1: Physical entity of the generalized variables in different energetic domains.

Energetic domain	Effort (e)	Flow (f)	Momentum ($p = \int edt$)	Displacement ($q = \int fdt$)
Linear mechanics	Force $un(F) = N$	Velocity $un(v) = \frac{m}{s}$	Linear momentum $un(p) = \frac{kg\,m}{s}$	Distance $un(x) = m$
Angular mechanics	Moment of force $un(M) = N\,m$	Angular velocity $un(\omega) = \frac{rad}{s}$	Angular momentum $un(L) = N\,m\,s$	Angle $un(\theta) = rad$
Electric	Voltage $un(V) = V$	Current $un(i) = A$	Flux linkage $un(\lambda) = V\,s$	Charge $un(q) = A\,s$
Magnetic	Magnetomotive force $un(\mathcal{F}) = A$	Flux rate $un(\dot{\Phi}) = \frac{Wb}{s}$	-	Flux $un(\Phi) = Wb$
Thermodynamic	Temperature $un(T) = K$	Entropy flow rate $un(\dot{S}) = \frac{J}{K\,s}$	-	Entropy flow $un(S) = \frac{J}{K}$

The essence of the bond graph method is to analyze the flow of power throughout the system. Each bond, denoted by a harpoon ($\rightharpoonup$), represents power being transmitted from one part of the system to another, with the sense as indicated. Each bond has a couple effort-flow associated to it.

The bonds connect elements to each other. There are five simple elements, able to have a single connection. Sources model the inflow (or outflow, in rare cases) of power into the model, defining either effort, with a source of effort (S_e), or flow, with a source of flow (S_f). Resistors (R) are elements that relate effort and flow, and model the "loss" of energy to an energetic domain not modeled. Capacitors (C) relate effort and generalized displacement, and can only store energy. Inductors (I) relate generalized momentum and flow, and can also store energy.

Then there are the elements of the junction structure, that distribute power. The balance of instantaneous power through those elements is always zero. Transformers (TF) are defined by a transformation ratio, m, that multiplies the input flow to provide the output flow. Gyrators (GY) are defined by a gyration ratio, r, that multiplies the input flow to provide the output effort. The 0-junction is such that all bonds share the same effort, and it results from power conservation that their flows sum algebraically to zero. At last, the 1-junction imposes a common flow among all bonds connected to it. Table 2.2 summarizes the elements discussed above.

The resistor, capacitor and inductor can still be generalized into field elements, in which multiple bonds are allowed to be connected to. For the linear case, the functions ϕ_R, ϕ_C and ϕ_I, defined in tab. 2.2, result as a matrices. Fields can be rewritten with a group of simple elements and structures of junction. However, this so called implicit form is not always obvious to obtain, and can even be impossible to obtain using linear elements.

Table 2.2: Basic elements for bond graph modeling.

Element	Notation	Characteristic equation	Examples
Source of effort	$\mathtt{S_e} \overset{e}{\underset{f}{\rightharpoonup}}$	$e = e(t)$	Batteries, force generators, centrifugal pumps
Source of flow	$\mathtt{S_f} \overset{e}{\underset{f}{\rightharpoonup}}$	$f = f(t)$	Current generators, velocity generators, volumetric pumps
Resistor	$\overset{e}{\underset{f}{\rightharpoonup}} \mathtt{R}$	$e = \phi_R(f)$ *or* $f = \phi_R^{-1}(e)$	Electrical resistors, mechanical dampers, hydraulic valves
Capacitor	$\overset{e}{\underset{\dot{q}}{\rightharpoonup}} \mathtt{C}$	$q = \phi_C(e)$ *or* $e = \phi_C^{-1}(q)$	Electrical capacitors, mechanical springs, hydraulic reservoirs
Inductor	$\overset{\dot{p}}{\underset{f}{\rightharpoonup}} \mathtt{I}$	$p = \phi_I(f)$ *or* $f = \phi_I^{-1}(p)$	Electrical inductors, mechanical inertia, hydraulic inertia
Transformer	$\overset{e_1}{\underset{f_1}{\rightharpoonup}} \overset{m}{\mathtt{TF}} \overset{e_2}{\underset{f_2}{\rightharpoonup}}$	$\begin{cases} e_1 = m\, e_2 \\ m\, f_1 = f_2 \end{cases}$	Electrical transformer, mechanical lever
Gyrator	$\overset{e_1}{\underset{f_1}{\rightharpoonup}} \overset{r}{\mathtt{GY}} \overset{e_2}{\underset{f_2}{\rightharpoonup}}$	$\begin{cases} e_1 = r\, f_2 \\ r\, f_1 = e_2 \end{cases}$	Electrical gyrator, DC motor
0-junction	$\rightharpoonup \mathtt{0} \rightharpoonup$	$\begin{cases} e_1 = e_2 = e_3 = \ldots = e_n \\ \sum_{i=1}^{n} f_i = 0 \end{cases}$	Kirchhoff′s first law
1-junction	$\rightharpoonup \mathtt{1} \rightharpoonup$	$\begin{cases} f_1 = f_2 = f_3 = \ldots = f_n \\ \sum_{i=1}^{n} e_i = 0 \end{cases}$	Kirchhoff′s second law, Second law of Newton

The attribution of causality is perhaps the most impressive part of this graphical modeling method. With a simple structured procedure the system governing equations are obtained, defining a state to describe the system, separating dependent and independent variables, ordering the equations, tearing algebraic loops and removing structural singularities. The procedure consists of drawing a vertical bar (|) on the part of the bond in which flow is imposed. Some elements have priorities over others and the causality is transmitted according to the properties of the junction structure elements. The standard procedure of causality assignment is:

1. Assign the preferencial causality to a source ($\rightharpoondown\!|\, \mathtt{S_f}$ or $\vdash\!\rightharpoonup \mathtt{S_e}$)

   a Transmit causality through the junction structure elements until no further progress is possible

   b Repeat step 1 until there are no more sources without causality assigned

2. Assign integral causality to a element that stores energy ($\vdash\!\rightharpoonup \mathtt{C}$ or $\rightharpoondown\!|\, \mathtt{I}$)

   a Transmit causality through the junction structure elements until no further progress is possible

   b Repeat step 2 until there are no more elements I or C without causality assigned

3. Assign an arbitrary causality to a resistor (R)

   a Transmit causality through the junction structure elements until no further progress is possible
   b Repeat step 3 until there are no more resistors without causality assigned

4. Assign an arbitrary causality to an arbitrary bond

   a Transmit causality through the junction structure elements until no further progress is possible
   b Repeat step 4 until the whole system is causal

The integral causality, mentioned in item 2, has this name as the characteristic equations for the elements are $e = \phi_C^{-1}\left(\int f\,dt\right) = \phi_C^{-1}(q)$ and $f = \phi_I^{-1}\left(\int e\,dt\right) = \phi_I^{-1}(p)$, for the capacitor and the inductor, respectively. The number of those elements in integral causality defines the order of the state space model, as the state variables are defined by the displacements (q) of the capacitors in integral causality and the momenta (p) of the inductors in integral causality. Those variables are grouped in a vector X. The sources contribute to the input vector (U) either with effort (e) or with flow (f). Writing the equations of all the elements with the assigned causalities, they can be rearranged into a state space model of the form $\dot{X} = A \cdot X + B \cdot U$, for the linear case, or $\dot{X} = \phi(X, U)$, for the general case.

2.3 Mechanical oscillators

The two existing architectures for resonant oscillators for energy harvesters are modeled in this section.

2.3.1 Direct excitation

This mass-spring-damper system is excited directly by a force, as shown in fig. 2.1(a). This is a less common architecture in energy harvesting, as it requires two clamping positions. The damper is a simple representation of the electromechanical conversion, as the conversion is, for the moment, out of the scope. Later on the resistor that models the damper will be replaced by a model of the conversion method. An initial bond graph model for the system is presented in fig. 2.1(b) and a reduced version of it in fig. 2.1(c).

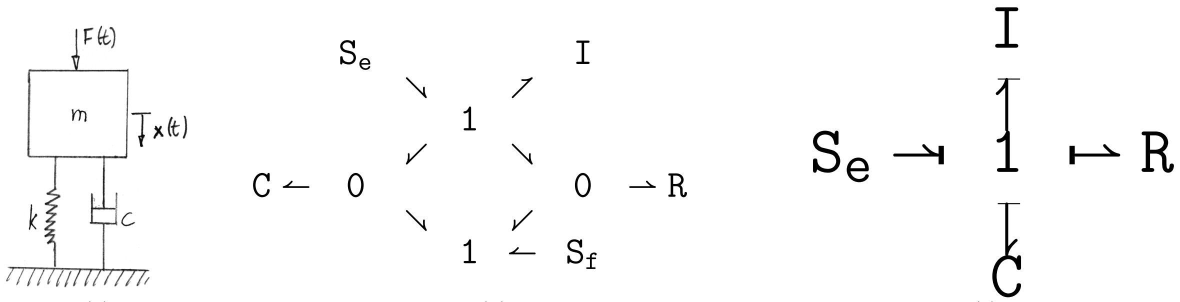

Figure 2.1: Models for a mass-spring-damper oscillator under direct excitation: (a) physical model, (b) initial bond graph model and (c) reduced bond graph model.

It can be seen that the initial bond graph has the same topology as the physical model. A set of rules exist to simplify fig. 2.1(b) into fig. 2.1(c) and can be seen, for instance in [Karnopp et al., 2000, Borutzky, 2004]. The final bond graph model could have been obtained directly from the observation that all elements share a common velocity. As both elements that store energy are in integral causality, it results that the system is of second order.

2.3.2 Base excitation

A more common architecture for resonant energy harvesters is a mass-spring-damper excited through base excitation. Analogously to the case of direct excitation, fig. 2.2 shows a physical model in (a), an initial bond graph model in (b) and a reduced bond graph model in (c).

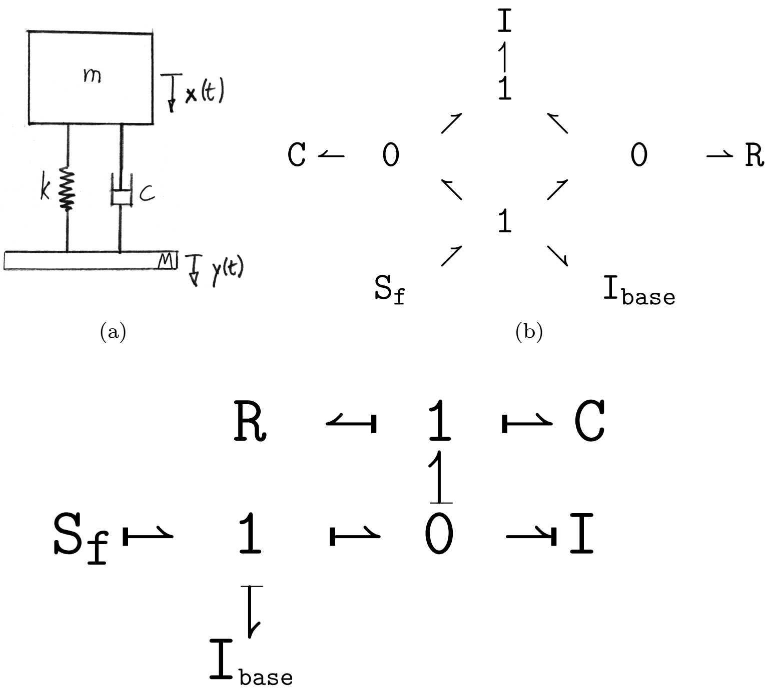

(a) (b) (c)

Figure 2.2: Models for a mass-spring-damper oscillator under base excitation: (a) physical model, (b) initial bond graph model and (c) reduced bond graph model.

This model also results to be of second order, as the base mass ($\mathtt{I}_{\mathtt{base}}$) is in derivative causality.

The bond graph model represents the topology of the system. This same model can be used to represent a bistable oscillator, for instance, changing the characteristic equation of the spring, represented by the capacitor (`C`).

Both reduced bond graph models urge that the element that defines the harvested power is the damper, as the sources only define either effort or flow.

2.4 Conversion methods

Bond graph models for the three most common conversion methods will be presented in this section. Their derivation will be accomplished from the equations that model the phenomena, framing them into the bond graph theory.

The first conversion method is the use of piezoelectric materials. Those are characterized by a non-centrosymmetric crystalline microstructure which is capable of generating electrical polarization while subject to mechanical strain [Ristic, 1983, Solymar and Walsh, 2004]. The polarization created is input to a power conditioning circuit as a difference of potential between two electrodes. This conversion method is extensively discussed in appendix A.

Electromagnetic conversion is based on Lenz's law (Faraday's law of induction), in which the generated voltage is proportional to the temporal variation of the magnetic flux [Feynman et al., 1964]. The variation of the magnetic flux is typically obtained through the relative motion of a permanent magnet and a coil, such that the outcome voltage is proportional to the coil-magnet relative velocity [Sari et al., 2009].

Electrostatic harvesters are based on the variation of the capacitance between two electrodes, which act as a voltage amplifier [He et al., 2010]. In fact, the electrostatic conversion method needs an external source of voltage, which may be provided internally with the support of electrets [Boisseau et al., 2010]. For this electromechanical coupling, the converted power is proportional to the maximum capacitance ratio [He et al., 2010, Kiziroglou et al., 2009, Murillo et al., 2009].

A comparison of the energy density achieved with each of them was performed in [Roundy, 2003] and is further discussed in appendix B. The study suggests that electromagnetic effects can provide the highest energy density, closely followed by piezoelectric materials. Electrostatic, however, provides a maximum theoretical energy density of approximately one order of magnitude lower than the other conversion methods.

2.4.1 Piezoelectric

Piezoelectric coupling is traditionally modeled with a linear relation among stresses (T), strain (S), electric displacement (D) and electric field (E). In eq. (2.1), c^E represents mechanical stiffness measured at constant electric field, ε^S is the electric permittivity measured at constant strain and e is a tensor composed of piezoelectric constants.

$$\begin{bmatrix} T_p \\ D_i \end{bmatrix} = \begin{bmatrix} c_{pq}^E & -e_{pk} \\ e_{iq} & \varepsilon_{ik}^S \end{bmatrix} \begin{bmatrix} S_q \\ E_k \end{bmatrix} \tag{2.1}$$

In accordance to [Liang and Liao, 2009], this model is simplified to describe a unimorph, as described in fig. 2.3. Equation 2.2 is obtained, relating force (F), velocity (v), current (I) and voltage (U) and using the derivative operator (s).

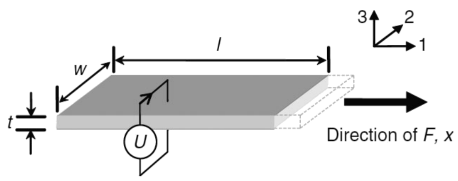

Figure 2.3: Sketch with main dimensions of unimorph. Reproduced from [Liang and Liao, 2009].

$$\begin{bmatrix} F \\ I \end{bmatrix} = \begin{bmatrix} \frac{k^E}{s} & \alpha_e \\ -\alpha_e & sC^S \end{bmatrix} \begin{bmatrix} v \\ U \end{bmatrix} \tag{2.2}$$

This equation is fully represented by the bond graph shown in fig. 2.4.

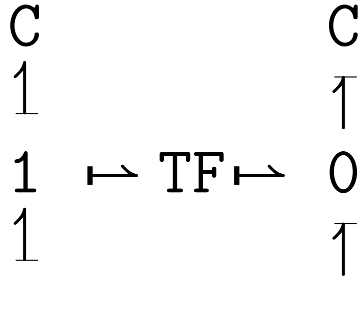

Figure 2.4: Bond graph model of piezoelectric coupling with mixed causality.

The bond graph model conveys that the piezoelectric conversion is a capacitive field, shown in its implicit form. The transformer (TF) separates the mechanical and electrical parts of the model and is the essence of the electromechanical coupling. This element defines the coupling such that electrical capacitance is reflected mechanically as stiffness and electric inductance is reflected as inertia.

Variations of eq. (2.1) are also standard in the literature, writing, for instance, strains and electric displacements as a function of the stresses and electric fields are represented with the same bond graph structure, only in different causalities.

2.4.2 Electrostatic

In accordance with Hoffmann et al [Hoffmann et al., 2009], the force between two capacitor electrodes is calculated as the derivative of the potential energy with respect to the position. This is valid as the energy field in the capacitor is conservative. For a parallel plate capacitor with relative motion of the plates on the direction perpendicular to the electrodes, the constitutive equations relating force (F), displacement (x), voltage (U) and charge (Q) are defined, for different causalities, as:

$$
\begin{aligned}
F &= \frac{Q^2}{2\epsilon A} \qquad U = \frac{Qx}{\epsilon A} \qquad && (a)\\
F &= \frac{\epsilon A U^2}{2x} \qquad Q = \frac{\epsilon A U}{x} \qquad && (b)\\
x &= \frac{\epsilon A U^2}{2F} \qquad Q = \frac{\epsilon A U}{x} \qquad && (c)
\end{aligned}
\tag{2.3}
$$

Equation 2.3 shows the constitutive relations for the capacitive field in integral causality (a), mixed causality (b) and derivative causality (c). The second mixed causality is not possible: it is impossible to describe the displacement (x) as a function of the force (F) and the charge (Q). This does not mandatorily mean that the physical system can achieve different positions independently of the force and voltage, but actually that the mathematical model cannot observe it. Moreover, the assumptions of this model are not valid for small scale – where border effects are predominant.

For relative motion of the parallel plates on the sense of changing the overlapping area the set of equations is different, as can be seen in eq. (2.4).

$$
\begin{aligned}
F &= \frac{-lQ^2}{2\epsilon w x^2} \qquad U = \frac{lQ}{\epsilon w x} \qquad && (a)\\
F &= \frac{-\epsilon w U^2}{2l} \qquad Q = \frac{\epsilon w x U}{l} \qquad && (b)\\
x &= Q\sqrt{\frac{2\epsilon w}{lF}} \qquad U = \frac{Ql}{\epsilon w x} \qquad && (c)
\end{aligned}
\tag{2.4}
$$

Here, the constitutive equations are shown in integral causality (a) and two different mixed causalities (b and c). The complete derivative causality is not possible, as it is impossible to describe displacement (x) as a function of voltage (U) and force (F). In this model, further analysis is required because of the negative signs, as the signs determine the direction of the power transfer (bonds).

The electrostatic conversion can be represented by a capacitive field. However, in opposition to the piezoelectric conversion, this field cannot be represented in the implicit form, due to its nonlinearity, with quadratic cross terms. Thus, the bond graph for the electrostatic conversion is shown in fig. 2.5.

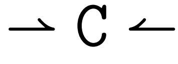

Figure 2.5: Bond graph model of electrostatic coupling.

2.4.3 Electromagnetic

The electromagnetic coupling was derived from fundamental physics, in disagreement with [Constantinou et al., 2006, Mann and Sims, 2009]. Later, it was found that Sari [Sari et al., 2009] proposed the same modeling. Taking Lenz's law (Faraday law of induction):

$$V = -N\left(\frac{d\vec{B}}{dt}\cdot\vec{A} + \vec{B}\cdot\frac{d\vec{A}}{dt}\right) \tag{2.5}$$

Where N is the number of active coils, $\vec{A}$ is the area of the coils and $\vec{B}$ is the magnetic induction. In opposition to [Constantinou et al., 2006, Mann and Sims, 2009], the area of the coils is constant $\left(\frac{d\vec{A}}{dt} = 0\right)$. The magnetic induction is a function of distance and, thus, the variation of the magnetic field over time is calculated through the chain rule as $\frac{dB}{dt} = \frac{dB}{dx}\frac{dx}{dt}$. Replacing this in eq. (2.5), eq. (2.6) is obtained.

$$V = -A\sum_{coils}\left(\frac{dB}{dx}\right)\dot{x} \tag{2.6}$$

Alternatively, an average behavior can be used, such as in eq. (2.7).

$$V = -NA\left.\frac{dB}{dx}\right|_{average}\dot{x} \tag{2.7}$$

On the mechanical side, further investigation is needed to derive the equation from fundamental physics. Nevertheless, in accordance to literature and using energy conservation arguments, the force can be obtained in analogy with eq. (2.7), resulting in eq. (2.8).

$$F = NA\left.\frac{dB}{dx}\right|_{average} i \tag{2.8}$$

Thus, the electromagnetic coupling can be completely modeled by a gyrator, shown in bond graph in fig. 2.6.

$$\xrightarrow[i]{U} \mathrm{GY} \xrightarrow[\dot{x}]{F}$$

Figure 2.6: Bond graph model of electromagnetic coupling.

In opposition to the piezoelectric coupling, here electric capacitance is reflected mechanically as inertia and electric inductance, as stiffness. Having in mind that the power conditioning circuit is predominantly capacitive, this results as an advantage for electromagnetic conversion while designing for harvesting vibrations of low frequencies.

2.5 Partial conclusions

Bond graph models were obtained for different subsystems present in energy harvesters. Even though this study is incomplete, bond graph models allow the observation of important characteristics of the subsystems, due to a simple and compact graphical representation. For instance, it is clear that a theoretical maximum for the harvested power cannot be defined looking exclusively at the mechanical oscillator. Another remark that should be reinforced is that piezoelectric and electromagnetic have at the core of their conversion behaviors that are dual of each other, such that the power conditioning circuit reflects on the mechanical oscillator in opposed forms.

Bibliography

A. Alabakhshizadeh, Y. Iskandarani, G. Hovland, and O.M. Midtgård. Analysis, Modeling and Simulation of Mechatronic Systems using the Bond Graph Method. *Modeling, Identification and Control*, 32(1): 35–45, 2011.

J.L. Baliño. Galerkin finite element method for incompressible thermofluid flows framed within the bond graph theory. *Simulation Modelling Practice and Theory*, 17(1):35 – 49, 2009. ISSN 1569-190X. Bond Graph Modelling.

J.L. Baliño, A.E. Larreteguy, and E.F. Gandolfo Raso. A general bond graph approach for computational fluid dynamics. *Simulation Modelling Practice and Theory*, 14(7):884 – 908, 2006. ISSN 1569-190X.

S Boisseau, G Despesse, and A Sylvestre. Optimization of an electret-based energy harvester. *Smart Materials and Structures*, 19(7):075015, 2010.

W. Borutzky. Bond graph modelling and simulation of multidisciplinary systems an introduction. *Simulation Modelling Practice and Theory*, 17(1):3 – 21, 2009. ISSN 1569-190X. Bond Graph Modelling¡/ce:title¿.

Wolfgang Borutzky. *Bond graphs – A Methodology for Modelling Multidisciplinary Dynamic Systems*, volume FS-14 of *Frontiers in Simulation*. SCS Publishing House, Erlangen, San Diego, 2004.

Peter Breedveld. Bond graphs. In *Encyclopedia of Life Support Systems*. EOLSS, 2003.

A Cammarano, S G Burrow, D A W Barton, A Carrella, and L R Clare. Tuning a resonant energy harvester using a generalized electrical load. *Smart Materials and Structures*, 19(5):055003, 2010.

François Cellier. Mathematical modeling of physical systems. Available at http://www.inf.ethz.ch/personal/fcellier/, 2011.

C. M. Chera, J. L. Baliño, and Geneviève Dauphin-Tanguy. Two-equation traffic flow models framed within the bond graph theory. In *SpringSim*, page 219, 2010.

P. Constantinou, P.H. Mellor, and P. Wilcox. Model of an electromagnetic vibration generator. In *Universities Power Engineering Conference, 2006. UPEC '06. Proceedings of the 41st International*, volume 1, pages 6 –10, sept. 2006.

Richard P. Feynman, Robert B. Leighton, and Matthew Sands. *The Feynman lectures on Physics*, volume II. Addison-Wesley, 1964.

P.J. Gawthrop and G.P. Bevan. Bond-graph modeling. *Control Systems, IEEE*, 27(2):24 –45, april 2007. ISSN 1066-033X.

Jürgen Greifeneder and François E. Cellier. Modeling multiphase systems using bond graphs. In *Proceedings ICBGM'2001, International Conference on Bond Graph Modeling and Simulation*, pages 285–291, Phoenix-AZ, USA, 2001. SCS.

C. He, M.E. Kiziroglou, D.C. Yates, and E.M. Yeatman. Mems energy harvester for wireless biosensors. In *Micro Electro Mechanical Systems (MEMS), 2010 IEEE 23rd International Conference on*, pages 172 –175, jan. 2010.

Daniel Hoffmann, Bernd Folkmer, and Yiannos Manoli. Fabrication, characterization and modelling of electrostatic micro-generators. *Journal of Micromechanics and Microengineering*, 19(9):094001, 2009.

C. R. Karnopp, D. L. Margolis, and R. C. Rosenberg. *System Dynamics: Modeling and Simulation of Mechatronic Systems*. Wiley-Interscience, 3rd edition, 2000.

Tom J. Kaźmierski and Steve Beeby, editors. *Energy Harvesting Systems*. Springer, 2011.

M.E. Kiziroglou, C. He, and E.M. Yeatman. Rolling rod electrostatic microgenerator. *Industrial Electronics, IEEE Transactions on*, 56(4):1101 –1108, april 2009. ISSN 0278-0046.

J.R. Liang and W.H. Liao. Piezoelectric energy harvesting and dissipation on structural damping. *Journal of Intelligent Material Systems and Structures*, 20(5):515–527, 2009.

A. Lundgren, H. Tiberg, L. Kvarnsjo, A. Bergqvist, and G. Engdahl. A magnetostrictive electric generator. *Magnetics, IEEE Transactions on*, 29(6):3150–3152, nov 1993.

B. P. Mann and N. D. Sims. Energy harvesting from the nonlinear oscillations of magnetic levitation. *Journal of Sound and Vibration*, 319(1-2):515 – 530, 2009. ISSN 0022-460X.

G. Murillo, G. Abadal, F. Torres, J.L. Lopez, J. Giner, A. Uranga, and N. Barniol. Harvester-on-chip: Design of a proof of concept prototype. *Microelectronic Engineering*, 86(46):1183 – 1186, 2009. ISSN 0167-9317. MNE 08: The 34th International Conference on Micro- and Nano-Engineering (MNE).

V. M. Ristic. *Principles of acoustic devices*. Wiley-Interscience, 1983.

Shadrach Joseph Roundy. *Energy scavenging for wireless sensor nodes with a focus on vibration to electricity conversion*. PhD thesis, University of California, Berkeley, 2003.

Ibrahim Sari, Tuna Balkan, and Haluk Kulah. An electromagnetic micro energy harvester based on an array of parylene cantilevers. *Journal of Micromechanics and Microengineering*, 19(10):105023, 2009.

Rahmatallah Shoureshi and David Carey. Bond graph modeling of an electroacoustic transducer. *Journal of the Franklin Institute*, 323(1):73 – 87, 1987. ISSN 0016-0032.

L. Solymar and D. Walsh. *Electrical properties of materials*. Oxford, 7th edition, 2004.

C.B. Williams and R.B. Yates. Analysis of a micro-electric generator for microsystems. *Sensors and Actuators A: Physical*, 52(13):8 – 11, 1996. ISSN 0924-4247. Proceedings of the 8th International Conference on Solid-State Sensors and Actuators Eurosensors IX.

Chapter 3

Existing mechanical oscillators

This section will present a review on energy harvesting, focusing on the mechanical oscillators. This review is a compilation of a search that identified over 350 articles in this field, in addition to patents, theses and books.

Different principles for mechanical oscillators are presented, following the evolution of the field. At the end of this chapter follows a published review paper on bistable energy harvesters, a recent development on the field.

3.1 Resonant oscillator

Vibration energy harvesters are in development for more than fifteen years, having as pioneers the works of [Lundgren et al., 1993, Williams and Yates, 1996], for instance. The first mechanical oscillators were implemented as resonant mass-spring-damper system, where the damper represents the electromechanical conversion. Despite the fact that those systems are simple and well understood, an in depth analysis shall be carried for those systems, as they are the foundations for the next developments in energy harvesting. Two possible architectures for resonant energy harvesters are shown in fig. 3.1.

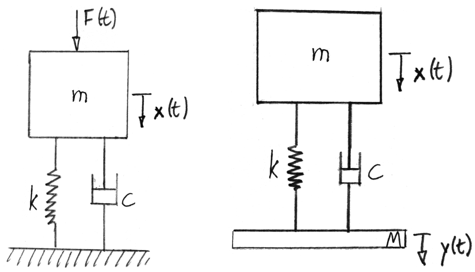

(a) (b)

Figure 3.1: Physical models for a mass-spring-damper oscillator under (a) direct excitation and (b) base excitation.

The physical model shown in fig. 3.1(a) is known as direct excitation and demands to be in mechanical contact with two parts that move relatively to each other. On the other hand, the architecture shown in fig. 3.1(b), of base excitation, requires a single contact point and, thus, is more suited for energy harvesting [Mitcheson et al., 2008]. Indeed, practical examples of directly excited energy harvesters are nearly nonexistent. However, due to theoretical interest, the dynamic behavior of both architectures shall be presented next.

3.1.1 Frequency response

The dynamic behavior of resonators is widely known and was derived in accordance to [Kelly, 1993, Thomson, 1965], for instance. As the systems are linear, the steady state frequency responses describe completely the systems. Those responses are written using the traditional definitions of natural frequency ($\omega_n = \sqrt{\frac{k}{m}}$), damping ratio ($\zeta = \frac{c}{2\sqrt{km}}$) and the input frequency is normalized such that $r = \frac{\omega}{\omega_n}$.

A mass-spring-damper system under direct excitation of a sinusoidal force input to the mass, $F = F_0 \sin(\omega t)$ produces an output measured as a displacement, given by $x = X \sin(\omega t - \phi)$, such that X and ϕ are given by eq. (3.1) and eq. (3.2), respectively. Those equations are also plotted in fig. 3.2 for different damping ratios, in the form of a Bode plot.

$$\frac{m\omega_n^2 X}{F_0} = \frac{1}{\sqrt{(1-r^2)^2 + (2\zeta r)^2}} \tag{3.1}$$

$$\phi = \tan^{-1}\left(\frac{2\zeta r}{1-r^2}\right) \tag{3.2}$$

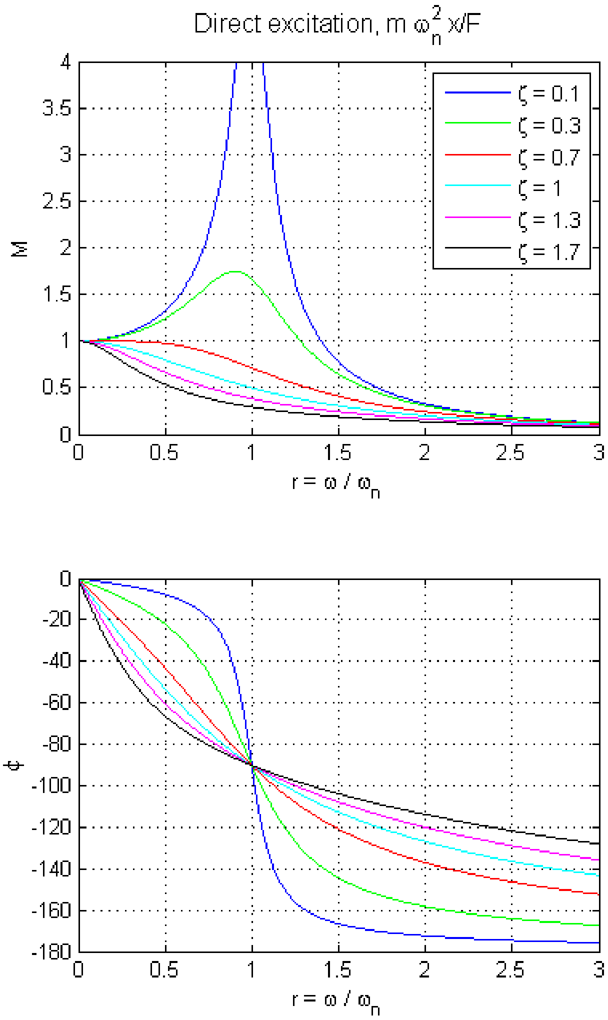

Figure 3.2: Plots of magnification and phase difference for direct excitation.

A traditional interpretation of the steady state behavior of second order oscillators is: at resonance, the work of the external forcing function is exclusively due to the damper; for frequencies lower than the resonant frequency, most of the work is against the spring force; for frequencies higher than the resonant frequency, most of the work is against the D'Alembert force.

For base excitation, also known as seismic motion, the response curve most commonly reported is the ratio between the proof mass motion and the base motion ($\frac{x}{y}$). This response, known as transmissibility, is more useful for vibration isolation analysis and is shown with the amplitude ratio in eq. (3.3) and the phase lag in eq. (3.4).

$$\frac{X}{Y} = T = \sqrt{\frac{1 + (2\zeta r)^2}{(1 - r^2)^2 + (2\zeta r)^2}} \tag{3.3}$$

$$\lambda = \tan^{-1}\left(\frac{2\zeta r^3}{1 + (4\zeta^2 - 1)\, r^2}\right) \tag{3.4}$$

However, in contrast to the case of direct excitation, the damper is not subject to the same displacements as the proof mass. Thus, for energy harvesting, it is more relevant to analyze the relative motion between the base and the proof mass normalized with respect to the base motion ($\frac{x-y}{y}$). This result is shown with the ratio of displacement amplitudes in eq. (3.5) and the phase lag in eq. (3.6).

$$\frac{X - Y}{Y} = \frac{Z}{Y} = \frac{r^2}{\sqrt{(1 - r^2)^2 + (2\zeta r)^2}} \tag{3.5}$$

$$\phi = \tan^{-1}\left(\frac{2\zeta r}{1 - r^2}\right) \tag{3.6}$$

Equations 3.5 and 3.6 are plotted in fig. 3.3 for different damping ratios.

3.1.2 Converted power

In order to compare the two oscillators, the converted power is calculated in agreement to [Mitcheson et al., 2004, Stephen, 2006], according to eq. (3.7). This formulation has an implicit hypothesis that all power lost on the damper is transformed into electrical. This hypothesis shall be refined later.

$$P = \frac{\int_{cycle} c\,(\dot{z})^2\, dt}{T} \tag{3.7}$$

Equation 3.7 is developed and the results are presented in eq. (3.8) for direct excitation and in eq. (3.9) for base excitation.

$$P = \frac{F_0^2}{m\omega_n} \frac{\zeta r^2}{(1 - r^2)^2 + (2\zeta r)^2} \tag{3.8}$$

$$P = mY_0^2\omega_n^3 \frac{\zeta r^6}{(1 - r^2)^2 + (2\zeta r)^2} \tag{3.9}$$

Equation 3.9 is plotted in fig. 3.4, with the damped power as a function of the damping ratio, ζ, and the normalized input frequency, r. Despite the fact that the numerical values of power have little sense,

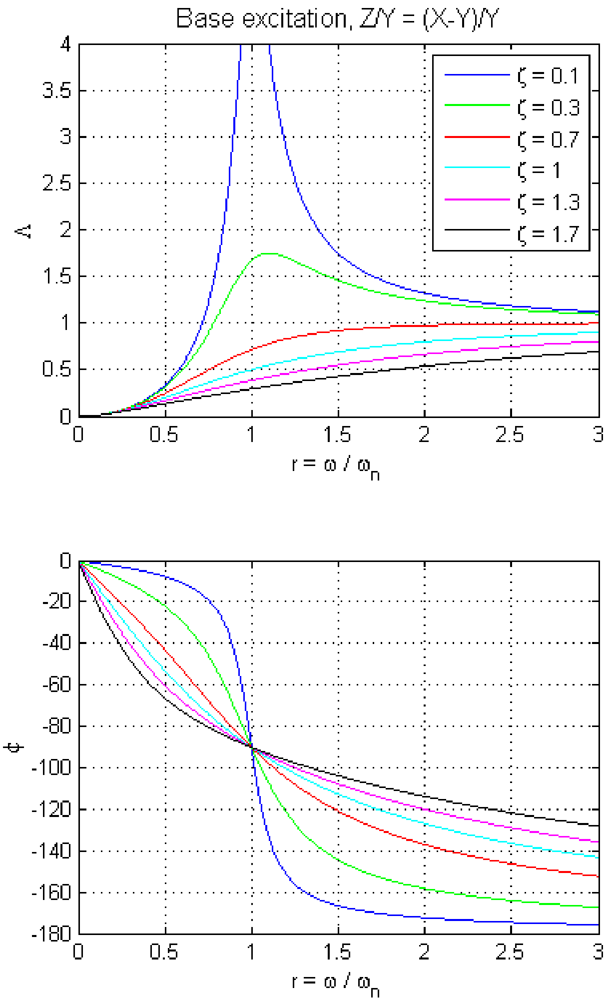

Figure 3.3: Plots of amplitude and phase difference for ratio between damper motion and base motion, for base excitation.

as they are dependent on the resonant frequency and the base motion amplitude, the plot can provide a good insight into the system's behavior.

It can be seen that there is a clear trend of more converted power for higher frequencies of input vibrations. This happens as vibrations of higher frequency carry more energy. As a matter of fact, the power of the input vibration is proportional to the acceleration squared divided by frequency [Mitcheson et al., 2008] or, equivalently, to the base displacement amplitude squared times the input frequency. Indeed, this trend will be removed, after some further analysis of this plot.

As the plot of fig. 3.4 also suggests the existence of an optimal damping coefficient for a given input frequency, the first partial derivative of the damped power with respect to the damping ratio is taken, according to eq. (3.10).

$$\begin{aligned} \frac{\partial P}{\partial \zeta} &= \frac{m Y_0^2 \omega^3 r^6 \left((1-r^2)^2 - (2\zeta r)^2 \right)}{\left((1-r^2)^2 - (2\zeta r)^2 \right)^2} \\ \therefore \frac{\partial P}{\partial \zeta} = 0 &\iff \zeta = \zeta_{ext} = \frac{\pm \left(r^2 - 1 \right)}{2r} \end{aligned} \tag{3.10}$$

Equation 3.10 shows that there exist a condition of extrema. Taking the second partial derivative with respect to the same variable shall define whether the extrema are maxima. This is carried through in

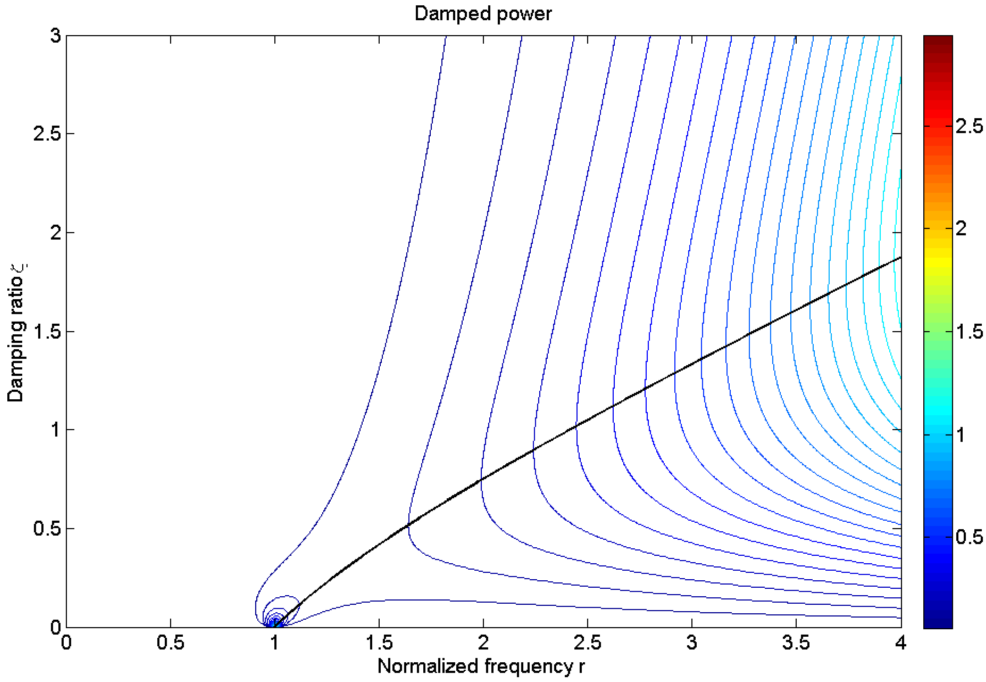

Figure 3.4: Damped power as function of the damping ratio and the normalized input frequency, for a resonant oscillator under base excitation. The black line is an optimal condition for damped power.

eq. (3.11).

$$\frac{\partial^2 P}{\partial \zeta^2} = 8mY_0^2\omega^3 r^8 \zeta \frac{\left((2\zeta r)^2 - 3\left(1-r^2\right)^2\right)}{\left((1-r^2)^2+(2\zeta r)^2\right)^3} \qquad \therefore \frac{\partial^2 P}{\partial \zeta^2}\left(\zeta = \zeta_{ext}\right) < 0 \text{ for } r > 1 \tag{3.11}$$

Thus, the condition for optimality is defined by eq. (3.12), which is plotted in fig. 3.4.

$$\zeta_{opt} = \frac{r^2 - 1}{2r} \text{ for } r > 1 \tag{3.12}$$

This condition for optimality can be understood from its physical principles, as it arises from a tradeoff: higher damping is wished for more damped power and lower damping is wished so that large strokes of harvesting are obtained. A final remark about plot of fig. 3.4 is that the scale of colors reaches larger values than the colors visualized on the plot. This happens as the damped power approaches infinity on the limit towards the point $(r, \zeta) = (1, 0)$, as can be seen both on eq. (3.8) and eq. (3.9). Indeed, this is a reason that pushes for the desire of a normalization of the damped power. However, the input power – a natural candidate – cannot be used as a reference, as it is exactly the damped power. Alternatively, the reference can contain only information from the input signal and the oscillator's mass, as $mY_0^2\omega^3$ [Mitcheson et al., 2004]. Using this reference, the normalized power is plotted in fig. 3.5, as a function of the normalized input frequency and the damping ratio.

This plot confirms that it is desirable to push the operation conditions towards resonance, as it amplifies the damped power. For an input frequency equal to the natural frequency, the normalized version of eq. (3.9) results such as shown in eq. (3.13).

$$\frac{P(\zeta, r = 1)}{mY_0^2\omega_n^3} = \frac{1}{4\zeta} \tag{3.13}$$

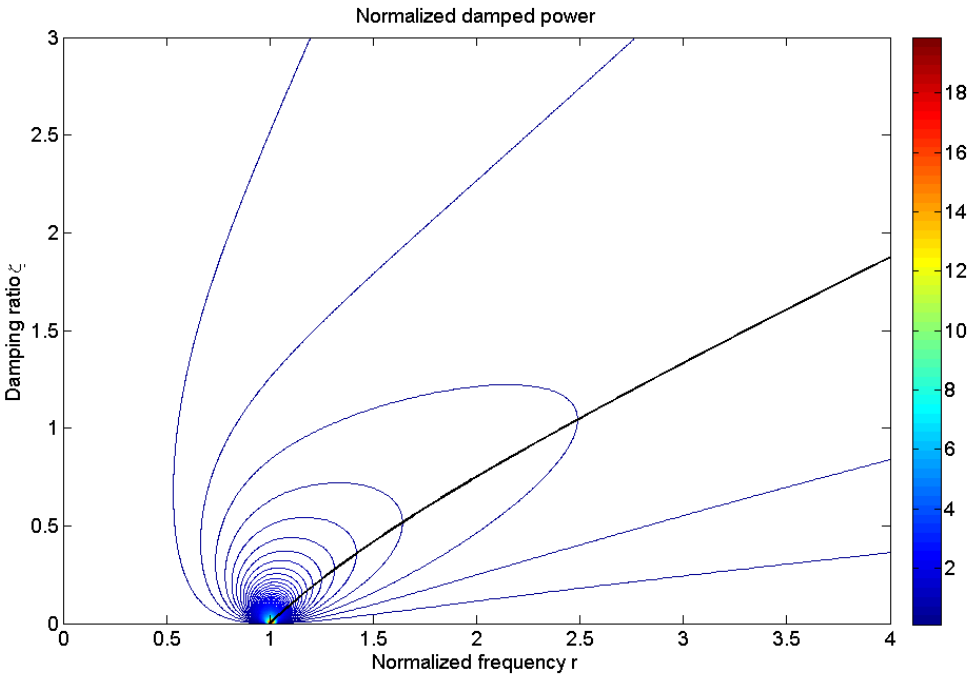

Figure 3.5: Normalized damped power as function of the damping ratio and the normalized input frequency, for a resonant oscillator under base excitation. The black line is an optimal condition for damped power.

Here the natural appearance of the quality factor, Q, is observed. The quality factor is a measure of the sharpness of the resonance peak, formally defined according to [Thomson, 1965], as shown in eq. (3.14). For this equation, ω_1 and ω_2 are the frequencies for which the system oscillations' power is half of the response at resonance.

$$Q = \frac{\omega_n}{\omega_2 - \omega_1} \tag{3.14}$$

For the case which the damping ratio is small, the quality factor can be expressed in a more direct expression [Feynman et al., 1964], according to eq. (3.15).

$$Q = \frac{1}{2\zeta} \tag{3.15}$$

Thus, sharp resonant peaks are desired in order to maximize the harvested power, i.e., the damping coefficient related to the electromechanical conversion must be minimized to increase the harvested power. The apparent paradoxicality of this statement is solved according to the tradeoff previously explained, as low damping results in large amplitude motion.

However, lowering the damping coefficient related to the electromechanical conversion leads a situation in which the residual mechanical damping, or parasitic damping, becomes relevant. Effects such as material hysteresis or air-induced drag (for small components) are possible mechanical damping sources. The widely accepted formulation for the converted power as a function of both the electromechanical damping ratio, ζ_e and the parasitic damping, ζ_p, was introduced in [Li et al., 2000], for base excitation, as shown in eq. (3.16).

$$P_{el} = mY_0^2\omega_n^3 \frac{\zeta_e r^6}{\left(1 - r^2\right)^2 + \left(2\left(\zeta_e + \zeta_p\right)r\right)^2} \tag{3.16}$$

In order to find out the optimal value of the electromechanical damping, the partial derivative of the converted power is taken, in accordance to [Mitcheson et al., 2004], as shown in eq. (3.17).

$$\begin{aligned} \frac{\partial P_{el}}{\partial \zeta_e} &= mY_0^2\omega^3 r^6 \frac{(1-r^2)^2+4r^2(\zeta_p^2-\zeta_e^2)}{((1-r^2)^2+(2(\zeta_e+\zeta_p)r)^2)^2} \\ \therefore \frac{\partial P_{el}}{\partial \zeta_e} &= 0 \text{ for } \zeta_e^{opt} = \frac{1}{2r}\sqrt{(1-r^2)^2+(2r\zeta_p)^2} \end{aligned} \tag{3.17}$$

For operation at resonance, eq. (3.17) is reduced to $\zeta_e^{opt} = \zeta_p$.

As mentioned before, the efficient operation with those parameters relies on large amplitudes of motion, i.e., large harvesting strokes. For reference, the damped power (eq. (3.9)) and the ratio between relative displacement of the proof mass with respect to the frame of the harvester and the base displacement, (eq. (3.5)) are plotted together in fig. 3.6, as a function of the damping ratio (ζ). The numerical values for the damped power are specific to the test conditions, with proof mass of 10 g and natural frequency of 10 Hz excited through base motion with a sinusoidal input of displacement amplitude of 1 mm at the resonant frequency ($f_{res} = f_n\sqrt{1-2\zeta^2}$). The numerical values of the transmissibility are independent of those parameters.

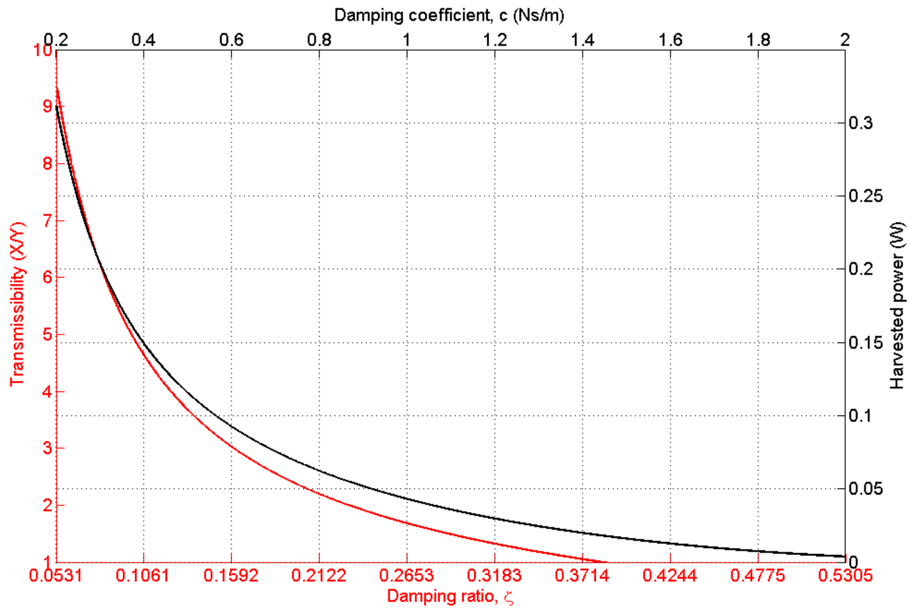

Figure 3.6: Converted power, in black, and ratio of relative displacement of the proof mass over displacement of the base motion, in red, at resonance, for different values of damping.

It can be seen in fig. 3.6 that the large converted power is obtained at the expense of a large amplification of the base motion. Indeed, the amplitude of motion of the proof mass reaches more than nine times the base displacement. However, vibration energy harvesters are frequently space limited, as they aim at be small systems. Thus, if on one hand, for small base displacements this model is correct, on the other hand, for larger base displacements nonlinearities should be introduced and this model should be refined.

Mitcheson et al [Mitcheson et al., 2004] introduced a limit for the stroke of the proof mass inside the harvester, denoted as Z_l. This model can be understood as a discontinuous stiffness, such increasing z beyond Z_l, the stiffness jumps from its regular value to infinity. In order to ensure that this stroke limit is not surpassed, the limit for the proof mass motion, Z_l, is imposed in eq. (3.5) and an optimal total damping ratio is obtained, according to eq. (3.18).

$$\zeta_{Z_l}^{opt} = \frac{1}{2r}\sqrt{r^4\left(\frac{Y_0}{Z_l}\right)^2-(1-r^2)^2} \tag{3.18}$$

This equation provides the optimal total damping ratio, i.e., including the parasitic damping, for the case in which the base motion amplitude and the optimal damping defined by eq. (3.17) would provide a relative displacement of the proof mass that exceeds its limit. In other words, if Z_l is not exceeded, for a given base displacement, the optimal damping value is given by eq. (3.17). Otherwise, the optimal damping is given by eq. (3.18).

3.2 Resonance-based oscillators

Another consequence of designing resonant systems with a very high quality factor is that the energy harvesters are specialized in a single fixed frequency and a slight mismatch with the input frequency will result in a dramatic decrease on the harvested power [Leland and Wright, 2006]. In contrast, as discussed before, the harvesting circuit reflects back in the oscillator, changing its resonant frequency. Moreover, it is common that the input vibrations are of broadband nature. Those issues lead to the introduction of different oscillators into the field of energy harvesting, as discussed next.

3.2.1 Tunable

In order to cope with the change of the resonant frequency while connected with the power conditioning circuit is to design an oscillator that can be tuned. Different designs were conceived, varying either the mass distribution or the system's stiffness, with an architecture sketched in fig. 3.7(a).

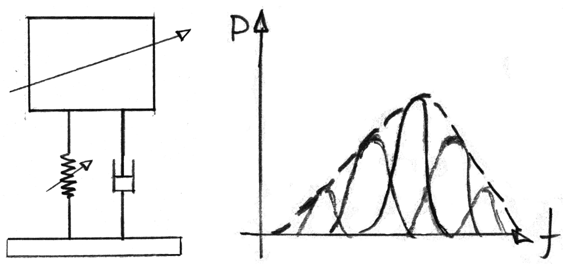

(a) (b)

Figure 3.7: Tunable mass-spring-damper oscillator under base excitation: (a) physical model and (b) typical shape of power response curve.

Different implementations of resonators with adjustable stiffness were developed using a tunable force that pushes the system towards buckling. A purely mechanical design was implemented by [Leland and Wright, 2006], in which a destabilizing force is applied on a simply supported piezoelectric bimorph, varying its stiffness for vibrations perpendicular to its main axis. Similarly, [Eichhorn et al., 2009] applies a destabilizing force to a piezoelectric bimorph cantilever using integrated arms such that the whole design is a single piece compliant mechanism. An electromagnetic energy harvester was built to be self tunable in closed loop control [Zhu et al., 2008, 2010a], actively controlling the magnitude of the repulsive force between an external magnet and one at the tip of a cantilever. Implementations were also developed based in different principles. [Challa et al., 2011] uses magnetic forces perpendicularly to the main axis of piezoelectric cantilevers to tune their resonant frequency. [Wu et al., 2008] introduced an energy harvester in which the mass distribution is adjustable, but, a study with further analyses was not found. Other implementations were also explored by different authors, as shown on the review of [Zhu et al., 2010b], for instance.

Apart from [Wu et al., 2008], all of the studies report an increase in the damping coefficient for frequencies further than the original one, which should be implementation dependent. The typical power harvested versus frequency plot is sketched in fig. 3.7(b). On the other hand, the variation of the damping ratio is predicted by theory, as tuning a linear oscillator resonant frequency will invariably change its quality factor. Indeed, eq. (3.15), valid for small damping coefficients, can be developed according to eq. (3.19).

$$Q = \frac{1}{2\zeta} = \frac{\omega_n}{cm} \tag{3.19}$$

A numerical study confirms that increasing the resonant frequency leads to a higher quality factor and that decreasing the resonant frequency leads to a lower quality factor [Hu et al., 2007].

3.2.2 Resonator under parametric excitation

A preliminary investigation of energy harvesting with parametric excitation was carried through by [Daqaq et al., 2009], but did not achieve conclusive results. This system is essentially a resonant oscillator subject to vibrations applied perpendicularly to the previous case.

3.2.3 Connected resonators

With the intention of broadening the peak of harvested power, one solution is to connect resonators in specific forms. As will be presented next, different configurations were explored.

Coupled

[Petropoulos et al., 2004] connected two resonators in series, as sketched on the physical model on fig. 3.8(a), obtaining a coupled oscillator with two masses. The shape of the power response curve obtained is shown in fig. 3.8(b). Despite the wider bandwidth of operation, the harvested power is smaller than for the simple system. No further examples were found.

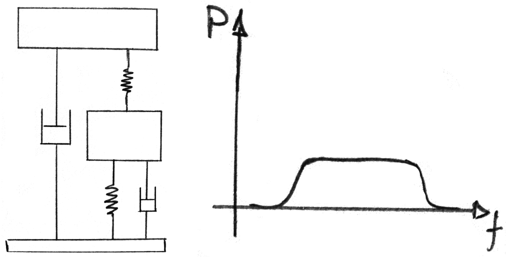

(a) (b)

Figure 3.8: Coupled mass-spring-damper oscillators in series, under base excitation: (a) physical model and (b) typical shape of power response curve.

Coupled in parallel

Using two identical cantilevers connected to the same proof mass, [Kim et al., 2011] obtained a system capable of oscillate in two different vibration eigenmodes. Designing the system to have the two eigenvalues close to each other, the response obtained is such as the one sketched in fig. 3.9(b). The physical model is sketched in fig. 3.9(a).

Arrays

Connecting several separate oscillators of similar resonant frequencies to the same base the bandwidth can be increased. A simple physical system is shown in fig. 3.10(a) and a typical response curve in fig. 3.10(b).

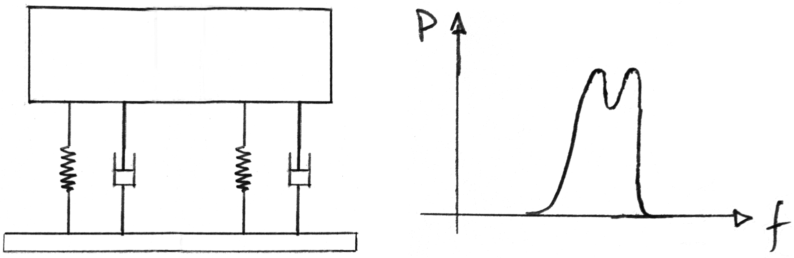

(a) (b)

Figure 3.9: Two mass-spring-damper oscillators coupled to the same proof mass, under base excitation: (a) physical model and (b) typical shape of power response curve.

[Zhu et al., 2010b] showed other array-based energy harvesters and reported that those suffer from a low volumetric efficiency, as only one resonator responds for each frequency while the others, practically, do not generate power.

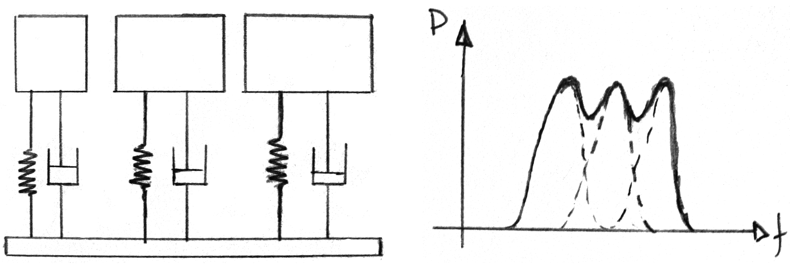

(a) (b)

Figure 3.10: Array of mass-spring-damper oscillators under base excitation: (a) physical model and (b) typical shape of power response curve.

3.2.4 Stoppers

Imposing an amplitude limiter to the resonator the bandwidth of the response can be widened. Using the properties of the classic resonator, but instead of avoiding to surpass the stroke limit, Z_l, the harvester is designed to operate at this condition. Implementations were reported in [Soliman et al., 2008b,a] and [Hoffmann et al., 2009], for instance, with a system modeled by the physical model shown in fig. 3.11(a) and obtaining a response curve of typical shape sketched in fig. 3.11(b). This solution for broadband input is subject to fatigue issues, in addition to high hysteresis.

3.2.5 Scrape-through

A different architecture for energy harvesting is such that a main oscillator is used to provide an impulse to a secondary resonator system. This method of having a main and a secondary resonator is broadly named frequency up-conversion. For scrape-through systems, in addition to frequency up-conversion, the impulse is transmitted due to a small overlap between the main oscillator and a secondary one. While moving, the main oscillator can displace a tip of each of the secondary resonators, transmitting energy to them in the form of strain. If the motion of the main mass continues on the same sense, the secondary oscillator experiences a sudden release and is, thus, allowed to oscillate in its own resonant frequency.

A simplified physical system is shown in fig. 3.12. Different authors explored this architecture [Rastegar et al., 2006, Lee et al., 2007, Kulah and Najafi, 2009, Liu et al., 2011, Özge Zorlu et al., 2011], but there

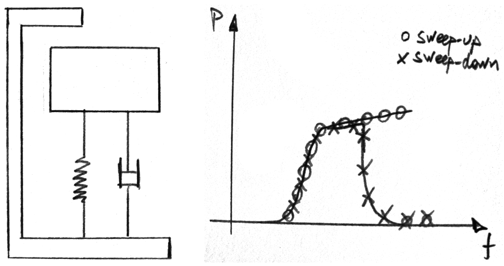

(a) (b)

Figure 3.11: Mass-spring-damper oscillator with amplitude limiters under base excitation: (a) physical model and (b) typical shape of power response curve.

is no typical power response plot.

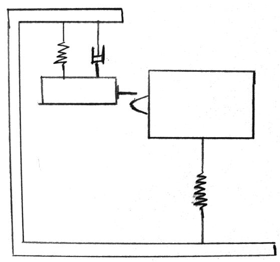

Figure 3.12: Simplified physical model for scrape-through oscillator for energy harvesting.

3.3 Duffing monostable oscillators

Using magnetic springs, different embodiments [Burrow and Clare, 2007, Burrow et al., 2008, Mann and Sims, 2009, Stanton et al., 2009, Barton et al., 2010] were proposed for Duffing oscillators with a single stable position. Further explanation about this oscillator will follow next. The physical model is the same as for the classic oscillator, only with a nonlinear spring. The typical oscillator is sketched in fig. 3.13(a) and its typical response curve in fig. 3.13(b). It results that the oscillator is subject to hysteresis and does not provide good results for random excitations [Daqaq, 2010].

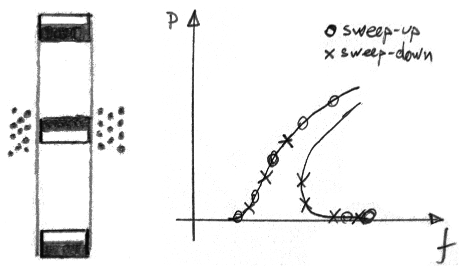

(a) (b)

Figure 3.13: Monostable nonlinear Duffing oscillator under base excitation: (a) typical embodiment, with three magnets and a coil (in section), and (b) typical shape of power response curve.

3.4 Bistable oscillators

On the next ten pages follows a review specific to bistable energy harvesters, published in a special edition on energy harvesting of the Journal of Intelligent Material Systems and Structures.

Bistable Vibration Energy Harvesters: a review

Sergio P. Pellegrini*, Nima Tolou*, Mark Schenk†, Just L. Herder*

* Department of Biomechanical Engineering, Faculty of Mechanical Engineering, Delft University of Technology, Mekelweg 2, 2628 CD Delft, The Netherlands

† Department of Engineering, Cambridge University, Trumpington St., Cambridge CB2 1PZ, United Kingdom

Abstract

Powering electronics without depending on batteries is an open research field. Mechanical vibrations prove to be a reliable energy source, but low-frequency broadband vibrations cannot be harvested effectively using linear oscillators. This article discusses an alternative for harvesting such vibrations, with energy harvesters with two stable configurations. The challenges related to nonlinear dynamics are briefly discussed. Different existing designs of bistable energy harvesters are presented and classified, according to their feasibility for miniaturization. A general dynamic model for those designs is described. Finally, an extensive discussion on quantitative measures of evaluating the effectiveness of energy harvesters is accomplished, resulting in the proposition of a new dimensionless metric suited for a broadband analysis.

Keywords: energy harvesting; nonlinear; bistable; Duffing equation.

1 Introduction

An evolving alternative to the use of batteries is the use of energy harvesters, which convert ambient energy into electricity. These devices can contribute to overcome the limitations related to batteries on power density [Paradiso and Starner, 2005], long-term duration [Roundy et al., 2003] and disposal. Long-life solutions for implantable devices or wireless sensor networks for structural health monitoring, for instance, could become feasible with the development of a reliable and continuous supply of energy.

Moreover, energy harvesters have advantages from a thermodynamical point of view. The decentralized generation of energy avoids the need for long range transmission and provides fewer energy conversions, both of which are subject to intrinsic losses. Additionally, it decreases the overall generation of entropy, as the energy is extracted from existing processes, moving towards a zero-waste overall system.

There are different possible energy sources for powering those devices, including solar, thermal or mechanical vibrations. The latter is considered to be the best alternative for environments without direct sunlight [Roundy et al., 2003, Mathúna et al., 2008, Kim et al., 2009].

Initially, the mainstream for vibration energy harvesters was to develop resonant linear systems, using electromagnetic, piezoelectric, electrostatic or magnetostrictive effects to transform mechanical energy into electrical potential energy. Regardless of the conversion mechanism, those harvesters are designed for specific vibrations, as linear oscillators provide large amplitude responses only when excited at resonance [Roundy et al., 2003]. This leads to higher manufacturing costs — demanding lower fabrication tolerances [Mann and Sims, 2009] — and to a very low efficiency for input vibrations of different frequencies — especially having in mind that these systems are usually designed to have a high resonance peak.

To cope with different input vibrations, energy harvesters with tunable resonance frequency were developed on open-loop [Leland and Wright, 2006, Eichhorn et al., 2009] and closed-loop [Zhu et al., 2010] configurations. Those harvesters have a more complex design and have a lower overall efficiency for the active case. In addition, an increase in damping was reported for frequencies further from the original resonance frequency.

Most application fields, such as structural monitoring or, more generally, wireless sensor networks, are subject to broadband vibrations. A tunable linear energy harvester does not provide good responses for broadband inputs, as it is specialized in a resonance frequency.

Thus, different approaches were developed to widen the bandwidth of the harvester, using, for example, arrays of linear oscillators, linear oscillators with amplitude stoppers or nonlinear oscillators (monostable oscillators with cubic nonlinearity). An extensive review on these strategies was made in [Zhu and Beeby, 2011]. This same review concludes that bistable energy harvesters are capable of coping with vibrations of frequency much lower than typical resonance frequencies, outweighing the increased complexity of design.

Indeed, important applications are subject to low frequency vibrations. Some examples are body-worn sensors and implantable devices. For human body motion, the frequencies that provide a fair amount of energy for harvesting are within the interval $0-30\,\mathrm{Hz}$ [von Büren et al., 2003, Ramlan et al., 2011, Huang et al., 2011]. Other applications, such as environmental monitoring, agricultural automation and security are typically lower than $40\,\mathrm{Hz}$ [Galchev et al., 2011]. Moreover, the scaling effect imposes that small objects perceive as low a vibration frequency that a large scaled object perceives as high. If the goal is to integrate energy harvesters into circuits, designing on MEMS scale, it is important to conceive harvesters designed for low frequencies.

As bistable oscillators enable energy harvesting from low frequency broadband vibrations, they may provide a solution to the challenge of scaling down harvesters to MEMS applications, side-stepping the issue of increasing resonance frequencies at these scales. However, to the authors' knowledge, no review paper focussed specifically on this topic.

For that purpose, section 2 presents a short history of the development of bistable energy harvesters, along with their specific characteristics. Section 3 introduces and classifies reported designs of those harvesters. Then, section 4 presents the mathematical modeling of the dynamic behavior of the bistable oscillators. Finally, section 5 discusses the methods for comparing the performance of energy harvesters and proposes a metric capable of handling the peculiarities inherent to nonlinear effects.

2 Bistable energy harvesters

Preliminary experimental results showed the potential of bistable energy harvesters in 2005 [Baker et al., 2005]. Later, numerical studies [Ramlan et al., 2010, Gammaitoni et al., 2009] implemented a model of an oscillator with a quartic bistable potential well and showed that bistable energy harvesters can provide more energy than its linear counterparts, for broadband vibration inputs of low frequencies. The result was also confirmed experimentally [Cottone et al., 2009].

Erturk and Inman [Erturk and Inman, 2011] compared the performance over a frequency range, between a linear energy harvester and a bistable one, as shown in Figure 1. The resonator provides larger power only for input frequencies close to its resonance frequency of 7.4 Hz. All frequencies were tested with a fixed RMS acceleration input of $0.35g$.

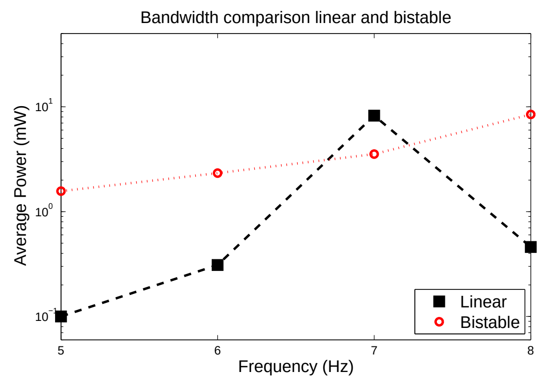

Figure 1: Power generated *versus* frequency of input vibration, for a bistable oscillator and a linear oscillator. Data from [Erturk and Inman, 2011].

However, designing a bistable energy harvester is challenging. In fact, Moon and Holmes [Moon and Holmes, 1979] made an experimental study on a bistable oscillator showing that, despite its deterministic characteristics, the oscillator behaves chaotically. Recent studies show that this behavior is limited to some ranges of frequencies and oscillation amplitudes, as illustrated in Figure 2. The plot is obtained for a harmonic excitation with fixed amplitude of 200 μm, which results in a tendency for larger open circuit voltages for larger frequencies, as the input power also increases. Figure 2 further allows an analysis of the hysteresis effects for bistable oscillators. Those are not as significant as for other nonlinear designs, such as the use of stoppers or the use of nonlinear monostable oscillators [Zhu and Beeby, 2011].

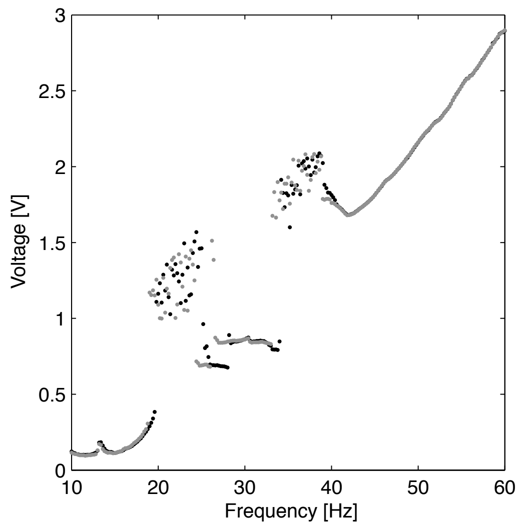

Figure 2: Voltage response over frequency, showing chaotic behavior at specific ranges. Frequency sweep-up is shown in gray and sweep-down in black. Image courtesy of [Cammarano et al., 2011].

Other numerical studies discussed the phenomenon of stochastic resonance [McInnes et al., 2008, Litak et al., 2010], in which large amplitude oscillations can be obtained given that sufficient energy is provided for the oscillator to overcome the potential barrier. Experimental studies confirmed that inter-well motion, whereby the system oscillates switching between the two stable equilibria, provides more energy than intra-well motion, with oscillations around one stable equilibrium configuration [Erturk and Inman, 2011, Stanton et al., 2010, Cammarano et al., 2011, Sneller et al., 2011].

Inter-well motion can happen in two different manners: periodically — with a large amplitude limit cycle — and chaotically. Chaotic motion provides bigger challenges for the processing of the generated electrical power [Erturk and Inman, 2011]. Thus, for energy harvesting purposes, the large amplitude limit cycle oscillation is the most desired behavior. An example of the characteristic behaviors is shown in

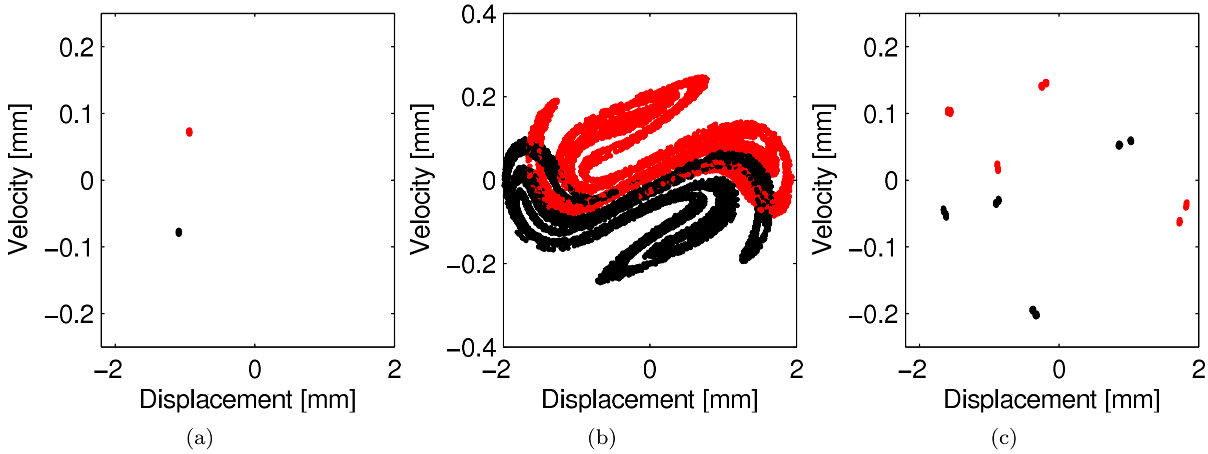

Figure 3: Stroboscopic map showing the characteristic dynamic behaviors of bistable oscillators, with (a) intra-well motion; (b) inter-well chaotic motion; and (c) inter-well periodic oscillations. Red (lighter) dots and black dots are in phase opposition. Image courtesy of [Cammarano et al., 2011].

Figure 3.

The complex non-resonant frequency response also generates challenges for the evaluation of the efficiency of the energy harvesters, as will be discussed in section 5.

3 Conceptual designs

Bistable energy harvesters have been designed using very different underlying physical principles, as will be shown with designs found in the literature. Two distinct design objectives have been developed: to use bistability as part of the vibration cycle or to use the inter-well motion for frequency up-conversion, aiming at energy harvesting of impact motion.

Bearing in mind that one goal of the field is to create small-scale harvesters, the presented energy harvesters will be classified according to their suitability for construction at MEMS scale. Ferrari et al [Ferrari et al., 2010b] report that the need for a permanent magnet in the oscillator imposes a harder MEMS fabrication process. Thus, a possible distinction is to classify the energy harvesters according to whether they use moving or stationary magnets. Further, there should be one class for devices that do not use any magnet, as this allows an even simpler fabrication process.

Following the classification suggested, the constructions found in literature are sketched and grouped in figures[1] . The classification is relatively independent of the conversion method, as it aims mostly at the design of the harvesters.

[1]For all following figures the hatched area denotes a patch with piezoelectric material; purely black blocks are concentrated masses; blocks with equal areas in white and black represent magnets; coils are shown either as points, when in section, or as lines, when in perspective; finally, the vibration direction is shown by a double ended arrow and is imposed in all parts marked as grounded.

3.1 Bistable oscillators

This subsection groups all energy harvesters that use bistability directly for energy conversion.

3.1.1 With internal magnets

Figure 4 groups the energy harvesters which have magnets as part of their oscillators. The first construction shown in Figure 4(a), is a piezoelectric energy harvester. This construction has been explored by several authors [Cottone et al., 2009, Stanton et al., 2010, Ferrari et al., 2010a, Andò et al., 2010, Lin and Alphenaar, 2010] and is composed of an elastic cantilever with patches of piezoelectric material and a magnet on the tip, in addition to an external magnet. The stiffness of the system is composed of the sum of the deformation of the elastic beam and the magnetic interaction, defining a potential energy landscape with two stable positions.

The next energy harvester, shown in Figure 4(b) has an electromagnetic conversion mechanism. The bistable energy potential is defined exclusively by magnetic interaction [Mann and Owens, 2010], with two magnets at the ends of a guiding tube and four magnets distributed radially. The oscillations of the central magnet generate a variable magnetic field through the coil, generating electric current.

Finally, the electromagnetic harvester sketched in Figure 4(c) was developed in [Cammarano et al., 2011]. The mechanism consists of a U-shaped iron core with a coil around it and a plate with four magnets on its end. Those magnets are arranged such that the ones on the same face of the plate show opposed polarities to the iron core. Here the system's bistability is defined by the higher magnetic permeability of the iron core, creating two preferred positions defined by the two closed magnetic circuits — either with the pair of magnets above or with the ones below the plate.

One relevant comment is that energy harvesters

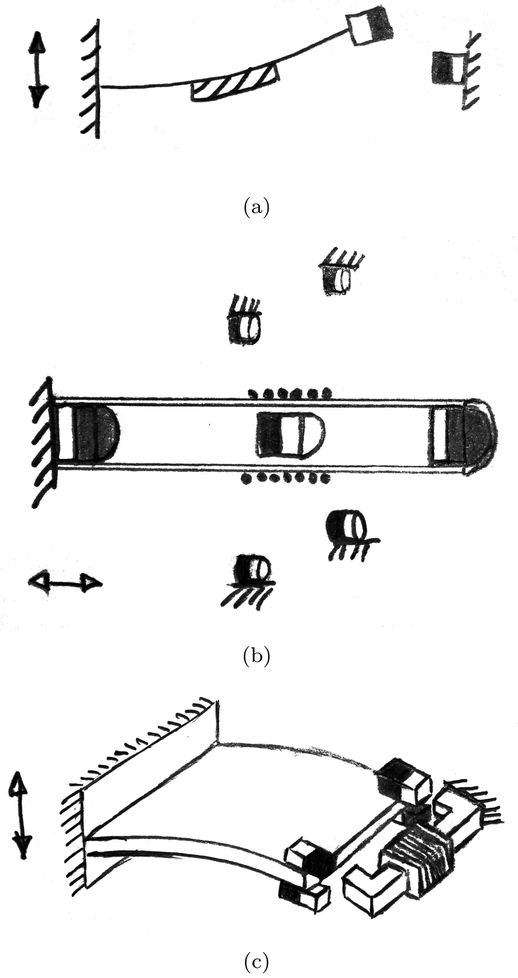

Figure 4: Sketches of energy harvesters with moving magnets: (a) cantilever with magnet repulsion; (b) pure magnetic interaction, with the four external magnets lying in the same plane and (c) two closed magnetic circuits define the stable configurations.

based on electromagnetic conversion methods will not mandatorily fall in this category. A harvester built such that the coil is moving — instead of the magnets — would fall into the next category, with better miniaturization possibilities.

3.1.2 With external magnets

Next, energy harvesters that rely exclusively on external fixed magnets are sketched in Figure 5.

The mechanism shown in Figure 5(a) was initially proposed in 1979 [Moon and Holmes, 1979], but only considered for energy harvesting thirty years later [Erturk et al., 2009]. Further analysis followed in [Erturk and Inman, 2011]. The harvester is composed of a ferromagnetic beam with a patch of piezoelectric material and two external magnets. Bistability is again obtained due to the higher magnetic permeability of ferroelectric materials.

The harvester in Figure 5(b) was proposed in [Ferrari et al., 2010b] and further developed in [Ferrari et al., 2011]. This piezoelectric energy harvester is similar to the previous one, with a modification that decreases the number of external magnets. As the attraction of ferromagnetic materials happens regardless of the magnetic polarization, the bistable energy landscape can be obtained using the two polarizations of one single magnet.

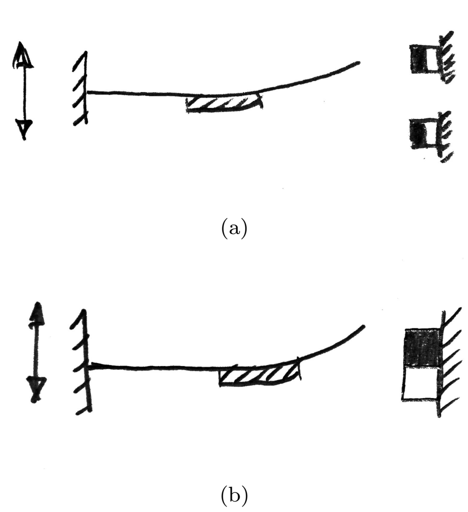

Figure 5: Sketches of energy harvesters that rely exclusively on external magnets: (a) a ferromagnetic cantilever interacts with two magnets and (b) a ferromagnetic cantilever interacting with two poles of the same magnet.

3.1.3 Mechanical bistability

The last class is shown in Figure 6, with sketches of energy harvesters that do not rely on magnets to obtain a bistable behavior.

The energy harvester in Figure 6(a) is a post-buckled beam with a central proof mass and patches of piezoelectric material [Sneller et al., 2011]. When applying a compressive force larger than the buckling load, the behavior of the system changes into a bistable structure, also known by the name of snap-through mechanism.

Finally, the harvester (b) is a bistable composite plate with piezoelectric patches and proof masses [Arrieta et al., 2010]. The two stable configurations are defined by two curvatures in different directions and result from the lay-up of the carbon fibers, with a 90° orientation shift between the layers.

3.2 Frequency up-conversion

In addition, there are the mechanisms which are of bistable nature, but do not use bistability directly in order to harvest energy. Those harvesters use the snap-through action — in other words, the inter-well motion — to generate an impulse for high frequency smaller linear oscillators. For those constructions, the

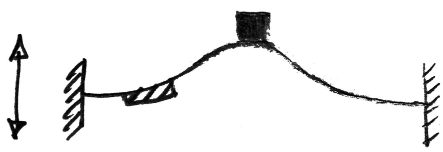

(a)

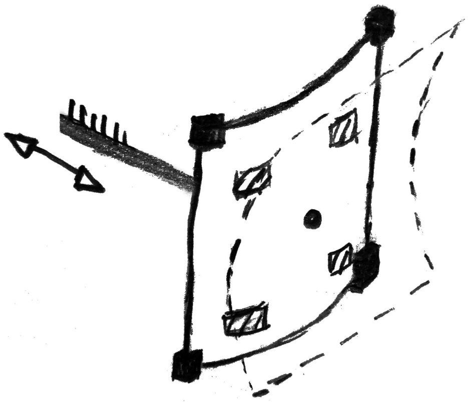

(b)

Figure 6: Sketches of energy harvesters that do not have any magnets: (a) a post-buckled beam and (b) a shell with two stable configurations, curved in different directions.

energy of intra-well oscillation is effectively not harvested.

A further subdivision of those harvesters according to the feasibility of small scale production was not executed, given the few examples in the literature, sketched in Figure 7.

Figure 7 (a) shows an energy harvester proposed in [Galchev et al., 2009a], further developed in [Galchev et al., 2009b] and modeled in [Galchev et al., 2011], in which a central spring-mass system is placed between two identical sub-systems. Each sub-system contains an actuation magnet, closer to the central proof mass, a spring, that acts as a membrane, a power generation magnet and a coil. The central proof mass has a magnetic permeability slightly higher than that of air, allowing the system to have two preferred positions. In the action of snap-through, the proof mass-spring system suddenly releases one of the sub-systems, which will then oscillate in its resonant frequency and generate electrical energy.

The mechanism in Figure 7(b) was proposed in [Jung and Yun, 2010a] and further developed in [Jung and Yun, 2010b]. The post-buckled beams have a single proof mass, supplied with cantilevers with piezoelectric patches. The inter-well oscillation of the proof mass generates an impulse to the cantilevers, that are set to oscillate in their own resonant frequency.

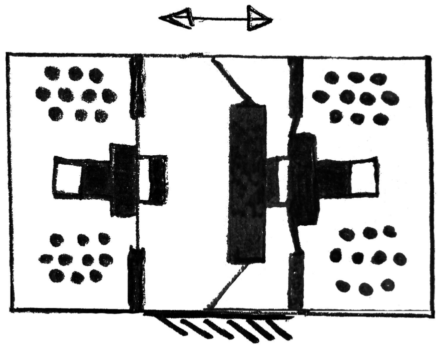

(a)

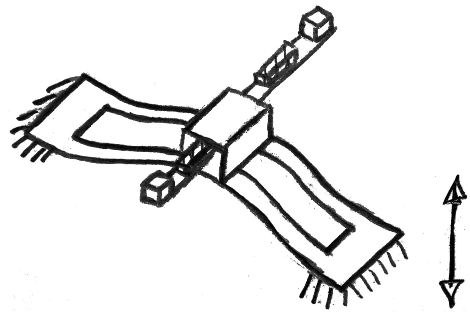

(b)

Figure 7: Sketches of energy harvesters that use bistability for frequency up-conversion: (a) the central mass is in equilibrium when in contact with either of the adjacent magnets; upon inter-well motion, an impulse is provided to one of the generation magnets, internal to the coils and (b) post-buckled beams provide an impulse to smaller resonant cantilevers.

4 Modeling the dynamics

It is imperative to stress that, despite the wide range of underlying principles used to design the oscillators, most of the authors reported the use of the Duffing equation to describe mathematically the dynamic behavior of the nonlinear oscillator.

An important exception should be pointed out for the energy harvester sketched in Figure 6(b). The dynamics of a simplified version of this harvester, without the proof masses, is modeled in [Arrieta et al., 2009] as two coupled modes with a quadratic nonlinear force field.

4.1 The Duffing oscillator

All the other harvesters dynamic behavior is described by a model, known as Duffing oscillator. The model is broad because its potential field is a composition of two symmetric opposed effects. The differential equation for the position of the vibrating mass of the oscillator is given in Equation 1.

$$\ddot{x} + \bar{c}\,\dot{x} - a\,x + b\,x^3 = F(t) \tag{1}$$

This equation can be interpreted as a balance of specific forces, or accelerations, in which the force of external vibrations, $F(t)$, is distributed among inertial effects, $\ddot{x}$, damping, $\bar{c}\,\dot{x}$, and the potential energy field, $-a\,x + b\,x^3$. The damping effects take into account both the energy dissipated mechanically, with friction, and the energy harvested.

The potential energy is the integral of $-a\,x + b\,x^3$. For clarification, the potential energy shall be written as a function of one single parameter, λ, instead of a and b.

$$U = -\frac{1}{2}\,\lambda\,x^2 + \frac{1}{4}\,x^4 \tag{2}$$

Equation 2, thus, shows that the potential energy landscape of a Duffing oscillator is a composition of a quadratic field, typical of linear systems, with a quartic one. Often, the bistable potential energy landscape is derived as a Taylor expansion of an exact formula. The relative importance of the two fields is dictated by the parameter λ. The parameter λ depends on the design and can be translated, for instance, into distance between magnets or buckling force.

An important transformation occurs when $\lambda = 0$. If for negative values of λ, the system had only one stable equilibrium position, now, for positive λ, the system has three equilibrium positions, one unstable and two stable. Plotting the equilibrium positions as a function of λ will result in a supercritical pitchfork bifurcation diagram [Seydel, 1994]. Commonly, Equation 2 is plotted for specific values of λ, either showing a monostable or a bistable behavior. Nevertheless, those plots are specific views of a single three-dimensional surface [Kovacic and Brennan, 2011]. Moreover, the bifurcation diagram is also implicit in that same plot, as clearly shown in Figure 8. This figure provides a complete overview of how the energy landscape varies as a function of the parameter λ.

5 Effectiveness measure

A central aspect of a review is to measure and compare how effectively the energy harvesters meet their design requirements, from the input vibration to the power harvested. However, comparing the effectiveness of energy harvesters is a challenge, due to the different harvesting scales, nature of the conversion methods and use of different test conditions. It is desirable that a metric is scale independent, and should therefore be dimensionless.

As, per definition, a metric will attribute more relevance to specific properties at the cost of ignoring others, it is important to understand which properties are important for each metric.

Some metrics for linear energy harvesters assign importance to high efficiency for energy harvesting at a single frequency. While this makes sense for linear harvesters, those metrics lose significance when comparing the efficiency of harvesters designed for a bandwidth of input vibrations. For nonlinear oscillators, in particular, an important aspect is related to the different dynamic responses, as discussed previously.

5.1 Single frequency metrics

First, metrics based on measures for a single input vibration are presented.

5.1.1 Quality factor based

Both metrics presented next are based on the quality factor, Q, a measure of the sharpness of the resonance peak defined for linear systems in forced harmonic vibration. A definition of the quality factor is provided in [Thomson, 1965], as shown in Equation 3.

$$Q = \frac{f_n}{f_2 - f_1} = \frac{f_n}{BW_{3\text{dB}}} \tag{3}$$

Here, f_n is the resonance frequency, f_1 and f_2 are the frequencies for which the system oscillations' power is half of the response at resonance. Thus, the quality factor is related to the $3\,dB$ bandwidth, but is defined exclusively for linear systems.

Richards [Richards et al., 2004] suggested a dimensionless efficiency metric for energy harvesters based on piezoelectric energy transduction. The metric is given by Equation 4.

$$\eta = \frac{\frac{1}{2}\frac{k^2}{1-k^2}}{\left(\frac{1}{Q} + \frac{1}{2}\frac{k^2}{1-k^2}\right)} \tag{4}$$

In the equation, Q represents the quality factor . The electromechanical coupling coefficient, k^2, is defined as a ratio of the electrical energy stored in the electric field over the mechanical strain energy input into the system for the case of energy harvesting. Q is a property of the oscillator and k^2 is a property of the piezoelectric material.

Roundy [Roundy, 2005] defined an effectiveness metric, also dimensionless, according to Equation 5.

$$e = k^2\,Q^2\,\frac{\rho}{\rho_0}\,\frac{\lambda}{\lambda_{\max}} \tag{5}$$

For this equation, ρ represents the density of the harvester and ρ_0 is a reference density, assumed to be $7.5\frac{g}{cm^3}$; λ is the transmission coefficient — a ratio of the energy delivered to an electrical load over the energy provided mechanically to the harvester — and $\lambda_{\max}$ is the theoretical maximum transmission coefficient.

5.1.2 Power density

Other metrics focused on the power generated by the energy harvesters. It will be preferred to write those metrics as a function of the root mean squared (RMS) power generated by the harvester, in opposition to the original definitions, which specified the metrics as a function of the "power output" or the "useful

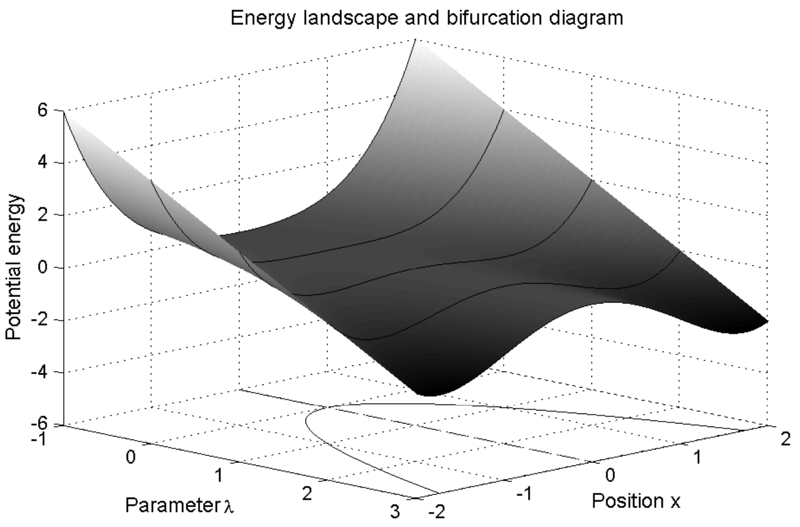

Figure 8: Potential energy *versus* position for different values of the system parameter λ. The supercritical pitchfork bifurcation can also be seen, with the stable branches corresponding to the valleys of the function and the unstable to peaks.

power output". This preference is justified as the RMS power is the most commonly reported.

It should be observed that the RMS power does not provide a complete characterization of the power that an energy harvester can supply to an electrical load, given that the rectification of the signal is also a dynamic process. This process is determined by the power conditioning circuit. Given that there is no consensus on the best topology for the conditioning circuit and that it is a common practice to report the RMS power output, it makes sense that the metrics are defined as a function of the RMS power.

One metric suggested in [Cao et al., 2007] is the specific power, or power density. It consists of the maximum power generated (i.e. at resonance) divided by the harvester's volume, as shown in Equation 6.

$$\mathrm{PD} = \frac{P_{\mathrm{RMS}}^{\mathrm{max}}}{V} \tag{6}$$

The simplicity of this metric allows its broad use. However, it does not take into account the use of input vibrations of different energetic levels.

Beeby et al [Beeby et al., 2007] suggested an index that takes into account this test condition. The normalized power density is the specific power divided by the input acceleration level squared, as shown in Equation 7.

$$\mathrm{NPD} = \frac{P_{\mathrm{RMS}}^{\mathrm{max}}}{a_{\mathrm{RMS}}^2\, V} \tag{7}$$

The normalized power density does not take into account the frequency of the input signal, as resonators are designed to operate at a specific frequency. Moreover, both of those metrics are scale dependent.

5.1.3 Proof mass displacement based

Alternatively, Mitcheson et al [Mitcheson et al., 2008] introduced a harvester effectiveness metric, according to Equation 8.

$$\mathrm{E_H} = \frac{P_{\mathrm{RMS}}^{\mathrm{max}}}{\frac{1}{2} Y_0 Z_l \omega^3 m} \tag{8}$$

In this equation, Y_0 is the amplitude of the input motion, Z_l is the maximum allowed amplitude for the internal motion of the proof mass and ω the frequency of the input vibration. This metric is a normalization of the output power with respect to the power dissipated in a optimally damped linear oscillator, considering the limits for the proof mass motion [Mitcheson et al., 2004].

5.1.4 Figures of merit

Given that the previous metric cannot differentiate volumes and proof mass densities of designs, the same authors created a variant of it, called volume figure of merit, $\mathrm{FoM_V}$ [Mitcheson et al., 2008]. The $\mathrm{FoM_V}$ normalizes the power output with an arbitrary reference case, defined by a harvester with same volume and with a proof mass made of gold, occupying half this volume. The normalization also includes the input vibration signal, as shown in Equation 9.

$$\mathrm{FoM_V} = \frac{P_{\mathrm{RMS}}^{\mathrm{max}}}{\frac{1}{16} Y_0\, \rho_{AU}\, V^{\frac{4}{3}}\, \omega^3} \tag{9}$$

For this equation, in addition to the definition in the previous equation, ρ_{AU} is the density of gold and V denotes the harvester's volume.

In the same paper, the authors point out that this index is intrinsically incapable of capturing the aspect of operation bandwidth. Having that in mind, they proposed the bandwidth figure of merit, as seen in Equation 10.

$$\mathrm{FoM_{BW}} = \mathrm{FoM_V} \frac{BW_{\mathrm{1dB}}}{\omega_m} \tag{10}$$

This index takes into account the bandwidth in which the generated power drop from the maximum is lower than a certain threshold. Mitcheson et al report that they preferred to include a 1 dB bandwidth,

$BW_{1\mathrm{dB}}$, in opposition to the more common $3\,dB$, in order to favor flatter frequency response curves. The frequency for which the maximum RMS power is obtained is ω_m.

The bandwidth figure of merit is a milestone for two reasons. Firstly, it gives direct relevance to bandwidth as a criterion to be analyzed. Secondly, the fact that it does not use the quality factor allows its use for arrays of linear oscillators and nonlinear oscillators. In other words, this index is a natural change from a mindset based on linear oscillators into the use of arrays of linear oscillators and nonlinear energy harvesters.

However, the bandwidth figure of merit is not directly applicable for nonlinear energy harvesters. For nonlinear oscillators, the response curve does not have a predefined shape. Nothing ensures, for instance, that the frequencies for which the harvester will provide a response within the a certain range, in dB, will lie in contiguous intervals. For example, for a specific input vibration amplitude of $2\,g$, where $g = 9.81\,\frac{m}{s^2}$, the harvester proposed in [Galchev et al., 2011] generates power over half of its peak response — in other words, within the $3\,dB$ range — over a discontinuous bandwidth. Plots of open circuit voltage of [Sneller et al., 2011] suggest similar results.

In addition, the concept of fixing a range in $3\,dB$, for instance, is not able to differentiate the cases of harvesters that maintain its efficiency at 40%, for instance, for a wide bandwidth from a harvester that has a sharp decay in response after the threshold.

5.2 Multiple frequency metric

Having those issues in mind, we propose a more complete efficiency evaluation of energy harvesters, with a parallel to fluid mechanics research on vortex-induced vibrations (VIV).

The phenomenon of VIV can happen when a bluff body is immersed in a flow. Due to the interaction of the fluid shear layers, vortices are shed downstream of the solid body, generating forces that impel the body. Those forces are periodic and their frequency is related to the flow velocity and the body geometry. Depending on the type of vortex shed and on the vortex shedding frequency, the body is set to resonate [Bearman, 1984]. From the essence of the VIV phenomenon, solid-fluid interaction, it results that the system has to be treated as a nonlinear oscillator. Specifically, it is of the interest of offshore engineering to suppress those oscillations as much as possible, as the vibrations impose a higher cost and reduce the life span of risers. There are some different constructions and manufacturers of VIV suppressors and the comparison among them is not well defined. In fact, Freire et al. [Freire et al., 2011] report that different metrics are used according to which suppression effect the authors want to highlight. Having that in mind, they developed a metric that provides a measure of the effectiveness of the suppression for the phenomenon in its entirety, for all values of flow velocity. An analogy could be made such that the flow velocity is seen as the frequency of the input vibration on a nonlinear oscillator.

The idea proposed can be simply stated as, instead of looking at the system response at a single frequency, to analyze the integral of the response over a predetermined frequency range. However, the existing metrics are not directly applicable for nonlinear energy harvesters, as the existence of a steady state – assumed for equation 8, for instance – is not assured. A possible performance index is shown in Equation 11.

$$\mathrm{I} = \frac{P_{\mathrm{RMS}}\, f}{m\, a_{\mathrm{RMS}}^2} \tag{11}$$

This non-dimensional group combines the electrical power generated, P_{RMS}, a property of the oscillator, m, and properties of the test condition, with the acceleration level, a_{RMS}, and the frequency, f. The symbol m represents the equivalent mass, that takes into account the mass of the part of the flexible structure that is effectively oscillating. However, as the parameter most often reported is the proof mass, it makes sense to use this value for m. Indeed, the equivalent mass is, in general, largely determined by the proof mass.

For the evaluation of the performance of nonlinear energy harvesters in multiple frequencies, we suggest to take the average over a specified frequency bandwidth, as shown in Equation 12.

$$\mathrm{I}_{\mathrm{a-b}} = \frac{\int_a^b I\,\mathrm{d}f}{b-a} \tag{12}$$

In this equation, a and b are specific frequencies and $b-a$ is the bandwidth of operation. The limits are not specified, as each design and application will have specific ranges of interest.

Equation 12 is a mean of the index of Equation 11 and is incapable of providing a complete overview of the performance of the harvester within the bandwidth of operation. Aiming at describing variability, the coefficient of variation is calculated according to Equation 13.

$$\mathrm{CV}_{\mathrm{a-b}} = \frac{\sqrt{\frac{\int_a^b I^2\,\mathrm{d}f}{b-a} - \left(I_{a-b}\right)^2}}{I_{a-b}} \tag{13}$$

The coefficient of variation can provide a better measure than the standard deviation because it is a relative number and, thus, allows a comparison of variability across different ranges of $b-a$ and for different energy harvesters.

A critique should be made because, as the system is nonlinear, the principle of superposition — an underlying assumption while taking the integral of the response — might not be respected [Åström and Murray, 2008]. Although theory does not ensure that the oscillator would behave the same as the index predicts when white noise is given as an input, an index based on the integral of different inputs can still be a valid metric in most cases.

Another direct consequence of the invalidity of the superposition principle is that the response of the energy harvester is a function of both the frequency and the amplitude of the input vibration. Equations 12 and 13 can also be applied for tests varying the motion amplitude or, alternatively, the acceleration amplitude.

One matter that remains open is how to deal with hysteresis. Possibilities such as taking two indexes — for sweep-up and sweep-down — or taking the average of them seem intuitive. Additionally, the sweep rate should be reported, as the hysteretic effects may depend on it. Indeed, for piezoelectric materials, hysteresis is rate-dependent [Smith et al., 2001].

6 Conclusions

This article presented and discussed bistable energy harvesters, specialized in transforming low-frequency broadband mechanical vibrations into electrical power. In contrast, for energy conversion from sources of determined single frequency vibrations, harvesters based on linear oscillators provide a more efficient outcome.

Despite the benefits, bistable energy harvesters challenges involve the complex nonlinear dynamic responses, with three response regimes — intra-well, chaos and large amplitude limit cycle. The latter of those is the most desirable, as it provides more electrical energy and is less problematic for the conditioning circuit.

A classification of the existing bistable energy harvesters was proposed, dividing them according to whether they use bistability directly for energy harvesting or for frequency up-conversion; if they rely on mechanical bistability or use magnets and, finally, whether those magnets are moving or fixed. This classification aims at sorting the harvesters on their feasibility for fabrication at MEMS scale.

In spite of the different underlying physics used to design bistable energy harvesters, the dynamic behavior is generally modeled with the same nonlinear equations, known as the Duffing oscillator.

A direct quantitative comparison of the harvesters proved to be hard, as most existing efficiency indexes do not capture the particularities of nonlinear oscillators for energy harvesting. Thus, we proposed a new metric, non-dimensional and suited for broadband analysis. It is expected that the new metric allows a fairer comparison of the different energy harvesters, and that the overview of the existing designs and the discussion on the main issues shall support the design of more effective bistable energy harvesters.

References

B. Andò, S. Baglio, C. Trigona, N. Dumas, L. Latorre, and P. Nouet. Nonlinear mechanism in mems devices for energy harvesting applications. *Journal of Micromechanics and Microengineering*, 20(12):125020, 2010.

A. Arrieta, S. Neild, and D. Wagg. Nonlinear dynamic response and modeling of a bi-stable composite plate for applications to adaptive structures. *Nonlinear Dynamics*, 58:259–272, 2009.

A. F. Arrieta, P. Hagedorn, A. Erturk, and D. J. Inman. A piezoelectric bistable plate for nonlinear broadband energy harvesting. *Appl. Phys. Lett.*, 97(10):104102, 2010.

K. J. Åström and R. M. Murray. *Feedback Systems: An Introduction for Scientists and Engineers.* Princeton University Press, 2008.

J. Baker, S. Roundy, and P. Wright. Alternative geometries for increasing power density in vibration energy scavenging for wireless sensor networks. In *3rd International Energy Conversion Conference*, page 12, San Francisco, CA. USA, 15-18 Aug 2005.

P. W. Bearman. Vortex shedding from oscillating bluff bodies. *Annual Review of Fluid Mechanics*, 16(1):195–222, 1984.

S. P. Beeby, R. N. Torah, M. J. Tudor, P. Glynne-Jones, T. O'Donnell, C. R. Saha, and S. Roy. A micro electromagnetic generator for vibration energy harvesting. *Journal of Micromechanics and Microengineering*, 17(7):1257, 2007.

A. Cammarano, S. G. Burrow, and D. A. W. Barton. Modelling and experimental characterization of an energy harvester with bi-stable compliance characteristics. *Proceedings of the Institution of Mechanical Engineers, Part I: Journal of Systems and Control Engineering*, 225(4):475–484, 2011.

X. Cao, W.-J. Chiang, Y.-C. King, and Y.-K. Lee. Electromagnetic energy harvesting circuit with feedforward and feedback dc-dc pwm boost converter for vibration power generator system. *Power Electronics, IEEE Transactions on*, 22 (2):679–685, Mar. 2007.

F. Cottone, H. Vocca, and L. Gammaitoni. Nonlinear energy harvesting. *Phys. Rev. Lett.*, 102:080601, Feb. 2009.

C. Eichhorn, F. Goldschmidtboeing, and P. Woias. Bidirectional frequency tuning of a piezoelectric energy converter based on a cantilever beam. *Journal of Micromechanics and Microengineering*, 19(9):094006, 2009.

A. Erturk and D.J. Inman. Broadband piezoelectric power generation on high-energy orbits of the bistable duffing oscillator with electromechanical coupling. *Journal of Sound and Vibration*, 330(10):2339 – 2353, 2011. Dynamics of Vibro-Impact Systems.

A. Erturk, J. Hoffmann, and D. J. Inman. A piezomagnetoelastic structure for broadband vibration energy harvesting. *Appl. Phys. Lett.*, 94(25):254102, 2009.

M. Ferrari, V. Ferrari, M. Guizzetti, B. Andò, S. Baglio, and C. Trigona. Improved energy harvesting from wideband vibrations by nonlinear piezoelectric converters. *Sensors and Actuators A: Physical*, 162(2):425 – 431, 2010a. Eurosensors XXIII, 2009.

M. Ferrari, V. Ferrari, M. Guizzetti, and D. Marioli. A single-magnet nonlinear piezoelectric converter for enhanced energy harvesting from random vibrations. *Procedia Engineering*, 5(0):1156 – 1159, 2010b. Eurosensors XXIV, 2010.

M. Ferrari, M. Baù, M. Guizzetti, and V. Ferrari. A single-magnet nonlinear piezoelectric converter for enhanced energy harvesting from random vibrations. *Sensors and Actuators A: Physical*, 172(1):287 – 292, 2011. Eurosensors XXIV, Sept. 2010.

C. M. Freire, I. Korkischko, and J. R. Meneghini. Defining a parameter of effectiveness for the suppression of vortex-induced vibration. In *Proceedings of the 30th International Conference on Ocean, Offshore and Artic Engineering*, Rotterdam, The Netherlands, Jun. 2011.

T. Galchev, H. Kim, and K. Najafi. Non-resonant bi-stable frequency-increased power scavenger from low-frequency ambient vibration. In *Solid-State Sensors, Actuators and Microsystems Conference, 2009. TRANSDUCERS 2009. International*, pages 632 –635, Jun. 2009a.

T. Galchev, H. Kim, and K. Najafi. A parametric frequency increased power generator for scavenging low frequency ambient vibrations. *Procedia Chemistry*, 1(1):1439 – 1442, 2009b. Proceedings of the Eurosensors XXIII conference.

T. Galchev, H. Kim, and K. Najafi. Micro power generator for harvesting low-frequency and nonperiodic vibrations. *Microelectromechanical Systems, Journal of*, 20(4):852 –866, Aug. 2011.

L. Gammaitoni, I. Neri, and H. Vocca. Nonlinear oscillators for vibration energy harvesting. *Appl. Phys. Lett.*, 94:164102, Apr. 2009.

H. Huang, G. Merrett, and N. White. Human-powered inertial energy harvesters: the effect of orientation, location and activity on obtainable power. In *Eurosensors XXV*. Elsevier Procedia Engineering, Sept. 2011.

S.-M. Jung and K.-S. Yun. A wideband energy harvesting device using snap-through buckling for mechanical frequency-up conversion. In *Micro Electro Mechanical Systems (MEMS), 2010 IEEE 23rd International Conference on*, pages 1207 –1210, Jan. 2010a.

S.-M. Jung and K.-S. Yun. Energy-harvesting device with mechanical frequency-up conversion mechanism for increased power efficiency and wideband operation. *Appl. Phys. Lett.*, 96(11):111906, 2010b.

H. Kim, Y. Tadesse, and S. Priya. *Energy Harvesting Technologies*, chapter Piezoelectric Energy Harvesting, pages 3–40. Springer, 2009.

I. Kovacic and M. J. Brennan, editors. *The Duffing equation: nonlinear oscillators and their phenomena*. Wiley, 2011.

Eli S. Leland and Paul K. Wright. Resonance tuning of piezoelectric vibration energy scavenging generators using compressive axial preload. *Smart Materials and Structures*, 15 (5):1413, 2006.

J.-T. Lin and B. Alphenaar. Enhancement of energy harvested from a random vibration source by magnetic coupling of a piezoelectric cantilever. *Journal of Intelligent Material Systems and Structures*, 21(13):1337–1341, 2010.

G. Litak, M. I. Friswell, and S. Adhikari. Magnetopiezoelastic energy harvesting driven by random excitations. *Appl. Phys. Lett.*, 96(21):214103, 2010.

B. P. Mann and B. A. Owens. Investigations of a nonlinear energy harvester with a bistable potential well. *Journal of Sound and Vibration*, 329(9):1215 – 1226, 2010.

B. P. Mann and N. D. Sims. Energy harvesting from the nonlinear oscillations of magnetic levitation. *Journal of Sound and Vibration*, 319(1-2):515 – 530, 2009.

C. Ó Mathúna, T. O'Donnell, R. V. Martinez-Catala, J. Rohan, and B. O'Flynn. Energy scavenging for long-term deployable wireless sensor networks. *Talanta*, 75(3):613 – 623, 2008. Special Section: Remote Sensing.

C. R. McInnes, D. G. Gorman, and M. P. Cartmell. Enhanced vibrational energy harvesting using nonlinear stochastic resonance. *Journal of Sound and Vibration*, 318(4-5):655 – 662, 2008.

P. D. Mitcheson, T. C. Green, E. M. Yeatman, and A. S. Holmes. Architectures for vibration-driven micropower generators. *Microelectromechanical Systems, Journal of*, 13(3): 429–440, 2004.

P. D. Mitcheson, E. M. Yeatman, G. K. Rao, A. S. Holmes, and T. C. Green. Energy harvesting from human and machine motion for wireless electronic devices. *Proceedings of the IEEE*, 96(9):1457–1486, Sept. 2008.

F. C. Moon and P. J. Holmes. A magnetoelastic strange attractor. *Journal of Sound and Vibration*, 65(2):275 – 296, 1979.

J. A. Paradiso and T. Starner. Energy scavenging for mobile and wireless electronics. *IEEE Pervasive Computing*, 4:18–27, Jan 2005.

R. Ramlan, M. Brennan, B. Mace, and I. Kovacic. Potential benefits of a non-linear stiffness in an energy harvesting device. *Nonlinear Dynamics*, 59:545–558, 2010.

R. Ramlan, M. J. Brennan, and B. R. Mace. On the optimum parameters of a device for harvesting energy from running and walking. *Proceedings of the Institution of Mechanical Engineers, Part I: Journal of Systems and Control Engineering*, 225(4):510–521, 2011.

C. D. Richards, M. J. Anderson, D. F. Bahr, and R. F. Richards. Efficiency of energy conversion for devices containing a piezoelectric component. *Journal of Micromechanics and Microengineering*, 14(5):717, 2004.

S. Roundy. On the effectiveness of vibration-based energy harvesting. *Journal of Intelligent Material Systems and Structures*, 16(10):809–823, 2005.

S. Roundy, P. K. Wright, and J. Rabaey. A study of low level vibrations as a power source for wireless sensor nodes. *Computer Communications*, 26(11):1131 – 1144, 2003. Ubiquitous Computing.

R. Seydel. *Practical bifurcation and stability analysis: from equilibrium to chaos*. Springer-Verlag, 2nd edition, 1994.

R. C. Smith, Z. Ounaies, and R. Wieman. A model for rate-dependent hysteresis in piezoceramic materials operating at low frequencies. Technical report, ICASE Report 2001-26, Sept. 2001.

A. J. Sneller, P. Cette, and B. P. Mann. Experimental investigation of a post-buckled piezoelectric beam with an attached central mass used to harvest energy. *Proceedings of the Institution of Mechanical Engineers, Part I: Journal of Systems and Control Engineering*, 225(4):497–509, 2011.

S. C. Stanton, C. C. McGehee, and B. P. Mann. Nonlinear dynamics for broadband energy harvesting: Investigation of a bistable piezoelectric inertial generator. *Physica D: Nonlinear Phenomena*, 239(10):640 – 653, 2010.

W. T. Thomson. *Vibration theory and applications*. Prentice-Hall, 1965.

T. von Büren, P. Lukowicz, and G. Tröster. Kinetic energy powered computing - an experimental feasibility study. In *Wearable Computers, 2003. Proceedings. Seventh IEEE International Symposium on*, pages 22 – 24, Oct. 2003.

D. Zhu and S. P. Beeby. *Energy Harvesting Systems*, chapter Kinetic Energy Harvesting, pages 1–78. Springer, 2011.

D. Zhu, S. Roberts, M. J. Tudor, and S. P. Beeby. Design and experimental characterization of a tunable vibration-based electromagnetic micro-generator. *Sensors and Actuators A: Physical*, 158(2):284 – 293, 2010.

Bibliography

David A. W. Barton, Stephen G. Burrow, and Lindsay R. Clare. Energy harvesting from vibrations with a nonlinear oscillator. *Journal of Vibration and Acoustics*, 132(2):021009, 2010.

S. G. Burrow, L. R. Clare, A. Carrella, and D. Barton. Vibration energy harvesters with non-linear compliance. In Mehdi Ahmadian, editor, *Active and Passive Smart Structures and Integrated Systems 2008*, volume 6928, page 692807. SPIE, 2008.

S.G. Burrow and L.R. Clare. A resonant generator with non-linear compliance for energy harvesting in high vibrational environments. In *Electric Machines Drives Conference, 2007. IEMDC '07. IEEE International*, volume 1, pages 715 –720, May 2007.

Vinod R Challa, M G Prasad, and Frank T Fisher. Towards an autonomous self-tuning vibration energy harvesting device for wireless sensor network applications. *Smart Materials and Structures*, 20(2): 025004, 2011.

Mohammed F. Daqaq. Response of uni-modal duffing-type harvesters to random forced excitations. *Journal of Sound and Vibration*, 329(18):3621 – 3631, 2010. ISSN 0022-460X.

Mohammed F. Daqaq, Christopher Stabler, Yousef Qaroush, and Thiago Seuaciuc-Osrio. Investigation of power harvesting via parametric excitations. *Journal of Intelligent Material Systems and Structures*, 20(5):545–557, 2009.

C. Eichhorn, F. Goldschmidtboeing, and P. Woias. Bidirectional frequency tuning of a piezoelectric energy converter based on a cantilever beam. *Journal of Micromechanics and Microengineering*, 19(9): 094006, 2009.

Richard P. Feynman, Robert B. Leighton, and Matthew Sands. *The Feynman lectures on Physics*, volume II. Addison-Wesley, 1964.

Daniel Hoffmann, Bernd Folkmer, and Yiannos Manoli. Fabrication, characterization and modelling of electrostatic micro-generators. *Journal of Micromechanics and Microengineering*, 19(9):094001, 2009.

Yuantai Hu, Huan Xue, and Hongping Hu. A piezoelectric power harvester with adjustable frequency through axial preloads. *Smart Materials and Structures*, 16(5):1961, 2007.

S. G. Kelly. *Fundamentals of Mechanical Vibrations*. McGraw-Hill, 1993.

In-Ho Kim, Hyung-Jo Jung, Bo Mi Lee, and Seon-Jun Jang. Broadband energy-harvesting using a two degree-of-freedom vibrating body. *Applied Physics Letters*, 98(21):214102, 2011.

Haluk Kulah and Khalil Najafi. Method and micro power generator for generating electrical power from low frequency vibration energy, 2009.

D.-G. Lee, G.P. Carman, D. Murphy, and C. Schulenburg. Novel micro vibration energy harvesting device using frequency up conversion. In *Solid-State Sensors, Actuators and Microsystems Conference, 2007. TRANSDUCERS 2007. International*, pages 871–874, Lyon, Jun. 2007.

Eli S. Leland and Paul K. Wright. Resonance tuning of piezoelectric vibration energy scavenging generators using compressive axial preload. *Smart Materials and Structures*, 15(5):1413, 2006.

Wen J. Li, Zhiyu Wen, Pak Kin Wong, Gordon M. H. Chan, and Philip H. W. Leong. A micromachined vibration-induced power generator for low power sensors of robotic systems. In *World Automation Congress - Eighth International Symposium on Robotics with Applications*, Hawaii, Jun 2000.

Huicong Liu, Cho Jui Tay, Chenggen Quan, Takeshi Kobayashi, and Chengkuo Lee. A scrape-through piezoelectric mems energy harvester with frequency broadband and up-conversion behaviors. *Microsyst. Technol.*, 17(12):1747–1754, December 2011. ISSN 0946-7076.

A. Lundgren, H. Tiberg, L. Kvarnsjo, A. Bergqvist, and G. Engdahl. A magnetostrictive electric generator. *Magnetics, IEEE Transactions on*, 29(6):3150–3152, nov 1993.

B. P. Mann and N. D. Sims. Energy harvesting from the nonlinear oscillations of magnetic levitation. *Journal of Sound and Vibration*, 319(1-2):515 – 530, 2009. ISSN 0022-460X.

P. D. Mitcheson, T. C. Green, E. M. Yeatman, and A. S. Holmes. Architectures for vibration-driven micropower generators. *Microelectromechanical Systems, Journal of*, 13(3):429–440, 2004.

P. D. Mitcheson, E. M. Yeatman, G. K. Rao, A. S. Holmes, and T. C. Green. Energy harvesting from human and machine motion for wireless electronic devices. *Proceedings of the IEEE*, 96(9):1457–1486, Sep. 2008.

Özge Zorlu, Emre Tan Topal, and Haluk Külah. A vibration-based electromagnetic energy harvester using mechanical frequency up-conversion method. *Sensors Journal, IEEE*, 11(2):481–488, 2011.

T. Petropoulos, E. M. Yeatman, and P. D. Mitcheson. Mems coupled resonators for power generation and sensing. *IEEE/ASME J. Microelectromech. Sys.*, 13(3):429–440, 2004.

J. Rastegar, C. Pereira, and H.-L. Nguyen. Piezoelectric-based power sources for harvesting energy from platforms with low-frequency vibration. In Edward V. White, editor, *Smart Structures and Materials 2006: Industrial and Commercial Applications of Smart Structures Technologies*, volume 6171, page 617101. SPIE, 2006.

M. Soliman, E.F. El-Saadany, E.M. Abdel-Rahman, and R.R. Mansour. Design and modeling of a wideband mems-based energy harvester with experimental verification. In *Microsystems and Nanoelectronics Research Conference, 2008. MNRC 2008. 1st*, pages 193 –196, oct. 2008a.

M S M Soliman, E M Abdel-Rahman, E F El-Saadany, and R R Mansour. A wideband vibration-based energy harvester. *Journal of Micromechanics and Microengineering*, 18(11):115021, 2008b. URL 1.

Samuel C. Stanton, Clark C. McGehee, and Brian P. Mann. Reversible hysteresis for broadband magnetopiezoelastic energy harvesting. *Appl. Phys. Lett.*, 95(17):174103, 2009. ISSN 00036951.

N.G. Stephen. On energy harvesting from ambient vibration. *Journal of Sound and Vibration*, 293(12): 409 – 425, 2006. ISSN 0022-460X.

William T. Thomson. *Vibration theory and applications*. Prentice-Hall, 1965.

C.B. Williams and R.B. Yates. Analysis of a micro-electric generator for microsystems. *Sensors and Actuators A: Physical*, 52(13):8 – 11, 1996. ISSN 0924-4247. Proceedings of the 8th International Conference on Solid-State Sensors and Actuators Eurosensors IX.

Xiaoming Wu, Jianhui Lin, Seiki Kato, Kai Zhang, Tianling Ren, and Litian Liu. A frequency adjustable vibration energy harvester. In *Proceedings of PowerMEMS 2008 + microEMS2008*, Sendai, Japan, Nov. 2008.

Dibin Zhu, Stephen Roberts, John Tudor, and Steve Beeby. Closed loop frequency tuning of a vibration-based micro-generator. In *PowerMEMS 2008+ microEMS2008*, pages 229–232, Sendai, Japan, Nov 2008.

Dibin Zhu, Stephen Roberts, Michael J. Tudor, and Stephen P. Beeby. Design and experimental characterization of a tunable vibration-based electromagnetic micro-generator. *Sensors and Actuators A: Physical*, 158(2):284 – 293, 2010a. ISSN 0924-4247.

Dibin Zhu, Michael J Tudor, and Stephen P Beeby. Strategies for increasing the operating frequency range of vibration energy harvesters: a review. *Measurement Science and Technology*, 21(2):022001, 2010b.

Chapter 4

Statically balanced energy harvester

Bistable energy harvesters can cope with low frequency, broadband vibrations. However, the complex dynamics is a challenge, as it narrows down the scope of vibrations that can be efficiently harvested. This complex dynamics arise from the energy landscape itself, i.e., from the fact that there are two stable configurations and an energy barrier between them. What would happen if this energy barrier is lowered? Moreover, on the limit case, what would happen if all the positions from the oscillator were stable? Would a neutrally stable oscillator provide a better energy harvester?

In order to answer those questions, first a brief review on static balancing is carried through, without aiming at completeness. Next, an analytical study of the dynamics of statically balanced oscillators is presented, with focus on the transduced power. Finally, the results achieved are discussed.

4.1 Panorama on static balancing

A perfectly statically balanced system is in equilibrium for a continuous set of positions, forming a balanced range of motion [Gallego and Herder, 2011]. It results that the work applied to set the system in motion is exclusively due to inertial effects (and friction, if relevant), i.e., an external force applied to a statically balanced system is reflected exclusively as acceleration.

4.1.1 Precedents

The idea of static balancing is not new [Herder, 2001], as counterweighting was already used in ancient Greece's mechane in theaters, for instance. In those systems, a lever is used to equalize the forces between two different masses, i.e., balancing is obtained with a weight-to-weight method. Alternatively, spring-to-weight balancing was proposed in 1932, with the Anglepoise lamp, in which springs are used to balance the mass of a desk lamp in all its allowed deployments. A different spring-to-weight balancer was proposed in 1939 [Ostler and Zwick, 1939], in which the force of a linear spring is used to equalize the force of a mass trough a spiral-shaped pulley.

An altogether different approach was proposed in [Wilkes, 1969], with the redistribution of strain over a thin flexible strip. The product, known as Rolamite, can provide a wide range of force-deflection behaviors, including static balancing.

4.1.2 Perspectives

Different perspectives on static balancing of mechanisms can be derived, all direct consequences of the definition.

The first relies on obtaining a motion for which the potential energy remains constant. [Radaelli et al., 2011] showed the design of a statically balanced mechanism with torsion springs designed through this perspective.

A different possibility is to focus on the derivative of the potential energy with respect to displacement: the overall internal forces of the system should sum (vectorially) to zero. This perspective was extensively discussed in [Herder, 2001], with a force-directed design leading to a basic balancer and a set of modification rules. A company called Intespring has been using this perspective to develop methods to balance systems of different weights [van Dorsser et al., 2007], including mechanisms that are self-adjustable to different weights [Barents et al., 2009, Wisse et al., 2009].

Taking the second derivative of potential energy, stiffness can be analyzed. This perspective consists of designing systems with zero stiffness and in equilibrium. The latter condition separates statically balanced from constant force mechanisms. [Schenk et al., 2007] varied the prestress level in order to obtain null eigenvalues of the stiffness matrix describing a tensegrity structure. Similarly, for a specific prestress level, [Guest et al., 2011] obtained an elastic shell capable of energy-free (quasi-static) motion for a constant curvature.

Still aiming at obtain zero stiffness, [Tolou et al., 2010] proposed to connect mechanisms with opposed force-deflection behaviors in parallel, essentially summing a positive to a negative constant stiffness. Different embodiments have been designed, connecting: two shifted bistable beams [Tolou et al., 2011], a bistable to a linear spring and a weight [Dunning, 2011, Tolou et al., 2012b], opposed constant force mechanisms [Tolou et al., 2012a] and a bistable to a shifted linear spring [Pluimers et al., 2012].

Finally, from a structural point of view, neutral stability is desired. On the theoretical ground, [Tarnai, 2003] analyzed a second order system, varying the parameters in order to turn to zero the determinant of the Hessian composed of the second derivatives of the potential energy with respect to the coordinate system. [Gallego and Herder, 2011] stated that neutral stability can be understood practically as a permanent buckling state throughout the range of motion.

All perspectives are closely related, as a statically balanced system can be understood and analyzed from each of them. However, at the conceptual design phase, different perspectives might lead to radically different embodiments. Even in their mathematical framework, the perspectives proposed by Tarnai and Schenk, for instance, result both at ensuring that the potential energy Hessian does not have full rank.

4.1.3 Approaches

There is no clear design method for statically balanced systems. So far, at least three distinct approaches seem to coexist: aiming directly at constant potential energy, focusing on strain redistribution between sub-systems or relying on a specific geometry to impose the matching of the forces.

4.2 Dynamic behavior of a statically balanced damped system

The literature of static balancing typically does not explore its dynamic properties. The application field of vibration isolation is, indeed, very related to static balancing, as there are embodiments that use negative stiffness similarly to the perspective of [Tolou et al., 2010], for instance. However, safety reasons impose that vibration isolators are designed as stable systems, i.e., passive vibration isolators are essentially second order systems with a very low resonance frequency [Platus, 1992, 1999]. Given that damping is a central aspect of energy harvesting, the dynamic behavior of a statically balanced damped system will be studied.

4.2.1 Physical model

As explained before, one of the properties of statically balanced systems is that its stiffness is zero. Thus, a physical model of a statically balanced system that converts mechanical energy into electrical is simply a mass connected to a damper. The case of direct excitation is sketched in fig. 4.1(a) and the case of base excitation is sketched in fig. 4.1(b).

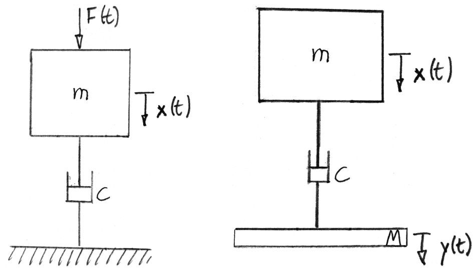

Figure 4.1: Physical models for a statically balanced damped oscillator under (a) direct excitation and (b) base excitation.

4.2.2 Frequency response

Taking the second law of Newton on those systems, they result as linear oscillators of first order. The differential equation was solved and the response was made dimensionless in analogy with the traditional definitions, with a corner frequency, defined as $\omega_c = \frac{c}{m}$, and normalizing the input frequency such that $r = \frac{\omega}{\omega_c}$.

For a direct excitation with a sinusoidal force input $F = F_0 \sin(\omega t)$, the velocity output is $\dot{x} = X_{dot} \sin(\omega t - \phi)$, such that X_{dot} and ϕ are given by eq. (4.1) and eq. (4.2), respectively. Those equations are also plotted in fig. 4.2, in the form of a Bode plot.

$$\frac{m\omega_c X_{dot}}{F_0} = \frac{1}{\sqrt{1+r^2}} \tag{4.1}$$

$$\phi = \tan^{-1}(r) \tag{4.2}$$

As seen in the plot, resonance is not present. Also, the system is completely defined by a line, in opposition to the second order system, defined by a surface dependent on input frequency and damping coefficient. Those are consequences of lowering the order of the dynamic system. Moreover, the common interpretation of the zones of influence of the spring, damper and mass, cannot be directly extended. For this simpler case, the shift in behavior is subject to the relative importance of the mass and the damping coefficient: for frequencies lower than the corner frequency, the damper does not offer great resistance and the mass moves almost freely; for frequencies higher than the corner frequency, both the damper and the mass react, resulting in lower velocities. Additionally, although the first order normalized amplitude response does not possess values larger than unity, this does not mean that large amplitude motion is not obtained, as the response is plotted for the normalized response for velocity.

For base excitation, analogously to the resonator, a transmissibility ratio – now for the velocities of the base and the proof mass – is derived and shown with the amplitude ratio in eq. (4.3) and the phase lag in eq. (4.4).

$$\frac{X_{dot}}{Y_{dot}} = T = \frac{1}{\sqrt{1+r^2}} \tag{4.3}$$

$$\lambda = \tan^{-1}(r) \tag{4.4}$$

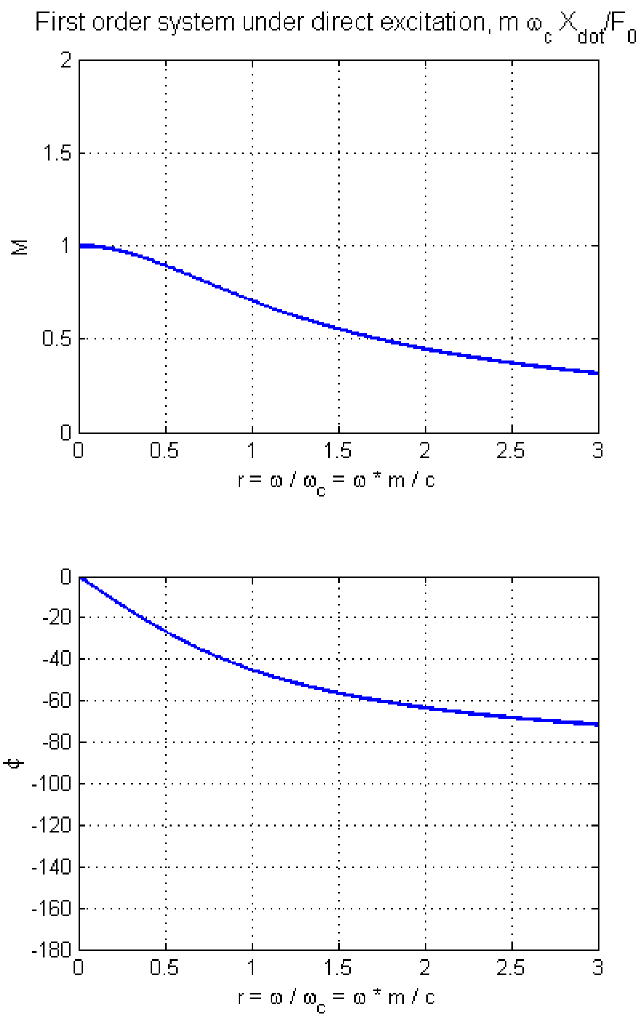

Figure 4.2: Plots of magnification and phase difference for direct excitation.

Again, this result is not best suited for energy harvesting. Aiming at analyzing the damped power, first the transfer function of the base motion to the damper relative motion ($\frac{\dot{x}-\dot{y}}{\dot{y}}$) is obtained and shown in eq. (4.5), with the amplitude, and in eq. (4.6), with the phase lag. This response is plotted in fig. 4.3.

$$\frac{X_{dot} - Y_{dot}}{X_{dot}} = \frac{Z_{dot}}{X_{dot}} = \frac{r}{\sqrt{1+r^2}} \tag{4.5}$$

$$\phi = \frac{\pi}{2} + \tan^{-1}(r) \tag{4.6}$$

Equations 3.5 and 3.6 are plotted in fig. 3.3 for different damping ratios. The general discussion carried through for the direct excitation case is valid here too.

4.2.3 Converted power

Assuming that the damping is exclusively due to the electromechanical conversion, eq. (3.7) can be used to calculate the converted power. The results are shown in eq. (4.7) for direct excitation and in eq. (4.8) for base excitation.

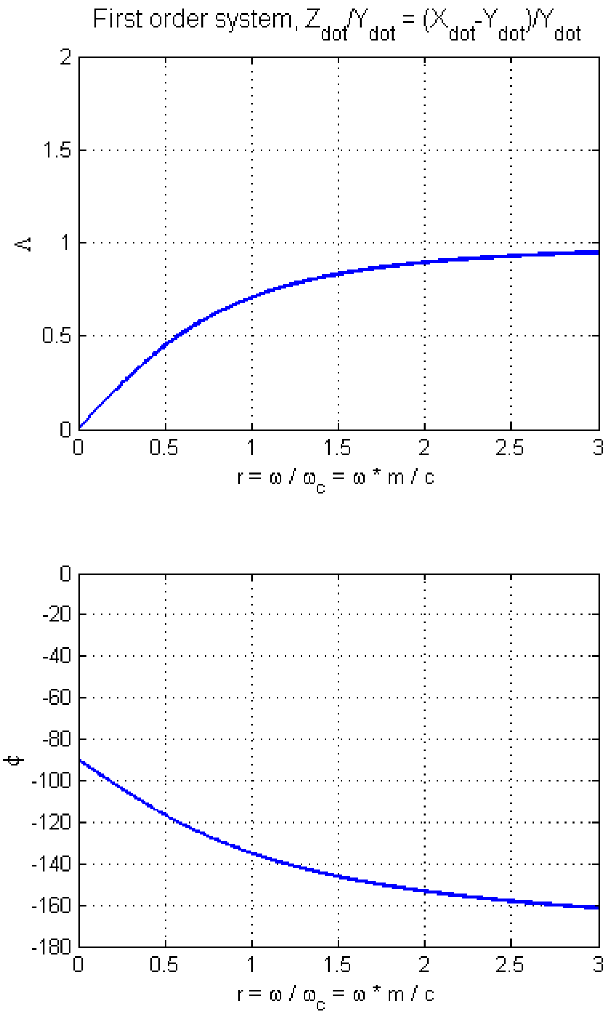

Figure 4.3: Plots of amplitude and phase difference for ratio between damper velocity and base velocity, for base excitation.

$$P_1 = \frac{F_0^2}{2m\omega_c}\frac{1}{1+r^2} \tag{4.7}$$

$$P_1 = \frac{mY_0^2\omega_c^3}{2}\frac{r^4}{1+r^2} \tag{4.8}$$

Equation 4.8 is plotted in fig. 4.4, with the damped power as a function of the damping coefficient, c, and the input frequency, f, in Hz. The numerical values of the damped power are dependent on the proof mass and the amplitude of the base motion, here 10 g and 1 mm respectively.

Again, the plot of fig. 4.4 is subject to a trend. This happens as the greater power for larger frequencies is a property of the input vibration, and not of the oscillator. Indeed, taking the partial derivative of damped power with respect to the input frequency, as shown in eq. (4.9), gives a positive function for an input frequency larger than zero, i.e., the power is strictly increasing with respect to the frequency of the input vibration.

$$\frac{\partial P_1}{\partial \omega} = \frac{2m^2Y_0^2c\omega^3\left(2c^2+m^2\omega^2\right)}{\left(c^2+m^2\omega^2\right)^2} \geq 0 \tag{4.9}$$

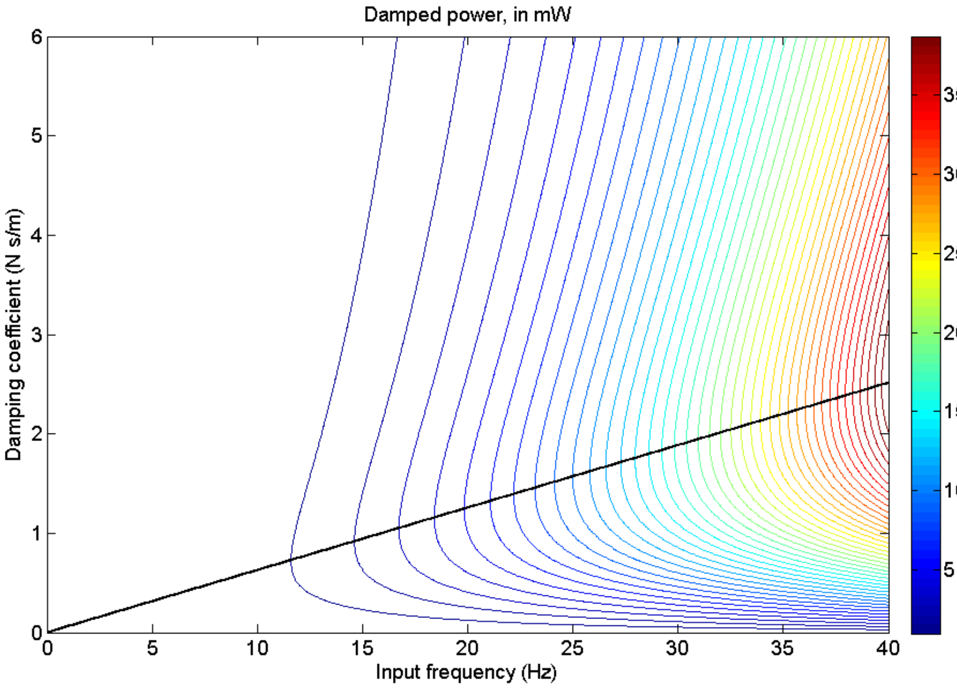

Figure 4.4: Damped power as function of the damping coefficient and the input frequency, for a statically balanced damped oscillator under base excitation. The black line is an optimal condition for damped power.

This trend can be partially removed using the same normalization as for the resonant oscillator, i.e., taking the ratio between the damped power and the power related to the proof mass and the vibration input, $mY_0^2\omega^3$. The plot shown in fig. 4.5 is obtained.

Both plots suggest the existence of an optimal damping. Indeed, from fig. 4.5 it can be understood that each oscillator, with a fixed damping coefficient, has an optimal input frequency vibration for energy conversion.

Optimal damping

This optimal damping turns out to be directly related to the corner frequency, as shall be shown analytically in this section. Taking the first derivative of the damped power, given by equation eq. (4.8), with respect to the damping coefficient, eq. (4.10) is obtained.

$$\begin{gathered}\frac{\partial P_1}{\partial c} = \frac{m^2Y_0^2\omega^4}{2}\frac{m^2\omega^2-c^2}{(m^2\omega^2+c^2)^2}\\ \therefore \frac{\partial P_1}{\partial c} = 0 \iff c = m\omega\end{gathered} \tag{4.10}$$

Equation 4.10 shows the existence of extrema. Taking the second partial derivative with respect to the same variable shall define whether the extrema are maxima. This is carried through in eq. (4.11).

$$\begin{gathered}\frac{\partial^2 P_1}{\partial c^2} = m^2Y_0^2\omega^4\frac{c\left(c^2-3m^2\omega^2\right)}{(c^2+m^2\omega^2)^3}\\ \therefore \frac{\partial^2 P_1}{\partial c^2}\left(c = m\omega\right) < 0\end{gathered} \tag{4.11}$$

Thus, the condition for optimality is defined by eq. (3.12), which is plotted in both fig. 3.4 and fig. 4.5 as dark bold lines.

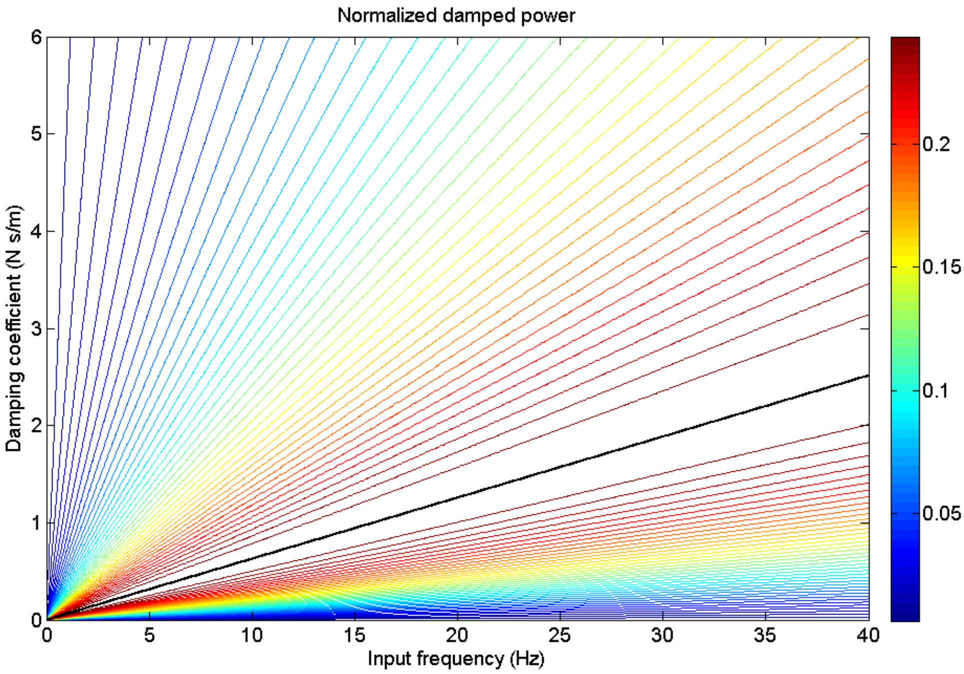

Figure 4.5: Normalized damped power as function of the damping coefficient and the input frequency, for a statically balanced damped oscillator under base excitation. The black line is an optimal condition for damped power.

4.3 Discussion and conclusion

An important remark is that the response of the statically balanced system, obtained from basic equations, turns out to be a limit case of the response of the second order system for null stiffness. This observation allows a direct comparison of the damped power for the resonant and the statically balanced oscillators. Subtracting the non-normalized expansions of eq. (3.9) and eq. (4.8), the condition shown in eq. (4.12). This result applies for both direct and base excitation.

$$P_1 > P_2 \iff \omega < \frac{\sqrt{2}}{2}\omega_n \tag{4.12}$$

This suggests that a statically balanced oscillator is better suited for vibrations with input frequency close to zero. However, those signals have less energy. Moreover, given that the stiffness can be tuned even up to zero, eq. (4.12) has little sense, as it is preferable then to tune the stiffness to match the resonance frequency to the vibration frequency, i.e., resonance is still preferred in energy harvesting.

Even though the statically balanced oscillator possesses no resonant frequency, there is still a preferred frequency for energy harvesting. This is the corner frequency, given by the ratio of the damping coefficient over the mass, and is the frequency in which the vibration power is damped the most effectively.

If statically balanced damped oscillators cannot be used to design better energy harvesters, they can be used to design more compact seismometers. Seismometers traditionally use large masses, in order to be able to measure low frequencies [Pérez and González, 1999]. Statically balanced oscillators can provide a wider band of measurement (region for which the amplitude plot of fig. 4.3 equals unity) with a much more compact system. Moreover, the facts that the damped power is strictly increasing and that the system is linear allows a full mapping of the frequency range.

Bibliography

Rogier Barents, Mark Schenk, Wouter D. van Dorsser, Boudewijn M. Wisse, and Just L. Herder. Spring-to-spring balancing as energy-free adjustment method in gravity equilibrators. In *ASME 2009 International Design Engineering Technical Conferences & Computers and Information in Engineering Conference IDETC/CIE 2009*, San Diego-CA, USA, Sept. 2009.

A. G. Dunning. Design of a zero stiffness six degrees of freedom compliant precision stage. Master's thesis, Delft University of Technology, 2011.

Juan A. Gallego and Just L. Herder. Buckling as a new perspective on static balancing of mechanisms. In *13th World Congress in Mechanism and Machine Science*, Guanajuato, México, Jun. 2011.

Simon D. Guest, Elizbar Kebadze, and Sergio Pellegrino. A zero-stiffness elastic shell structure. *Journal of Mechanics of Materials and Structures*, 6(1-4):203–212, 2011.

Just L. Herder. *Energy-free Systems: theory, conception, and design of statically balanced spring mechanisms*. PhD thesis, Delft University of Technology, Delft, The Netherlands, 2001.

Joseph Ostler and Kurt Zwick. Power equalizing device, 1939.

Roque Calero Pérez and José Antonio Carta González. *Fundamentos de mecanismos y máquinas para ingenieros*. McGraw-Hill, 1999.

David L. Platus. Negative-stiffness-mechanism vibration isolation systems. In Colin G. Gordon, editor, *Vibration Control in Microelectronics, Optics, and Metrology*, volume 1619, pages 44–54. SPIE, 1992.

David L. Platus. Negative-stiffness-mechanism vibration isolation systems. In Eddy A. Derby, Colin G. Gordon, Daniel Vukobratovich, Paul R. Yoder, Jr., and Carl H. Zweben, editors, *Optomechanical Engineering and Vibration Control*, volume 3786, pages 98–105. SPIE, 1999.

Pieter Pluimers, Nima Tolou, Brian D. Jensen, Larry Howell, and Just L. Herder. A compliant on/off connection mechanism for preloading statically balanced compliant mechanisms. In *Proceedings of the ASME 2012 International Design Engineering Technical Conferences & Computers and Information in Engineering Conference IDETC/CIE 2012*, Chicago-IL, USA, Aug. 2012.

Giuseppe Radaelli, Juan A. Gallego, and Just L. Herder. An energy approach to static balancing of systems with torsion stiffness. *Journal of Mechanical Design*, 133(9):091006, Sept. 2011.

M. Schenk, S.D. Guest, and J.L. Herder. Zero stiffness tensegrity structures. *International Journal of Solids and Structures*, 44(20):6569 – 6583, 2007. ISSN 0020-7683.

T. Tarnai. Zero stiffness elastic structures. *International Journal of Mechanical Sciences*, 45:425–431, 2003.

N. Tolou, P. J. Pluimers, B. D. Jensen, S. Magleby, L. L. Howell, and J. L. Herder. Near-zero-stiffness linear motion stage with high orthogonal and out-of-plane stiffness. In *DSPE 2012*, Deurne, The Netherlands, Sept. 2012a.

Nima Tolou, Vincent A. Henneken, and Just L. Herder. Statically balanced compliant micro mechanisms (sb-mems): Concepts and simulation. *ASME Conference Proceedings*, 2010(44106):447–454, 2010.

Nima Tolou, Pablo Estevez, and Just L. Herder. Collinear-type statically balanced compliant micro mechanisms (sb-mems) experimental comparison between pre-curved and straight beams. In *Proceedings of the ASME 2011 International Design Engineering Technical Conferences & Computers and Information in Engineering Conference IDETC/CIE 2011*, Washington-DC, USA, Aug. 2011.

Nima Tolou, Pieter Pluimers, Brian D. Jensen, Spencer Magleby, Larry Howell, and Just L. Herder. Constant force micro mechanism out of carbon nanotube forest. In *Proceedings of the 12th euspen International Conference*, Stockholm, Sweden, Jun 2012b.

Wouter D. van Dorsser, Just L. Herder, Boudewijn M. Wisse, and Rogier Barents. Balancing device, 2007.

Donald F. Wilkes. Roller-band devices, 1969.

Boudewijn M. Wisse, Rogier Barents, Wouter D. van Dorsser, and Just L. Herder. Apparatus for exercising a force on a load, 2009.

Chapter 5

Statically balanced frequency up-conversion energy harvester

Given that a statically balanced damped oscillator is not good for energy harvesting, another design paradigm had to be conceived. This chapter shall first introduce this newly conceived paradigm, along with a comparative discussion with the existing designs that are the closest to it. Next, a simple system of concentrated parameters is modeled, providing a qualitative analysis of the model performance and a sensitivity analysis for its parameters. Finally, three different concepts are proposed for the statically balanced suspension, being one of those innovative.

5.1 Design paradigm

Conceptually, it is hypothesized that a statically balanced mass – with no damping, in opposition to the previous chapter – should present a dynamic response similar to that of a mass under no influence of a gravity field. A linear model for this system is a memoryless model, i.e., a static system. For a statically balanced non-damped system under base excitation, intuition suggests that the mass should remain still for vibrations of all sort of frequencies and move only if the amplitude of the input vibration is larger than the statically balanced stroke. Thus, taking damping away from the static balanced system should provide an oscillator capable of using integrally the linear momentum composed of the product of the proof mass and the relative velocity between the proof mass and the base.

Moreover, the behavior of resonators in energy harvesting is fairly well understood. As discussed previously, those classic oscillators operate best if allowed to resonate. Shifting the electromechanical damping from the statically balanced system to a secondary resonator seems, thus, to allow a combination of the best properties of both statically balanced systems and damped resonators. The proposed design paradigm can be described as two part system, as a statically balanced non-damped system that provides an impulse, while reaching its ends-of-stroke, to a secondary resonator, which converts mechanical power into electrical.

This basic idea of separating the electromechanical damping from the main oscillator is already present with frequency up-conversion energy harvesters. However, the use of statically balanced oscillators on the form it is being proposed is, to the author's knowledge, innovative and seems to have potential for harvesting vibrations of large amplitude, such as human motion, a current technical challenge.

Of the two existing sorts of frequency up-conversion harvesters, the one based on bistable oscillators impose challenges related to the complex nonlinear dynamics. In contrast, a statically balanced frequency up-conversion energy harvester would allow the harvesting of vibration inputs that would provide intra-well motion for the bistable oscillator – not harvested for bistable frequency up-conversion. It could be hypothesized that the bistable design benefits from the negative stiffness between the stable equilibria positions, i.e., that if inter-well motion takes place, it gains momentum from the potential energy field.

However, the potential energy is a conservative field: the energy recovered after the unstable equilibrium is passed had to be spent beforehand.

The second class that uses frequency up-conversion is the one of scrape-through oscillators. In principle, any energy landscape is allowed for the main oscillator, i.e., even a statically balanced scrape-through energy harvester can be designed. As a matter of fact, despite the fact that they do not claim it, [Rastegar et al., 2006] showed a sketch, reproduced here in fig. 5.1, that can be understood as being statically balanced.

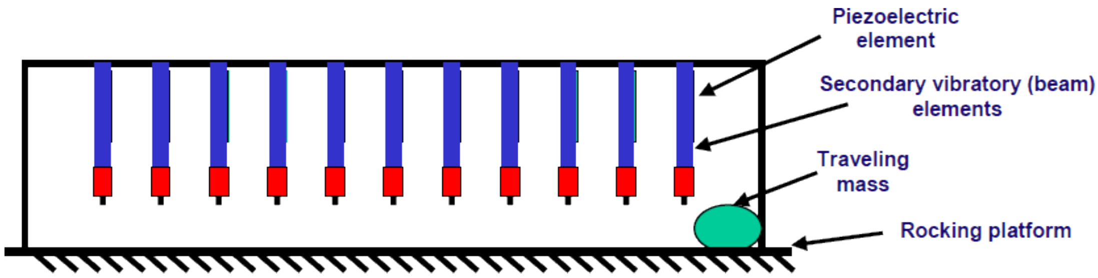

Figure 5.1: A sketch presented for scrape-through frequency up-conversion energy harvesting. It results from the flat shape of the rocking platform that the main oscillator is statically balanced. Reproduced from [Rastegar et al., 2006].

However, scrape-through oscillators are not well suited for smaller scales, as decreasing the free path, i.e., the length between two consecutive secondary resonators, leads to less energy harvested. This happens as the kinetic energy of the proof mass is proportional to the momentum squared and the momentum acquired by the proof mass depends on the allowed travel range. Thus, a conceptual comparison with the existing alternatives suggests that a statically balanced frequency up-conversion energy harvester in which the secondary resonators are triggered only at the ends-of-stroke can provide more effective small energy harvesters for large amplitude input vibrations.

5.2 Dynamic behavior

This section will present the dynamic characteristics of this new design paradigm. First a lumped parameter model is proposed, with the derivation of the governing equations. Then, this model is implemented numerically in Matlab. Finally, a sensitivity analysis for the different parameters that define the model is presented.

5.2.1 Model

The simplest model capable of modeling the desired behavior is conceived with concentrated parameters as shown in fig. 5.2. A spring and a damper connect a proof mass, m_1, to the mass of the main oscillator, m. A statically balanced suspension connects the main oscillator mass to the base, M.

Defining variables for the relative position of the oscillators' masses according to eq. (5.1) and eq. (5.2), a system of equations that describe the system's dynamics can be derived from basic laws.

$$z = x - y \tag{5.1}$$
$$z_1 = x_1 - x \tag{5.2}$$

The overall system is of fourth order, with two equations derived with Newton's Second Law, for the masses m and $m1$, and the derivatives of the two constraint equations shown above. The system results

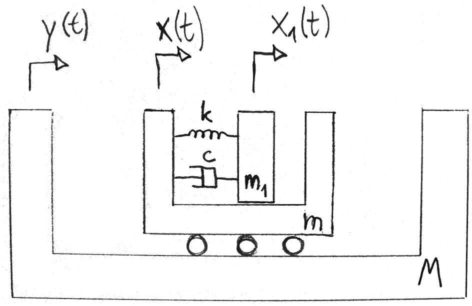

Figure 5.2: Simple physical model for statically balanced frequency up-conversion. The statically balanced suspension is presented schematically with rollers.

as shown in eq. (5.3) and relates the state variables, z_1, p_1, z, p, to the input variable, $\dot{y}$, that describes the velocity of the base.

$$\begin{cases} \dot{z}_1 = \frac{1}{m_1}p_1 - \frac{1}{m}p \\ \dot{p}_1 = -kz_1 - \frac{c}{m_1}p_1 + \frac{c}{m}p \\ \dot{z} = \frac{1}{m}p - \dot{y} \\ \dot{p} = kz_1 + \frac{c}{m_1}p_1 - \frac{c}{m}p \end{cases} \tag{5.3}$$

Equation 5.3 can also be rewritten explicitly as a state-space model, according to eq. (5.4).

$$\begin{bmatrix} \dot{z}_1 \\ \dot{p}_1 \\ \dot{z} \\ \dot{p} \end{bmatrix} = \begin{bmatrix} 0 & \frac{1}{m_1} & 0 & -\frac{1}{m} \\ -k & -\frac{c}{m_1} & 0 & \frac{c}{m} \\ 0 & 0 & 0 & \frac{1}{m} \\ k & \frac{c}{m_1} & 0 & -\frac{c}{m} \end{bmatrix} \begin{bmatrix} z_1 \\ p_1 \\ z \\ p \end{bmatrix} + \begin{bmatrix} 0 \\ 0 \\ -1 \\ 0 \end{bmatrix} \dot{y} \tag{5.4}$$

Given that there is a limited available stroke, $2L_{tot}$, conditions should be enforced for when each of the two masses reaches its ends-of-stroke. For the mass of the secondary oscillator, this condition can be modeled as a stiffening effect, according to a model linear by parts, shown in eq. (5.5). L_1 is the maximum allowed amplitude of motion for the internal proof mass and k_{low} and k_{high} are two constant values of stiffness.

$$k = \begin{cases} k_{low} & \text{for } L_1 - |z_1| \geq 0 \\ k_{high} & \text{for } L_1 - |z_1| < 0 \end{cases} \tag{5.5}$$

As for the main oscillator, there is a collision when the maximum allowed amplitude of motion, L, is reached. A simple model, rigorously valid for the central impact of two spheres [Hoppmann II, 2002], is taken as a first approximation. The model is shown in equations 5.6 and 5.7, as function of two parameters: the coefficient of restitution, e, and the outer mass ratio, $\lambda = \frac{m}{M}$.

$$(M\dot{y})_{new} = \frac{1 - e\lambda}{1 + \lambda} M\dot{y} + \frac{1 + e}{1 + \lambda} p \tag{5.6}$$

$$(p)_{new} = \frac{\lambda(1 + e)}{1 + \lambda} M\dot{y} + \frac{\lambda - e}{1 + \lambda} p \tag{5.7}$$

Another simplifying assumption, that the motion of the base is not affected by the dynamics of the energy harvester, determines that eq. (5.6) is ignored. An equivalent formulation of this hypothesis is to state that the energy that the base is capable of supplying is infinite, i.e., that the base is actively compensating for the power harvested at all instants.

In order to solve this system of differential equations, it should be realized that the equations 5.5 and 5.7 impose that a purely analytical solution is not possible. Those equations impose that the solution is dependent both on the frequency and the amplitude of the input vibration, i.e., that the system is nonlinear. Thus, a MatLab script was conceived in order to obtain a numerical solution for the system.

5.2.2 Numerical implementation

All the simulations presented here are for a vibration input of 1 Hz and 20 mm of amplitude of motion and a total mass for the harvester $m_{tot} = m + m_1 = 8$ g.

Matlab numerical integration algorithms

As a first approach, MatLab algorithms for solving ordinary differential equations were used. However, even using very tight tolerances (10^{-15} for absolute tolerance and 10^{-10} for the relative one), different algorithms provided different outcomes for the average damped power. Table 5.1 summarizes the different results obtained for a simulation of 5 seconds, with a natural frequency $f_n = 3000$ Hz, impact conditions of the outer mass ratio $\lambda = 10^{-3}$ and coefficient of restitution $e = 0.95$, total available stroke of $2L_{tot} = 60$ mm, stroke ratio $L^* = \frac{L_1}{L} = 5$ and inner mass ratio $m^* = \frac{m_1}{m} = 0.2$.

Table 5.1: Different results obtained using different MatLab solvers.

MatLab command	Average power (μW)
ode45	609.20
ode23	804.22
ode113	*
ode15s	7245.45
ode23s	677.39
ode23t	386.75
ode23tb	326.65

* omitted, as plot of evolution of z presents numerical instability (wiggles), a mathematical solution not possible in physical systems

Given the large disagreement among the solvers, none of them will be used. Instead, numerical integrations algorithms of fixed time step were implemented.

Implementation of numerical solvers

Following the recommendation of [Cellier and Kofman, 2006], both the forward Euler and the backward Euler algorithms were implemented. This procedure of simulating the system twice ensures that the results – if they agree between each other – are true to the physical model.

The forward Euler is a first order method in which the state value for the next time step is calculated with a Taylor approximation of the derivative at the current time step, according to eq. (5.8). This algorithm is fast but might be unstable.

$$x_{t+1} = x_t + \Delta t \, \dot{x}_t \tag{5.8}$$

On the other hand, in the backward Euler the state value for the next time step is calculated with the derivative at the next time step. This method, shown in eq. (5.9), possesses an algebraic loop – situation in which the incognita is calculated as a function of itself. For the case in which the derivative is a linear function of the state, solving this algebraic loop demands a matrix inversion, reason for which this algorithm is slower, but intrinsically (numerically) stable.

$$x_{t+1} = x_t + \Delta t\, \dot{x}_{t+1} \tag{5.9}$$

Convergence analysis

There are three sources of errors while using numerical methods and the three of them should be addressed. The first, named global relative error, is set to be $5 \cdot 10^{-3}$. This is calculated according to eq. (5.10) where $P(n)$ is the average damped power calculated with n time steps. The second error source, called roundoff error is of the order of 10^{-15}, as a 64-bit system was used and Matlab uses double precision in its calculations by default. Using single precision – of the order 10^{-6} – would provide faster calculations, but another software should be used. Finally, the accumulation error should not be relevant if the time step is small enough to stabilize the numerical solver.

$$\text{relative error}(n) = \frac{|P(n) - P(n/2)|}{P(n/2)} \tag{5.10}$$

Using the same parameters as in the previous subsection, the number of time steps is doubled until the determined level of precision is reached. The results of this procedure are shown in fig. 5.3.

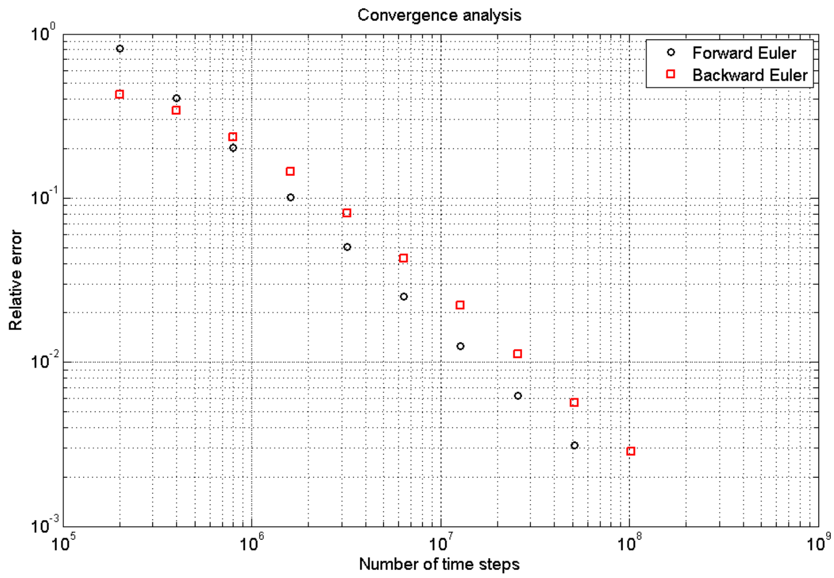

Figure 5.3: Convergence analysis for forward and backward Euler. The number of time steps is increased until the relative error reaches less than 0.5%.

In order to tie this discussion on numerical methods, another plot is shown in fig. 5.4. Here, the average damped power is plotted for each number of time steps tested. It is seen that the results agree up to precision level determined, allowing the conclusion that the numerical implementation is faithful to physical model.

Sensitivity analysis

The validation of the numerical implementation, with the convergence analysis was executed only for the parameter values stated above. Different values for the parameters might lead the numerical method to

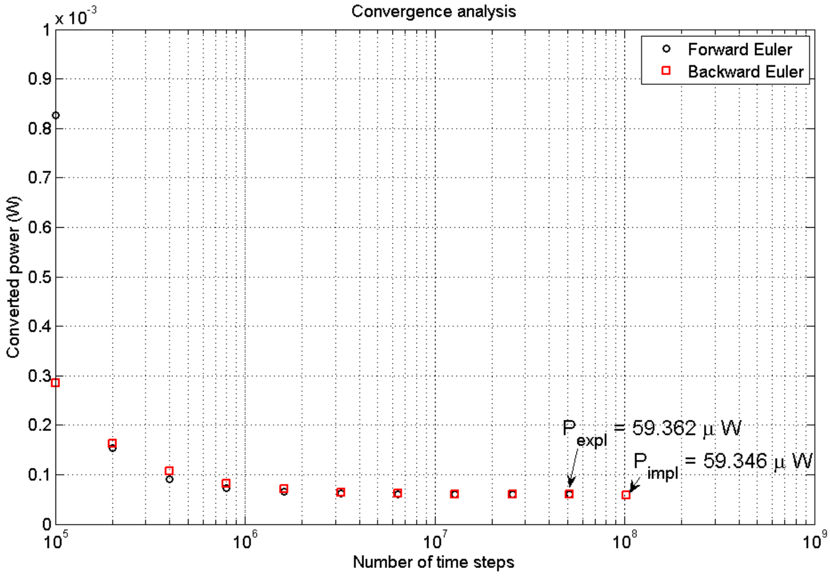

Figure 5.4: Convergence analysis for forward and backward Euler. The average damped power calculated as a function of the number of time steps.

have a lower convergence rate, i.e., for different parameters more time steps might be necessary. In that sense, it is not assured that this sensitivity analysis provides precise quantification of the optimal values. Nevertheless, a fair qualitative analysis of the design parameters is presented in this section, with trends for the damped power.

The results presented here were obtained with a forward Euler with $5.12{\cdot}10^7$ time steps for 5 s of simulation time. Each parameter is studied separately, keeping the other parameters constant. The standard values for the parameters are $f_n = 1000$ Hz for the natural frequency, $\lambda = 10^{-3}$ for the outer mass ratio, $e = 0.8$ for the coefficient of restitution, $2L_{tot} = 40$ mm for the total available stroke, $L^* = \frac{L_1}{L} = 1$ for the stroke ratio and $m^* = \frac{m_1}{m} = 1$ for the inner mass ratio.

The parameter with the greatest influence on the damped power is the total available stroke. Figure 5.5a shows the damped power as a function of the ratio between the total available stroke and the amplitude of the base motion, $\frac{L_{tot}}{A}$. It results that the damped power increases for larger strokes, up to a level slightly over three times the amplitude of motion of the input vibration. For even larger strokes, the damped power experiences a dramatic drop, as collisions do not take place.

With the second greatest influence, the ratio between the inner strokes, $L^* = \frac{L_1}{L}$, defines the damped power as shown in fig. 5.5b. It can be seen that, if L and L_1 compete for the total available stroke, larger values should be provided for the statically balanced stroke, L.

Next, the damped power is influenced by the inner mass ratio $m^* = \frac{m_1}{m}$ as shown in fig. 5.5c. A significant drop occurs for values close to two. Further investigation is required to understand the reasons for this effect.

The final parameter with a large influence on the damped power is the coefficient of restitution, e. Figure 5.5d shows that the harvester should be designed aiming at elastic collisions.

With a lower influence, the ratio between the base mass and the intermediate mass, λ, can be used to determine the total mass of the harvester as a function of the mass of the base. According to fig. 5.5e, there is minimal variation on the damped power for ratios lower than 10^{-3}.

Finally, the least relevant parameter results to be the natural frequency of the secondary oscillator, ω_n. Figure 5.5f shows a relative variation of less than 1% throughout the range tested.

If on one hand, the numerical solution allows the analysis of optimal design parameters, comparing different numerical scenarios among themselves, the results for the harvested power should not be analyzed

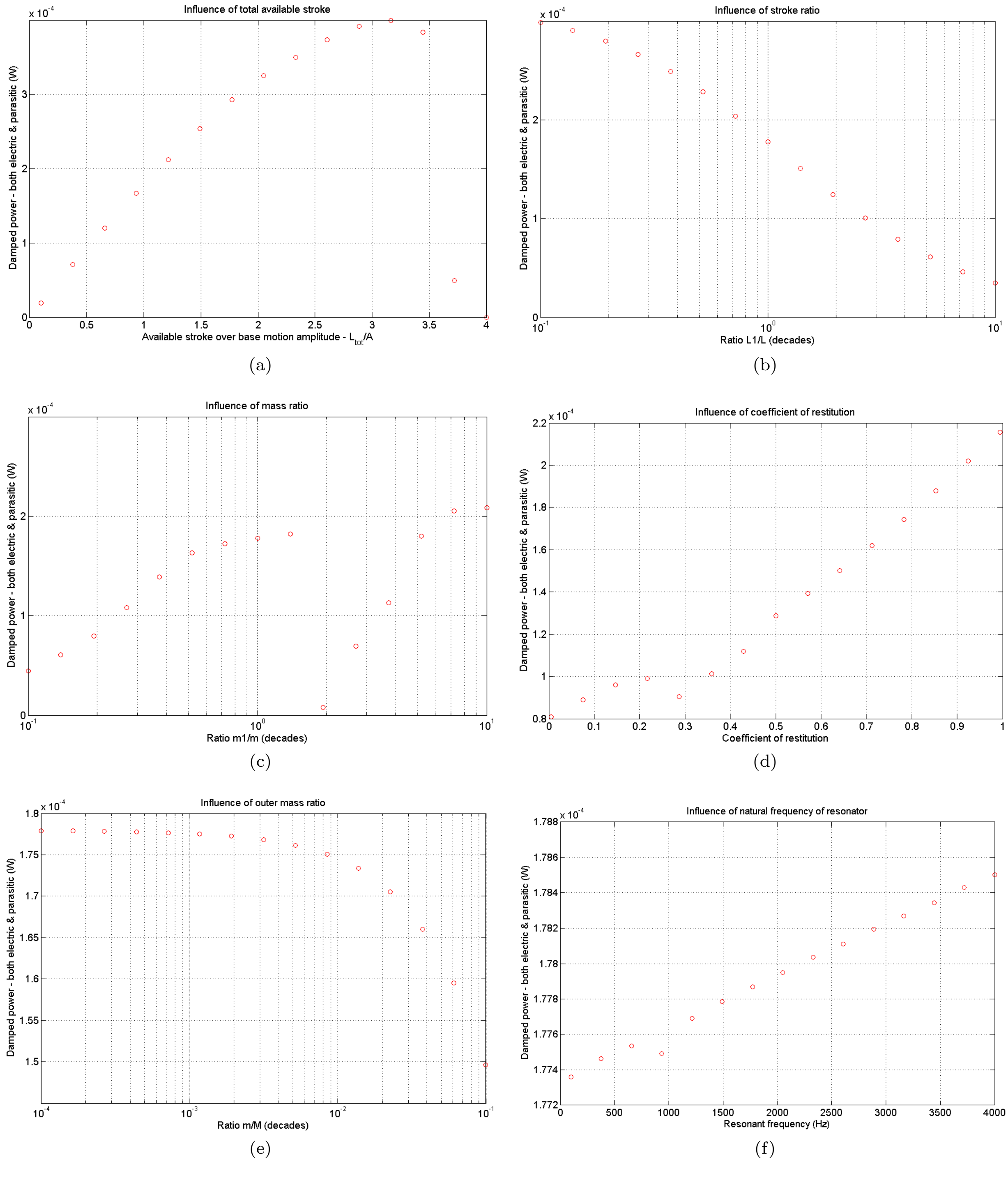

Figure 5.5: Sensitivity analysis for all parameters on the damped power, with the influences of: (a) the ratio of total stroke over the amplitude of the base motion, (b) the stroke ratio, (c) the inner mass ratio, (d) the coefficient of restitution, (e) the outer mass ratio and (f) the natural frequency of the secondary oscillator.

quantitatively, for two main reasons. The first is related to the modeling itself, as the obtained model relies on hypotheses that are valid for a certain range of conditions. Secondly, numerical integration always leads to the sum of errors, as discussed before.

As much as those issues are addressed, the results should not be considered as if they could provide a maximum limit for harvested power, but actually as an indicator of the order of magnitude that can be achieved with this architecture. Additionally, a multi-parameter optimization was not performed, i.e., the point in the parameter space selected for the indication of maximum power might be close to a local maximum, different than the global one.

Nevertheless, results are presented for a total stroke L_{tot} = 34.7 mm, a stroke ratio L^* = .1, a mass ratio m^* = 4, a perfect elastic collision e = 1, an outer mass ratio $\lambda = 10^{-4}$ and a natural frequency f_n = 2000 Hz. A damped power of 517.6 μW is obtained. Using the normalization with respect to the harvester's mass and the test conditions proposed in eq. (11) of the paper of section 3.4, a value of 65.22% is obtained. This result is summarized in tab. 5.2.

Table 5.2: Indication of order of magnitude for the maximum achievable damped power.

Harvester total mass	8 g
Vibration frequency	1 Hz
Vibration amplitude	20 mm
Damped power	517.6 μW
Normalized damped power	65.22 %

5.3 Statically balanced suspension conceptual design

As energy harvesters are small systems, the use of compliant mechanisms seems better suited, as they provide the opportunity of designing high precision, compact mechanisms with reduced assembly costs and lower need of maintenance [Gallego and Herder, 2009]. Moreover, for the case of energy harvesters, the elimination of backlash eliminates the nonlinearity associated with hysteresis, allowing a smoother dynamic behavior. Thus, it is set as a goal to design a system at least partially compliant.

However, the design of statically balanced compliant mechanisms is not evident and most often results in an unperfect balancing, due to the nonlinearities and manufacturing uncertainty intrinsic to this type of mechanisms. Thus, more attention shall be given to the design of the statically balanced suspension.

For that purpose, three different concepts are proposed, with two variations for each of them. A comparison among them and discussion are followed by the concept selection. Finally, a finite element model is developed for the chosen concept.

5.3.1 Selection criteria

Three criteria are defined in order to evaluate the alternative designs that shall be presented. The first and most important one is defined as balancing quality. Any deviation from the statically balanced behavior shall lead either to a linear oscillator with low resonant frequency or to a weakly bistable mechanism, both changing qualitatively the dynamic behavior of the system. Of the two deviations, the one towards bistability is preferred, as the potential energy landscape of the linear system slows down the oscillator while it approaches the stoppers.

Next, the separation among the eigenfrequencies is considered. It is important that the system oscillates in a single mode, while excited with large amplitude low frequency vibrations. In order to achieve that, the other vibration modes should be of high resonant frequency.

Finally, the compactness of the system is evaluated. Given that space is limited, suspensions with a large statically balanced stroke and a small overall size should be privileged.

5.3.2 Concept 1 – Rolamite

The first concept is based on the Rolamite [Wilkes, 1969]. Here, the main oscillator is a mass suspended by two flexible strips partially rolled. Different force deflection behaviors can be achieved, depending on the width of the strips: a constant width provides a statically balanced mechanism and a width that varies linearly provides a constant force.

This principle can be explained looking at the strain energy stored in the strips. For the statically balanced case, the constant width implies that no work is needed to (quasi-statically) move the system and the strain is redistributed throughout the length of the strips. For the strip with linearly increasing width, work needs to be executed into the system and the constant force level depends on the rate of increase of the width with respect to the length of the strip.

From the flexibility of Rolamite, it results that this principle can be applied for harvesting energy both in the direction of gravity and perpendicularly to it, leading to two possible variations discussed next.

Fist variation

The first variation presented is for harvesting motion on the vertical direction. The constant force generated by the Rolamite compensates the weight of the mechanism, resulting in a statically balanced system. The ends-of-stroke are defined by the contact of the central mass with two other masses, clamped to the base. When the main oscillator hits the ends-of-stroke, an impulse is transmitted to the secondary oscillators. The electromechanical conversion of energy occurs in this secondary oscillator, either using piezoelectric or electromagnetic conversion. A possible embodiment is shown in fig. 5.6. The secondary oscillator is schematically represented as cantilevers, in gray.

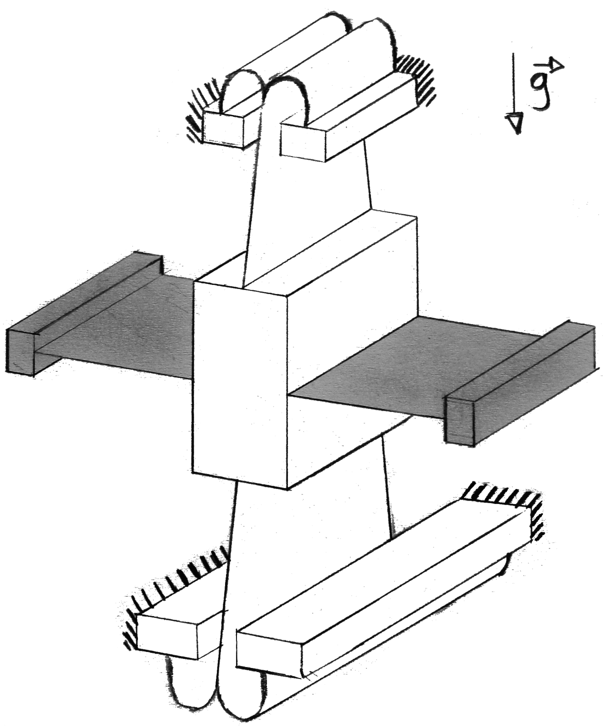

Figure 5.6: Constant force Rolamite balancing the weight of the mechanism, resulting in a statically balanced main oscillator. The secondary oscillator, in gray, is triggered when the main oscillator hits its ends-of-stroke.

Second variation

Another possibility is to use strip of constant width to harvest motion perpendicularly to the direction of gravity. This is shown in fig. 5.7, with gravity in the direction of the width of the Rolamite strip.

An additional variation is implemented with the connection to the secondary oscillator. The resonators, represented in gray, act here as the ends-of-stroke of the main oscillator. It results that this system is an inversion of the one presented in fig. 5.2, with the main oscillator internally to the secondary oscillators. This inversion might prove useful for applications such as powering nodes for structural monitoring, as the energy harvesters are physically close to sensitive vibration sensors. It is thus preferable that the internal collisions reflect back to the base in a single frequency than in a wide range of frequencies.

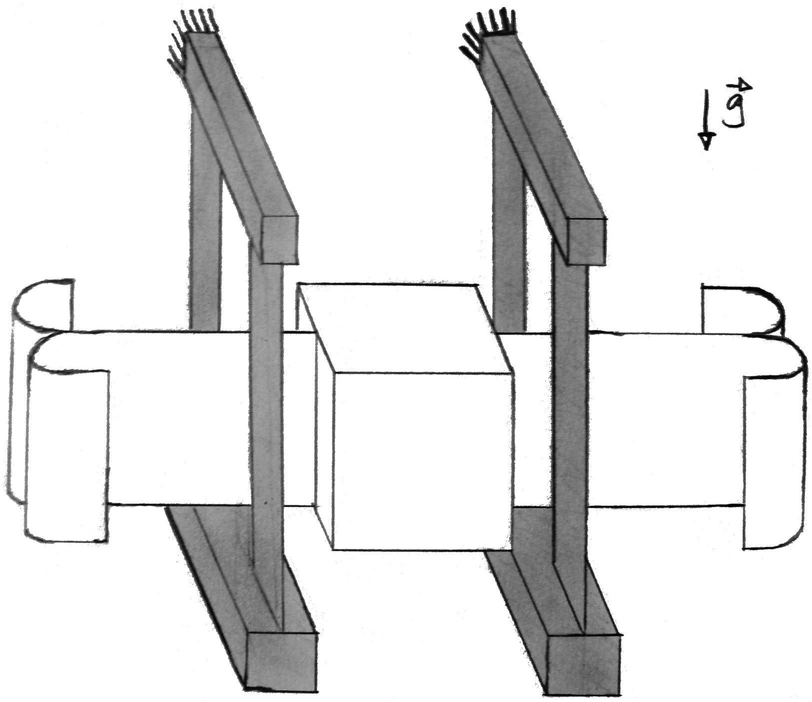

Figure 5.7: Statically balanced Rolamite as the suspension for the main oscillator. The secondary oscillator, in gray, is triggered to oscillate directly by the main oscillator.

The presented variations on the positioning of the secondary oscillators are also applicable to the next concepts. However, the resonators are going to be omitted from the sketches, for clarity.

5.3.3 Concept 2 – Subsystems of constant stiffness

This concept is a new embodiment based on the work of [Tolou, 2012]. It consists of obtaining a statically balanced mechanism connecting in parallel two subsystems of constant stiffness, one negative and one positive. To achieve a good balancing quality, two adjustments need to be performed: one to ensure that the stiffness of the two subsystems have the same absolute value and another to obtain the desired constant force level. For motion perpendicularly to the direction of gravity, the tuning should aim for zero force. For any other direction of motion, the system should be tuned to compensate for the weight. One advantage of this tuning *a posteriori* is that the design is more robust to manufacturing uncertainties. Two different forms are proposed for tuning this system, next.

Fist variation

The tuning possibility is schematically shown in fig. 5.8, with double ended arrows denoting length adjustments. The constant force level is achieved varying the length of the connection between the subsystems, marked as (1) in the figure. The positive stiffness is tuned varying the free length of the beams of the folded suspension, with the adjustments marked as (2).

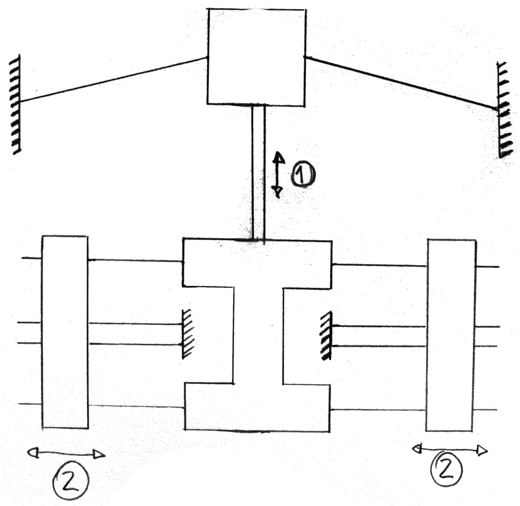

Figure 5.8: Statically balanced system obtained with the sum of two subsystems of constant stiffness. Two length adjustments are needed: (1) denotes the adjustment for the constant force level and (2) denotes the adjustment of the positive stiffness.

Second variation

Another possibility is to tune the negative stiffness. Applying a buckling force to the bistable beams is capable of doing that [Dunning et al., 2012]. This alternative to match the negative stiffness to the positive one is shown by single ended arrows, denoted by (2), in fig. 5.9.

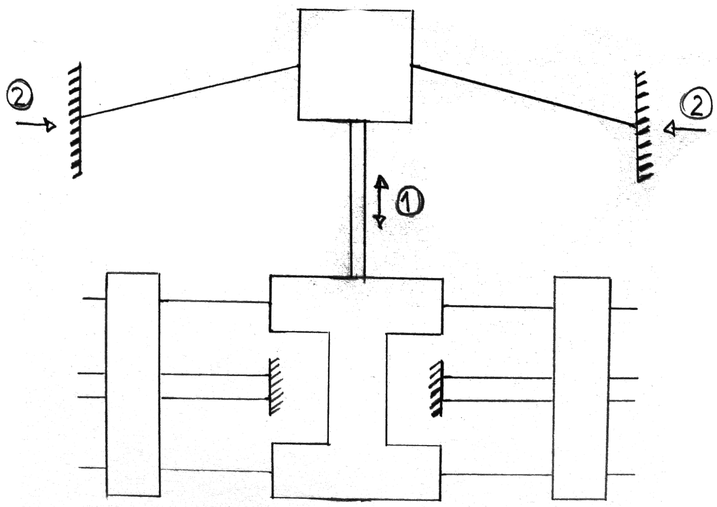

Figure 5.9: Statically balanced system obtained with the sum of two subsystems of constant stiffness. A length adjustment, for the constant force level, is denoted as (1) and a force adjustment, to match the stiffnesses and reach a constant force, is denoted by (2).

5.3.4 Concept 3 – Statically balanced folded suspension

The final concept is the development of a principle introduced in [Gallego, 2012], which is applying a constant critical load to buckle the folded suspension. The challenge for this principle – solved here in two different ways – is to ensure that a constant destabilizing force is provided in spite of the parasitic shift (motion perpendicular to the mechanism's direction of motion) of the intermediate rigid beams.

The use of buckling forces for softening mechanisms in not new. However, the approach of imposing critical load so that static balancing is achieved is new. Indeed, the only application examples of this perspective were presented in [Gallego and Herder, 2011], the paper that introduced this approach.

Fist variation

For the first embodiment, the critical load is transmitted to the folded suspension by the compression of a ring, capable of providing a buckling force in spite of rotations around its principal axis. This rolling motion can be combined with a variable thickness of the intermediate beam, such that the distance between the grounded beam (on top) and the intermediate beam is constant throughout the range of motion of the mechanism, as shown in fig. 5.10. The shape of the intermediate beam is defined by the parasitic shift of the flexible parts of the folded suspension.

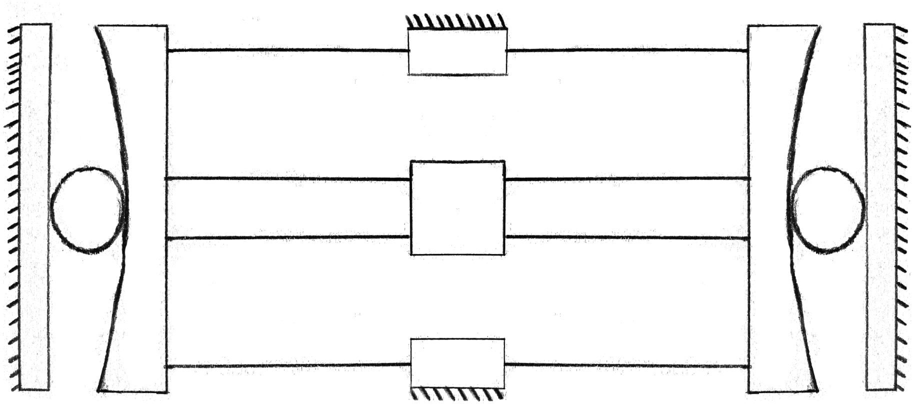

Figure 5.10: First embodiment for statically balanced folded suspension. The critical buckling load is provided by the compression of rings, which are free to rotate around their own main axis.

There are three main challenges related to this embodiment. The first is the variation of the point of application of the force, that inevitably changes and generates an uneven loading on the flexible beams of the folded suspension. Next, there is a possibility that the ring suffers a skewing motion, while operating. This can be mitigated with the use of elastic bands to ensure the positioning of the ring, such as in [Herder and Horward, 1997]. Finally, it requires a fine control of the radii of the ring, in order to control the stiffness of this subsystem and obtain the required load.

Second variation

Alternatively, this constant force can be applied using zero free-length springs, as in fig. 5.11. The proposed design can be understood as a two-layered mechanism: in the first layer is the standard folded suspension and in the second layer is a frame that applies a constant force to the folded suspension. The two layers are connected by two pivots, in the middle of the intermediate beams of the folded suspension.

The frame can be understood as a composition of four basic gravity equilibrators, proposed in [Herder, 2001], without the mass. It is essential that the springs are not connected to grounded positions, but to the vertical links of the frame, so that a constant force is generated. The geometrical conditions for the frame are defined by eq. (5.11).

$$r_1 k_1 a_1 = r_2 \frac{F_{crit}}{2} \tag{5.11}$$

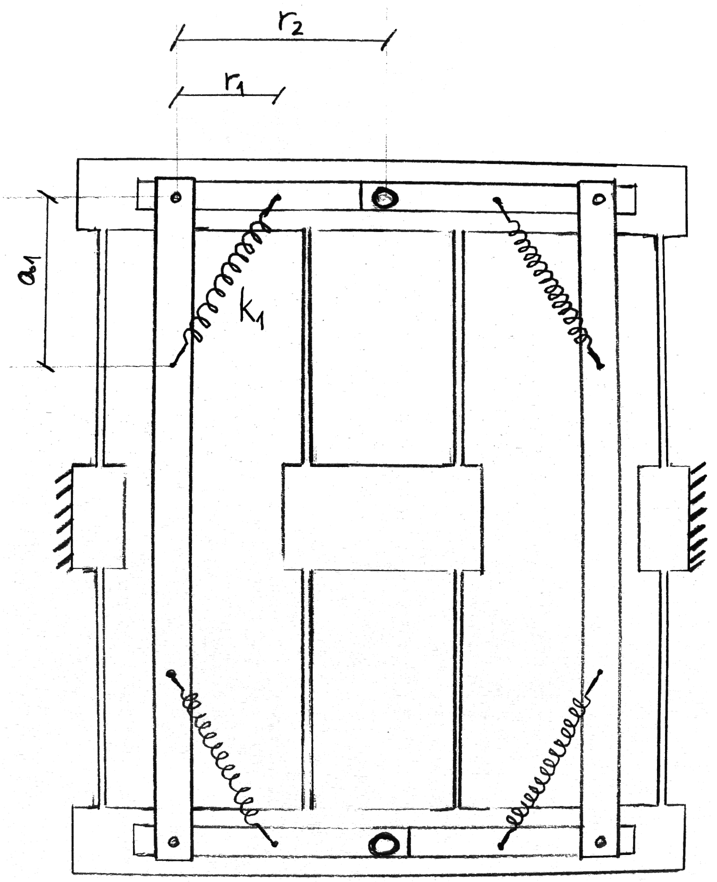

Figure 5.11: Final embodiment for a statically balanced folded suspension. The critical buckling load is provided by a constant force mechanism with zero free-length springs.

5.3.5 Concept selection

The first concept is capable of providing an excellent balancing quality, as deviations from the statically balanced behavior are only due to non-homogeneity in the thickness and the tolerances and imperfections related to cutting the strip, both being small. However, this concept fails to meet the next two criteria, as, for one, it is hard to miniaturize and, then, the design has an intrinsic low stiffness on the direction perpendicular to the strip. This latter point can be amended with the addition of rings internally to the rolled part of the strip. Nevertheless, the addition of movable parts is not desirable at small scales, in addition to the fact that it increases the inertia of the system.

The second concept can provide a compact mechanism with high separation between the eigenfrequencies. However, the balancing quality is achieved through *a posteriori* tuning, i. e., good balancing quality is only achieved at the expense of having two tunable adjustments. This imposes implementation challenges, demanding a compromise in compactness.

Finally, the third concept is able to provide a compact system with high separation between the resonant frequencies of the different modes of oscillation. The balancing quality has not been proven, but it is suggested to be good. In addition to those points, the fact that this is a new concept for the design of statically balanced mechanisms pushes for the selection of this solution.

Thus, the folded suspension is selected for further analysis. A summary of this discussion for the concept selection is presented in tab. 5.3.

Table 5.3: Summary of concept selection. The final grades vary within the range ±20

	Weight	1 – Rolamite	2 – Constant stiffness subparts	3 – SB folded suspension
Balancing quality	5	++	+	+
Eigenfreq. separation	3	−	++	++
Compactness	2	−−	+	++
		3	13	15

5.3.6 Numerical analysis

In order to validate the concept, a numerical analysis was executed in ANSYS, with the code shown in Appendix C. A nonlinear finite element model was implemented for the smallest working part of the statically balanced folded suspension, i.e., a single beam under critical load. Each of the eight beams of the folded suspension deflects equally. This was implemented in ANSYS using BEAM3 elements, constraining all degrees of freedom of one end of the beam and allowing the other end to move only perpendicularly to the beam.

The geometry of the beam is defined with a length of 40 mm, a width of 5 mm and a thickness of 1 mm. The material properties are set as E = 113.9 GPa for the Young's modulus and ν = 0.3 for the Poisson's ratio, typical values for titanium alloys. The prestress level, near the critical load is set to 294 N and was determined empirically. This force is applied in fifty steps of calculation. After the application of the prestress, a lateral deflection is imposed to the beam and the reactive force of the beam is obtained and plotted in fig. 5.12.

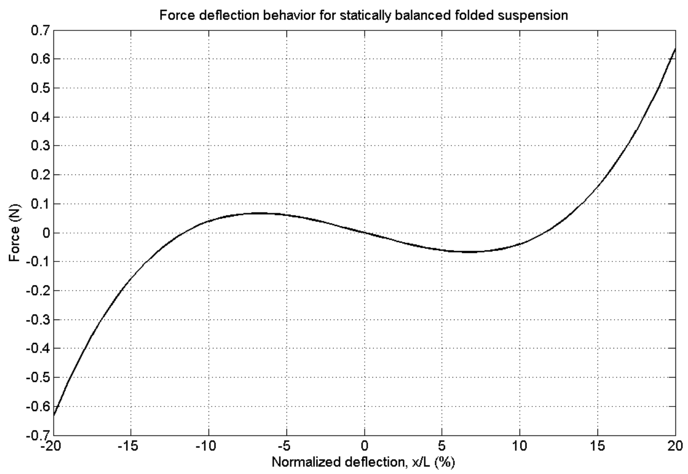

Figure 5.12: Numerically obtained force deflection behavior for buckled beam, the minimal part of the statically balanced folded suspension. The deflection is normalized with respect to the total length of the beam.

It can be seen that a force lower than $0.1\,N$ is achieved even for large deflections, in a range of ±14% of the lateral deflection over the beam length. Having in mind that the folded suspension is composed of eight beams, it is expected that the forces should reach a maximum of around $0.8\,N$ within 28% of the lateral deflection over length ratio.

There are two forms of evaluating those forces and the balancing quality. The first is to put it in contrast with the required preload, which is of $1176\,N$. However, as this force is applied only once, a more effective form of determining the balancing quality is to compare the preloaded case with a situation with no preload. This normalization is executed and shown in fig. 5.13.

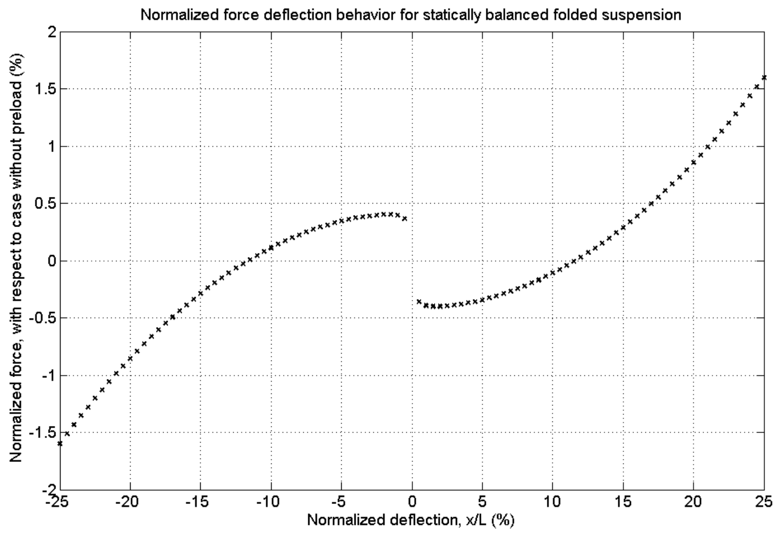

Figure 5.13: Numerically obtained force deflection behavior for buckled beam, the minimal part of the statically balanced folded suspension. The deflection is normalized with respect to the total length of the beam and the force is normalized with respect to the case of no buckling force.

As the force used for the normalization increases for larger displacements, this plot shows a even larger stroke. Indeed, for lateral displacements within ±21% of total beam length a balancing quality of over 99% is achieved.

5.4 Conclusion

This section introduced a new design paradigm for energy harvesting. This new paradigm provides a clear mindset shift, from a frequency-centered design to an amplitude-centered design. If, on one hand, existing nonlinear energy harvesters are an indicator of this shift, as there is a dependence on both frequency and amplitude, the statically balanced frequency up-conversion design is clearly amplitude-dependent.

A lumped parameter model was proposed for this paradigm and a numerical simulation was implemented. After ensuring that the numerical model is faithful to the physical model, of continuous time, sensitivity analysis was performed for each of the parameters. An indicator for the maximal power proved to be in the range of 0.5 mW for a vibration input with frequency of 1 Hz and amplitude of motion of 20 mm and a total mass for the harvester of 8 g. This result is far better than the current state of the art.

Six different embodiments were considered, being two of them radically innovative. A compact mechanism with good balancing quality was conceived, with the balancing of a traditional component for precision engineering. Numerical simulation in ANSYS were used to verify the hypotheses. The outcome is a statically balanced folded suspension, with over 99% of stiffness reduction for a large stroke.

Two additional recommendations are suggested for this design. First, that the vertical links of the frame are constrained so that they do not move in the direction defined by their main axis. Also, given that a constant force is needed only for a short range of motion (the parasitic shift is small), regular springs can be used, as long as the free-length is “hidden” behind the vertical links.

Bibliography

François E. Cellier and Ernesto Kofman. *Continuous system simulation*. Springer, 2006.

A. G. Dunning, N. Tolou, P. J. Pluimers, L. F. Kluit, and J. L. Herder. Bi-stable compliant mechanisms: Corrected finite element modeling for stiffness tuning and preloading incorporation. *Journal of Mechanical Design*, In press, 2012.

Juan A. Gallego. *Statically Balanced Compliant Mechanisms: Theory and Synthesis*. PhD thesis, Delft University of Technology, 2012.

Juan A. Gallego and Just L. Herder. Synthesis methods in compliant mechanisms: an overview. In *Proceedings of the ASME IDETC/CIE*, San Diego, Aug-Sep 2009.

Juan A. Gallego and Just L. Herder. Buckling as a new perspective on static balancing of mechanisms. In *13th World Congress in Mechanism and Machine Science*, Guanajuato, México, Jun. 2011.

Just L. Herder. *Energy-free Systems: theory, conception, and design of statically balanced spring mechanisms*. PhD thesis, Delft University of Technology, Delft, The Netherlands, 2001.

Just L. Herder and Marcel J. Horward. Manipulating pliers, 1997.

W. H. Hoppmann II. *Harris' shock and vibration handbook*, chapter Effects of impact on structures, pages 9.1–13. McGraw-Hill, 2002.

J. Rastegar, C. Pereira, and H.-L. Nguyen. Piezoelectric-based power sources for harvesting energy from platforms with low-frequency vibration. In Edward V. White, editor, *Smart Structures and Materials 2006: Industrial and Commercial Applications of Smart Structures Technologies*, volume 6171, page 617101. SPIE, 2006.

Nima Tolou. *Statically balanced compliant mechanisms for micro-precision*. PhD thesis, Delft University of Technology, 2012.

Donald F. Wilkes. Roller-band devices, 1969.

Chapter 6

Conclusions

The outcomes of this thesis can be summarized in the following points:

1 A compilation of the mechanical oscillators used for energy harvesting.

2 The introduction of bond graph modeling to a new field. Energy harvesting should profit from the integrative view provided by bond graph models.

3 The conceptual proposal of a new architecture, of statically balanced energy harvesters.

- **a** The rejection of this new architecture, based on an analytical study on the energy harvested. It results that resonators perform better than this new architecture.

4 The conceptual proposal of another new architecture, of statically balanced frequency up-conversion energy harvesters.

- **a** This new system is modeled and analyzed numerically, with a proof that the numerical results are faithful to the continuous time model.
- **b** A sensitivity analysis for all the parameters that regulate the model's performance.
- **c** A numerical confirmation that this architecture can provide results far better than the current state of the art, aiming at low frequency and large amplitude vibrations of broadband – typical for human motion, for instance. A harvested power in the order of 0.5 mW was obtained for a harvester of 8 g and an input vibration of 1 Hz and 20 mm amplitude.

5 The proposal of a new mechanism, a statically balanced folded suspension.

- **a** Numerical results confirm that this mechanism is capable of a large balanced stroke (±21% of lateral displacement over beam length with over 99% of stiffness reduction).
- **b** For being compact, having a high quality of balancing and being based on a widely accepted existing mechanism, this mechanism has potential to become a new standard for precision engineering.

Recommendations for future work follow as:

I Further development of bond graph modeling in energy harvesting, with:

  Ia the modeling of different power conditioning circuits,

  Ib the application to a real full example.

II For the statically balanced frequency up-conversion energy harvester:

  IIa further numerical analysis, testing different input vibrations,

  IIb the integral design of a harvester, focusing also on the conversion method and the power conditioning circuit,

  IIc the construction of a prototype.

III For the statically balanced folded suspension, in addition to the recommendations already suggested at the end of chapter 5:

  IIIa the construction and testing of a prototype,

  IIIb the design of a compliant version of the prestressing frame.

Bibliography

A. Alabakhshizadeh, Y. Iskandarani, G. Hovland, and O.M. Midtgård. Analysis, Modeling and Simulation of Mechatronic Systems using the Bond Graph Method. *Modeling, Identification and Control*, 32(1): 35–45, 2011.

APC International, Ltd. Piezoelectric constants. Available at http://www.americanpiezo.com, 2002.

APC International, Ltd. *Physical and piezoelectric properties of APC materials.* Available at http://www.americanpiezo.com, 2011.

M. F. Ashby. *Materials selection in mechanical design.* Butterworth Heinemann. Elsevier Science & Technology, 4th edition, 2010.

J.L. Baliño. Galerkin finite element method for incompressible thermofluid flows framed within the bond graph theory. *Simulation Modelling Practice and Theory*, 17(1):35 – 49, 2009. ISSN 1569-190X. Bond Graph Modelling.

J.L. Baliño, A.E. Larreteguy, and E.F. Gandolfo Raso. A general bond graph approach for computational fluid dynamics. *Simulation Modelling Practice and Theory*, 14(7):884 – 908, 2006. ISSN 1569-190X.

Rogier Barents, Mark Schenk, Wouter D. van Dorsser, Boudewijn M. Wisse, and Just L. Herder. Spring-to-spring balancing as energy-free adjustment method in gravity equilibrators. In *ASME 2009 International Design Engineering Technical Conferences & Computers and Information in Engineering Conference IDETC/CIE 2009*, San Diego-CA, USA, Sept. 2009.

David A. W. Barton, Stephen G. Burrow, and Lindsay R. Clare. Energy harvesting from vibrations with a nonlinear oscillator. *Journal of Vibration and Acoustics*, 132(2):021009, 2010.

S Boisseau, G Despesse, and A Sylvestre. Optimization of an electret-based energy harvester. *Smart Materials and Structures*, 19(7):075015, 2010.

D.-A. Borca-Tasciuc, M.M. Hella, and A. Kempitiya. Micro-power generators for ambient intelligence applications. In *Soft Computing Applications (SOFA), 2010 4th International Workshop on*, pages 19 –24, Jul. 2010.

W. Borutzky. Bond graph modelling and simulation of multidisciplinary systems an introduction. *Simulation Modelling Practice and Theory*, 17(1):3 – 21, 2009. ISSN 1569-190X. Bond Graph Modelling¡/ce:title¿.

Wolfgang Borutzky. *Bond graphs – A Methodology for Modelling Multidisciplinary Dynamic Systems*, volume FS-14 of *Frontiers in Simulation.* SCS Publishing House, Erlangen, San Diego, 2004.

Peter Breedveld. Bond graphs. In *Encyclopedia of Life Support Systems.* EOLSS, 2003.

British Petroleum. BP statistical review of world energy June 2011. Available at bp.com/statisticalreview, 2011.

M. Brokate, A. Pokrovskii, D. Rachinskii, and O. Rasskazov. *The science of hysteresis*, volume Mathematical modeling and applications, chapter Differential equations with hysteresis via a canonical example, pages 125–292. Elsevier, 2006.

S. G. Burrow, L. R. Clare, A. Carrella, and D. Barton. Vibration energy harvesters with non-linear compliance. In Mehdi Ahmadian, editor, *Active and Passive Smart Structures and Integrated Systems 2008*, volume 6928, page 692807. SPIE, 2008.

S.G. Burrow and L.R. Clare. A resonant generator with non-linear compliance for energy harvesting in high vibrational environments. In *Electric Machines Drives Conference, 2007. IEMDC '07. IEEE International*, volume 1, pages 715 –720, May 2007.

W. D. Callister Jr. *Materials science and engineering: an introduction.* Willey, 7th edition, 2007.

A Cammarano, S G Burrow, D A W Barton, A Carrella, and L R Clare. Tuning a resonant energy harvester using a generalized electrical load. *Smart Materials and Structures*, 19(5):055003, 2010.

A. A. Cavalheiro. *Influence of potassium and lithium additives on the relaxor ceramic magnesium lead niobate (PMN).* PhD thesis, Instituto de Química de Araraquara da Universidade Estadual Paulista "Júlio de Mesquita Filho", 2002.

François Cellier. Mathematical modeling of physical systems. Available at http://www.inf.ethz.ch/personal/fcellier/, 2011.

François E. Cellier and Ernesto Kofman. *Continuous system simulation.* Springer, 2006.

Vinod R Challa, M G Prasad, and Frank T Fisher. Towards an autonomous self-tuning vibration energy harvesting device for wireless sensor network applications. *Smart Materials and Structures*, 20(2): 025004, 2011.

C. M. Chera, J. L. Baliño, and Geneviève Dauphin-Tanguy. Two-equation traffic flow models framed within the bond graph theory. In *SpringSim*, page 219, 2010.

P. Constantinou, P.H. Mellor, and P. Wilcox. Model of an electromagnetic vibration generator. In *Universities Power Engineering Conference, 2006. UPEC '06. Proceedings of the 41st International*, volume 1, pages 6 –10, sept. 2006.

Mohammed F. Daqaq. Response of uni-modal duffing-type harvesters to random forced excitations. *Journal of Sound and Vibration*, 329(18):3621 – 3631, 2010. ISSN 0022-460X.

Mohammed F. Daqaq, Christopher Stabler, Yousef Qaroush, and Thiago Seuaciuc-Osrio. Investigation of power harvesting via parametric excitations. *Journal of Intelligent Material Systems and Structures*, 20(5):545–557, 2009.

A. G. Dunning. Design of a zero stiffness six degrees of freedom compliant precision stage. Master's thesis, Delft University of Technology, 2011.

A. G. Dunning, N. Tolou, P. J. Pluimers, L. F. Kluit, and J. L. Herder. Bi-stable compliant mechanisms: Corrected finite element modeling for stiffness tuning and preloading incorporation. *Journal of Mechanical Design*, In press, 2012.

Ecertec. *Ultrax powders & ceramics 2001-2002.* Available at http://www.ecertec.com, 2001.

C. Eichhorn, F. Goldschmidtboeing, and P. Woias. Bidirectional frequency tuning of a piezoelectric energy converter based on a cantilever beam. *Journal of Micromechanics and Microengineering*, 19(9): 094006, 2009.

Etrema Products Inc. *Data sheet terfenol-D.* Available at http://www.etrema-usa.com, 2011.

Richard P. Feynman, Robert B. Leighton, and Matthew Sands. *The Feynman lectures on Physics*, volume II. Addison-Wesley, 1964.

Juan A. Gallego. *Statically Balanced Compliant Mechanisms: Theory and Synthesis.* PhD thesis, Delft University of Technology, 2012.

Juan A. Gallego and Just L. Herder. Synthesis methods in compliant mechanisms: an overview. In *Proceedings of the ASME IDETC/CIE*, San Diego, Aug-Sep 2009.

Juan A. Gallego and Just L. Herder. Buckling as a new perspective on static balancing of mechanisms. In *13th World Congress in Mechanism and Machine Science*, Guanajuato, México, Jun. 2011.

Á. F. García. Histéresis en un tubo en forma de u que gira alrededor de un eje. Available at http://www.sc.ehu.es/sbweb/fisica, Dec. 2010.

P.J. Gawthrop and G.P. Bevan. Bond-graph modeling. *Control Systems, IEEE*, 27(2):24 –45, april 2007. ISSN 1066-033X.

V. Giurgiutiu. Actuators and smart strucutres. In S. G. Braun, editor, *Encyclopedia of vibration*, pages 58–81. Elsevier, Oxford, 2001.

Jürgen Greifeneder and François E. Cellier. Modeling multiphase systems using bond graphs. In *Proceedings ICBGM'2001, International Conference on Bond Graph Modeling and Simulation*, pages 285–291, Phoenix-AZ, USA, 2001. SCS.

Simon D. Guest, Elizbar Kebadze, and Sergio Pellegrino. A zero-stiffness elastic shell structure. *Journal of Mechanics of Materials and Structures*, 6(1-4):203–212, 2011.

C. He, M.E. Kiziroglou, D.C. Yates, and E.M. Yeatman. Mems energy harvester for wireless biosensors. In *Micro Electro Mechanical Systems (MEMS), 2010 IEEE 23rd International Conference on*, pages 172 –175, jan. 2010.

Just L. Herder. *Energy-free Systems: theory, conception, and design of statically balanced spring mechanisms.* PhD thesis, Delft University of Technology, Delft, The Netherlands, 2001.

Just L. Herder and Marcel J. Horward. Manipulating pliers, 1997.

Horace Herring and Cutler Cleveland. Rebound effect. In Cutler J. Cleveland, editor, *Encyclopedia of Earth.* [First published in the Encyclopedia of Earth November 18, 2008; Last revised Date November 18, 2008; Retrieved May 8, 2012], http://www.eoearth.org/article/Rebound_effect.

Daniel Hoffmann, Bernd Folkmer, and Yiannos Manoli. Fabrication, characterization and modelling of electrostatic micro-generators. *Journal of Micromechanics and Microengineering*, 19(9):094001, 2009.

W. H. Hoppmann II. *Harris' shock and vibration handbook*, chapter Effects of impact on structures, pages 9.1–13. McGraw-Hill, 2002.

Yuantai Hu, Huan Xue, and Hongping Hu. A piezoelectric power harvester with adjustable frequency through axial preloads. *Smart Materials and Structures*, 16(5):1961, 2007.

Intergovernmental panel on climate change. Available at http://www.ipcc.ch.

S. John, J. Sirohi, G. Wang, and N. M. Wereley. Comparison of piezoelectric, magnetostrictive, and electrostrictive hybrid hydraulic actuators. *Journal of intelligent material systems and structures*, 18: 1035–1048, 2007.

C. R. Karnopp, D. L. Margolis, and R. C. Rosenberg. *System Dynamics: Modeling and Simulation of Mechatronic Systems.* Wiley-Interscience, 3rd edition, 2000.

Tom J. Kaźmierski and Steve Beeby, editors. *Energy Harvesting Systems.* Springer, 2011.

S. G. Kelly. *Fundamentals of Mechanical Vibrations.* McGraw-Hill, 1993.

Hyunuk Kim, Yonas Tadesse, and Shashank Priya. *Energy Harvesting Technologies*, chapter Piezoelectric Energy Harvesting, pages 3–40. Springer, 2009.

In-Ho Kim, Hyung-Jo Jung, Bo Mi Lee, and Seon-Jun Jang. Broadband energy-harvesting using a two degree-of-freedom vibrating body. *Applied Physics Letters*, 98(21):214102, 2011.

T. King and M. Pozzi. *Smart technologies*, chapter Piezoelectric Materials, pages 141–170. World Scientific, 2003.

M.E. Kiziroglou, C. He, and E.M. Yeatman. Rolling rod electrostatic microgenerator. *Industrial Electronics, IEEE Transactions on*, 56(4):1101 –1108, april 2009. ISSN 0278-0046.

Haluk Kulah and Khalil Najafi. Method and micro power generator for generating electrical power from low frequency vibration energy, 2009.

D.-G. Lee, G.P. Carman, D. Murphy, and C. Schulenburg. Novel micro vibration energy harvesting device using frequency up conversion. In *Solid-State Sensors, Actuators and Microsystems Conference, 2007. TRANSDUCERS 2007. International*, pages 871–874, Lyon, Jun. 2007.

Eli S. Leland and Paul K. Wright. Resonance tuning of piezoelectric vibration energy scavenging generators using compressive axial preload. *Smart Materials and Structures*, 15(5):1413, 2006.

Wen J. Li, Zhiyu Wen, Pak Kin Wong, Gordon M. H. Chan, and Philip H. W. Leong. A micromachined vibration-induced power generator for low power sensors of robotic systems. In *World Automation Congress - Eighth International Symposium on Robotics with Applications*, Hawaii, Jun 2000.

J.R. Liang and W.H. Liao. Piezoelectric energy harvesting and dissipation on structural damping. *Journal of Intelligent Material Systems and Structures*, 20(5):515–527, 2009.

Huicong Liu, Cho Jui Tay, Chenggen Quan, Takeshi Kobayashi, and Chengkuo Lee. A scrape-through piezoelectric mems energy harvester with frequency broadband and up-conversion behaviors. *Microsyst. Technol.*, 17(12):1747–1754, December 2011. ISSN 0946-7076.

A. Lundgren, H. Tiberg, L. Kvarnsjo, A. Bergqvist, and G. Engdahl. A magnetostrictive electric generator. *Magnetics, IEEE Transactions on*, 29(6):3150–3152, nov 1993.

Nadim Maluf and Kirt Williams. *An Introduction to Microelectromechanical Systems Engineering*. Artech House, 2nd edition, 2004.

B. P. Mann and N. D. Sims. Energy harvesting from the nonlinear oscillations of magnetic levitation. *Journal of Sound and Vibration*, 319(1-2):515 – 530, 2009. ISSN 0022-460X.

Cian Ó Mathúna, Terence O'Donnell, Rafael V. Martinez-Catala, James Rohan, and Brendan O'Flynn. Energy scavenging for long-term deployable wireless sensor networks. *Talanta*, 75(3):613 – 623, 2008. ISSN 0039-9140. Special Section: Remote Sensing.

P. D. Mitcheson, T. C. Green, E. M. Yeatman, and A. S. Holmes. Architectures for vibration-driven micropower generators. *Microelectromechanical Systems, Journal of*, 13(3):429–440, 2004.

P. D. Mitcheson, E. M. Yeatman, G. K. Rao, A. S. Holmes, and T. C. Green. Energy harvesting from human and machine motion for wireless electronic devices. *Proceedings of the IEEE*, 96(9):1457–1486, Sep. 2008.

Morgan ElectroCeramics. *Piezoelectric ceramics*. Available at http://www.morganelectroceramics.com/, 2011.

G. Murillo, G. Abadal, F. Torres, J.L. Lopez, J. Giner, A. Uranga, and N. Barniol. Harvester-on-chip: Design of a proof of concept prototype. *Microelectronic Engineering*, 86(46):1183 – 1186, 2009. ISSN 0167-9317. MNE 08: The 34th International Conference on Micro- and Nano-Engineering (MNE).

Omega Piezo. *Ceramic components*. Available at http://www.omegapiezo.com, 2011.

D. de S. Onça. *"When the sun shines, they slip into the shade...": global warming ideology*. PhD thesis, Faculdade de Filosofia, Letras e Ciências Humanas da Universidade de São Paulo, 2011.

Joseph Ostler and Kurt Zwick. Power equalizing device, 1939.

Özge Zorlu, Emre Tan Topal, and Haluk Külah. A vibration-based electromagnetic energy harvester using mechanical frequency up-conversion method. *Sensors Journal, IEEE*, 11(2):481–488, 2011.

Ming-Jen Pan, Paul W. Rehrig, John P. Kucera, Seung Eek E. Park, and Wesley S. Hackenberger. Comparison of actuator properties for piezoelectric and electrostrictive materials. In Christopher S. Lynch, editor, *Smart Structures and Materials 2000: Active Materials: Behavior and Mechanics*, volume 3992, pages 80–90. SPIE, 2000.

Roque Calero Pérez and José Antonio Carta González. *Fundamentos de mecanismos y máquinas para ingenieros*. McGraw-Hill, 1999.

T. Petropoulos, E. M. Yeatman, and P. D. Mitcheson. Mems coupled resonators for power generation and sensing. *IEEE/ASME J. Microelectromech. Sys.*, 13(3):429–440, 2004.

David L. Platus. Negative-stiffness-mechanism vibration isolation systems. In Colin G. Gordon, editor, *Vibration Control in Microelectronics, Optics, and Metrology*, volume 1619, pages 44–54. SPIE, 1992.

David L. Platus. Negative-stiffness-mechanism vibration isolation systems. In Eddy A. Derby, Colin G. Gordon, Daniel Vukobratovich, Paul R. Yoder, Jr., and Carl H. Zweben, editors, *Optomechanical Engineering and Vibration Control*, volume 3786, pages 98–105. SPIE, 1999.

Pieter Pluimers, Nima Tolou, Brian D. Jensen, Larry Howell, and Just L. Herder. A compliant on/off connection mechanism for preloading statically balanced compliant mechanisms. In *Proceedings of the ASME 2012 International Design Engineering Technical Conferences & Computers and Information in Engineering Conference IDETC/CIE 2012*, Chicago-IL, USA, Aug. 2012.

Giuseppe Radaelli, Juan A. Gallego, and Just L. Herder. An energy approach to static balancing of systems with torsion stiffness. *Journal of Mechanical Design*, 133(9):091006, Sept. 2011.

J. Rastegar, C. Pereira, and H.-L. Nguyen. Piezoelectric-based power sources for harvesting energy from platforms with low-frequency vibration. In Edward V. White, editor, *Smart Structures and Materials 2006: Industrial and Commercial Applications of Smart Structures Technologies*, volume 6171, page 617101. SPIE, 2006.

V. M. Ristic. *Principles of acoustic devices*. Wiley-Interscience, 1983.

Shad Roundy, Paul K. Wright, and Jan Rabaey. A study of low level vibrations as a power source for wireless sensor nodes. *Computer Communications*, 26(11):1131 – 1144, 2003. ISSN 0140-3664. Ubiquitous Computing.

Shadrach Joseph Roundy. *Energy scavenging for wireless sensor nodes with a focus on vibration to electricity conversion*. PhD thesis, University of California, Berkeley, 2003.

Ibrahim Sari, Tuna Balkan, and Haluk Kulah. An electromagnetic micro energy harvester based on an array of parylene cantilevers. *Journal of Micromechanics and Microengineering*, 19(10):105023, 2009.

M. Schenk, S.D. Guest, and J.L. Herder. Zero stiffness tensegrity structures. *International Journal of Solids and Structures*, 44(20):6569 – 6583, 2007. ISSN 0020-7683.

Rahmatallah Shoureshi and David Carey. Bond graph modeling of an electroacoustic transducer. *Journal of the Franklin Institute*, 323(1):73 – 87, 1987. ISSN 0016-0032.

M. Soliman, E.F. El-Saadany, E.M. Abdel-Rahman, and R.R. Mansour. Design and modeling of a wideband mems-based energy harvester with experimental verification. In *Microsystems and Nanoelectronics Research Conference, 2008. MNRC 2008. 1st*, pages 193 –196, oct. 2008a.

M S M Soliman, E M Abdel-Rahman, E F El-Saadany, and R R Mansour. A wideband vibration-based energy harvester. *Journal of Micromechanics and Microengineering*, 18(11):115021, 2008b. URL 1.

L. Solymar and D. Walsh. *Electrical properties of materials*. Oxford, 7th edition, 2004.

Samuel C. Stanton, Clark C. McGehee, and Brian P. Mann. Reversible hysteresis for broadband magnetopiezoelastic energy harvesting. *Appl. Phys. Lett.*, 95(17):174103, 2009. ISSN 00036951.

N.G. Stephen. On energy harvesting from ambient vibration. *Journal of Sound and Vibration*, 293(12): 409 – 425, 2006. ISSN 0022-460X.

T. Tarnai. Zero stiffness elastic structures. *International Journal of Mechanical Sciences*, 45:425–431, 2003.

William T. Thomson. *Vibration theory and applications*. Prentice-Hall, 1965.

N. Tolou, P. J. Pluimers, B. D. Jensen, S. Magleby, L. L. Howell, and J. L. Herder. Near-zero-stiffness linear motion stage with high orthogonal and out-of-plane stiffness. In *DSPE 2012*, Deurne, The Netherlands, Sept. 2012a.

Nima Tolou. *Statically balanced compliant mechanisms for micro-precision.* PhD thesis, Delft University of Technology, 2012.

Nima Tolou, Vincent A. Henneken, and Just L. Herder. Statically balanced compliant micro mechanisms (sb-mems): Concepts and simulation. *ASME Conference Proceedings*, 2010(44106):447–454, 2010.

Nima Tolou, Pablo Estevez, and Just L. Herder. Collinear-type statically balanced compliant micro mechanisms (sb-mems) experimental comparison between pre-curved and straight beams. In *Proceedings of the ASME 2011 International Design Engineering Technical Conferences & Computers and Information in Engineering Conference IDETC/CIE 2011*, Washington-DC, USA, Aug. 2011.

Nima Tolou, Pieter Pluimers, Brian D. Jensen, Spencer Magleby, Larry Howell, and Just L. Herder. Constant force micro mechanism out of carbon nanotube forest. In *Proceedings of the 12th euspen International Conference*, Stockholm, Sweden, Jun 2012b.

TRS Technologies. *Single crystal piezoelectrics.* Available at http://www.trstechnologies.com, 2010a.

TRS Technologies. *Electrostrictors.* Available at http://www.trstechnologies.com, 2010b.

United Nations. “Report of the World Commission on Environment and Development.” General Assembly Resolution 42/187, 11 December 1987.

U.S. Energy Information Administration. History of energy consumption in the United States, 1775-2009. Available at http://www.eia.gov, 2011.

Wouter D. van Dorsser, Just L. Herder, Boudewijn M. Wisse, and Rogier Barents. Balancing device, 2007.

R. Vepa. *Dynamics of smart structures.* Wiley, 2010.

Donald F. Wilkes. Roller-band devices, 1969.

C.B. Williams and R.B. Yates. Analysis of a micro-electric generator for microsystems. *Sensors and Actuators A: Physical*, 52(13):8 – 11, 1996. ISSN 0924-4247. Proceedings of the 8th International Conference on Solid-State Sensors and Actuators Eurosensors IX.

Boudewijn M. Wisse, Rogier Barents, Wouter D. van Dorsser, and Just L. Herder. Apparatus for exercising a force on a load, 2009.

Xiaoming Wu, Jianhui Lin, Seiki Kato, Kai Zhang, Tianling Ren, and Litian Liu. A frequency adjustable vibration energy harvester. In *Proceedings of PowerMEMS 2008 + microEMS2008*, Sendai, Japan, Nov. 2008.

Dibin Zhu, Stephen Roberts, John Tudor, and Steve Beeby. Closed loop frequency tuning of a vibration-based micro-generator. In *PowerMEMS 2008+ microEMS2008*, pages 229–232, Sendai, Japan, Nov 2008.

Dibin Zhu, Stephen Roberts, Michael J. Tudor, and Stephen P. Beeby. Design and experimental characterization of a tunable vibration-based electromagnetic micro-generator. *Sensors and Actuators A: Physical*, 158(2):284 – 293, 2010a. ISSN 0924-4247.

Dibin Zhu, Michael J Tudor, and Stephen P Beeby. Strategies for increasing the operating frequency range of vibration energy harvesters: a review. *Measurement Science and Technology*, 21(2):022001, 2010b.

Appendix A

Electromechanical materials

In materials science, there are four known mechanisms of converting energy between electromagnetical and mechanical fields. Those will be briefly discussed and average properties of commonly used alloys will be compared. More explanations about each property, in specific, will follow later.

A.1 Energy conversion phenomena

A.1.1 Piezoelectricity

This property was discovered in 1880 and is a linear effect for which the material can generate an electric field when subject to mechanical strain – with the direct piezoelectric effect – or, inversely, deform when subject to an electric field [Solymar and Walsh, 2004, Ristic, 1983]. This macroscopic property results from the non-centrosymmetric crystalline microstruture, which is a necessary condition. The direct piezoelectric effect is explained with the generation of electric dipoles while the lattice is deformed, i.e. the strain-induced relative displacement of the ions result in an overal electrical polarization.

Piezoelectric materials are capable of both expanding and contracting, depending on the sense of application of the electrical field. Although the phenomenon is described by a linear model with third-rank tensors, the relation strain-electric field is not perfectly linear due to hysteresis. Vepa [Vepa, 2010] reports that the Bouc-Wen model is commonly employed to model it.

Pyroelectricity

There are important sub-classifications of piezoelectric materials. The widest of those is the one of pyroelectric materials, as it encompasses half of the twenty crystallographic classes that exhibit piezoelectric properties. Pyroelectric materials are piezoelectric materials that present a spontaneous polarization in a certain range of temperature. The resulting polarization remains until a critical temperature, known as Curie temperature, is reached. Microscopically, the Curie temperature is the limit above which all the coherence of dipole orientation is lost. Above this temperature all piezoelectric properties are lost and the material is considered to be paraelectric.

Ferroelectricity

If the polarization of a pyroelectric crystal can be changed with the application of an external electric field, the material is said to be ferroelectric. The name ferroelectric is in analogy to the classification of ferromagnetic. Following the analogy, polarization correlates to magnetization and the material also has Weiss domains – regions of the crystal in which all the dipoles have the same orientation. The directions of the resultant electric dipoles can be changed with the application of a strong external electric field. Given the arrangement of the grains, the electric dipoles will assume the closest allowed direction.

Under this classification are the two of the most used piezoelectric materials: the polymer polyvinylidene fluoride (PVDF) and the ceramic lead zirconate titanate (PZT). PZTs are usually classified as soft or hard, also in analogy to magnets, and their main differences will be explored on table A.1. PVDF is important for being a piezoelectric ductile material, despite its lower coupling properties.

Relaxor ferroelectricity

A regular ferroelectric material possesses a sharp phase transition, close to the Curie temperature, into a paraelectric behavior. This transition is commonly characterized with a plot of the relative permittivity over temperature, that shows a peak at the Curie temperature [Ecertec, 2001]. However, some materials that exhibit a diffuse phase transition around the critical temperature. Moreover, for those materials, the temperature in which this transition occurs varies with the frequency of application of the electric field [Cavalheiro, 2002]. Those materials are called relaxor ferroelectrics.

The most common ceramic is the lead magnesium niobate (PMN) and is typically changing its phase into a paraelectric behavior at room temperature. Thus, a higher Curie temperature is obtained with the addition of lead titanate (PT) and the commercially available mateiral is the PMN-PT. A more extensive comparison between average properties of PMN-PTs and PZTs shall be made on tab. A.1.

Manufacturing

Before comparing the electromechanical conversion phenomena, it is important to discuss the manufacturing methods, as those determine the microstructure of the resulting material and, thus, define its overall performance. Both PZT and PMN alloys can be manufactured through sintering or single crystal growth (although PZT single crystals are hard to manufacture and less common).

Sintering is known for long and basically consists of four stages: first, oxides of lead, zirconium and titanium are mixed and heated; then, the resulting powder is mixed along with a binder; next, this mixture is compacted and modeled into the desired shape; and finally, this “green compact” is burned, typically at around $1000°C$, depending on the ceramic composition. The performance of the finished material is very sensitive to the way the powder is processed, especially to grain size.

If on one hand the process allows a very wide range of manufacturable shapes, this happens at the expense of a non-uniform microstructure, i.e., the sintered piece is composed of several grains oriented in different directions. The existence of multiple grains leads to a lower mechanical performance, due to the presence of grain boundaries. Additionally, the resulting sintered piezoelectric piece needs to be poled as it shows no net piezoelectric effect due to the random orientation of the several existing Weiss domains. This process consists of slowly cooling the material through the Curie temperature under the influence of a strong electric field (typically, $2kV/mm$ or more). The poling process increases the volume of the Weiss domains. However, the existence of multiple grains imposes that a perfect alignment of the polarization direction of all Weiss domains is impossible. King and Pozzi [King and Pozzi, 2003] report that a level of polarization of at least 80% can be obtained.

Alternatively, single crystals can be manufactured. The fact that the whole material is coherently oriented provides more intense electromechanical coupling, lower hysteretic losses and a higher maximum usable strain. Despite the superior properties, single crystals can only be manufactured in simple topologies and shapes, such as plates, discs, rings and tubes [TRS Technologies, 2010a]. To create more complex shapes, it would be necessary to cut the crystal without generating grain boundaries. The traditional form of cutting crystals is through cleavage, defined by Callister [Callister Jr., 2007] as the “successive and repeated breaking of atomic bonds along specific crystallographic planes”.

However, it may happen that the desired shape for the mechanism does not allow cleavage, as its outer surfaces might not coincide with the desired crystallographic planes. Moreover, Vepa reports that there exists a particular direction in which single crystals should be sliced, in order to maximize the piezoelectric properties. Single crystals can also be poled, as a single crystal can contain more than one Weiss domain.

A.1.2 Electrostriction

Electrostriction is characterized by a quadratic relation between electric field and mechanical strain. It is not limited by symmetry and is present all materials [Giurgiutiu, 2001], to a larger or smaller extent. The quadratic relation is translated not only in non-linearity, but also in the fact that negative strain cannot be obtained. Moreover, there is no inverse effect [Solymar and Walsh, 2004], i.e., electrostriction does not predict polarization due to the application of mechanical strains. Nowadays, the material most used for its electrostrictive properties is the PMN, presented before as a relaxor ferroelectric. Thus, PMN shows both behaviors.

A.1.3 Piezomagnetism

The magnetic counterpart of piezoelectricity is piezomagnetism. In 1983, Ristic reported piezomagnetism to be a weak effect and, even though a quarter of a century passed, there is still no widely available material that can correspond to the expectations as well as their electric counterparts.

A.1.4 Magnetostriction

The magnetic counterpart of electrostriction is called magnetostriction and is a property of all ferromagnetic materials [Vepa, 2010]. In opposition to electrostriction, though, magnetostrictive materials can also respond to mechanical strains, producing magnetic fields [Solymar and Walsh, 2004]. An advantage that arises from the inherent differences between electrical and magnetic fields is that more energy can be stored in a magnetic field, as intense electric fields need insulation for safety reasons. However, due to the need of a magnetic circuit armature, magnetoactive induced-strain actuators will always have a lower power density as their electric counterparts [Giurgiutiu, 2001].

Nowadays, the magnetostrictive material more used is Terfenol-D. This material has superior behavior for cyclic loading and a higher coupling factor [Etrema Products Inc., 2011]. Other materials are the ones know by the trade name Metglas 2605SC and Galfenol. The differential of the latter is the fact that it is ductile, even though it has a much lower maximum strain [John et al., 2007].

A.2 Material properties

Relevant properties that define the behavior of the electromechanical materials are discussed next. Some typical values for some materials are presented, for reference. A brief comparison among the electromechanical conversion phenomena is presented at the end of this section.

A.2.1 Coupling properties

One of the properties that define the performance of piezoelectric materials is the electromechanical coupling coefficient. This property provides a measure of how effectively energy is converted and is defined according to eq. (A.1) and is always smaller than one.

$$k = \sqrt{\frac{\varepsilon_{stored}}{\varepsilon_{supplied}}} \tag{A.1}$$

This coefficient cannot be near 100% – even for single crystals – due to thermodynamical limitations, as the second law imposes that there is no energy transformation can occur without entropy generation, commonly translated in heat. In fact, Ristic [Ristic, 1983] affirms that the energy losses are twofold, with part of the supplied energy being dissipated in the material and another part radiated into the surroundings.

If the coupling coefficient measures efficiency, sensitivity is measured with the piezoelectric constants, d. Those are reported either in $\frac{pm}{V}$ or in $\frac{pC}{N}$ and couple linearly the electric and mechanical fields, as shown in eq. (A.2).

$$\begin{aligned} S &= s^E\,T + d\,E \\ D &= d\,T + \varepsilon^T\,E \end{aligned} \tag{A.2}$$

Those equations simply say that both strain, S, and electric displacement, D, vary linearly with the stress, T, and the electric field, E. They are first order Taylor approximations in which the constants are the partial derivatives with respect to one independent variable, maintaining the other independent variable constant. It results, by energy conservation, that the coefficient d appears in both equations.

Anisotropy

It is essencial to reinforce that piezoelectricity is a property that arises from asymmetry. That basic observation leads to an anisotropic macroscopic behavior. As a matter of fact, eq. (A.2) is a system of nine equations, coupling the six strain and stress directions with the three electrical displacement and field components. Indeed, piezoelectric properties are often reported for specific directions, with two subscript indexes: the first denoting the direction of the electrodes and the second indicating the relevant direction for stress or strain. Those indexes vary between 1 and 6, following the convention shown in fig. A.1.

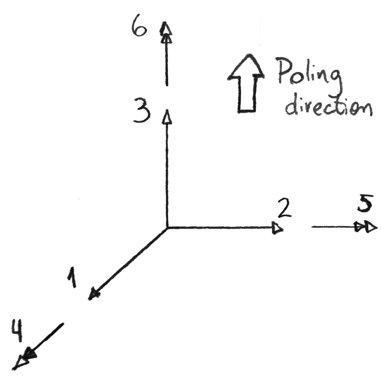

Figure A.1: Convention for directions notation

For the coupling coefficient, five different values are reported: k_{33}, k_{31}, k_{15}, k_p, k_t. The last two, planar and relative to the thickness, are usually measured for thin discs polled axially and correspond to electrodes on the caps of the disc and strain radially, for k_p, or axially, for k_t [APC International, Ltd., 2002]. Usually, the highest coupling factors for a given material are, in order, k_{33}, k_{15} and k_t.

A.2.2 Hysteresis

In simple words, hysteresis is a phenomenon that happens when a system can provide different stable outputs given the same external conditions, depending, for instance, on the history of those conditions [Brokate et al., 2006, García, 2010].

Mechanical

For a first analysis, the mechanical hysteresis properties of piezoelectric ceramics were studied. Ashby [Ashby, 2010] reports that technical ceramics have one of the lowest mechanical hysteretic losses. A quantitative measure of the losses is provided by the loss coefficient, defined as a ratio of the energy lost in one cycle over the maximum energy stored mechanically with the strain, according to eq. (A.3).

$$\eta = \frac{\oint \sigma dE}{2\pi \oint_0^{\sigma_{\max}} \sigma dE} \tag{A.3}$$

It is very unusual that the manufacturers report directly numerical values for hysteresis on the specifications of the materials. One single value was obtained from [Morgan ElectroCeramics, 2011] for the material PZT807I, where the number $8.6\,10^{-4}$ is reported as "internal friction". However, the resonance factors, Q, and the phase lag, δ, here between stress and strain are frequently reported. For small damping ($\eta < 1\%$), these properties can be related according to eq. (A.4).

$$\eta = \frac{1}{Q} = \tan\delta \tag{A.4}$$

Those other values are often reported [APC International, Ltd., 2011, Morgan ElectroCeramics, 2011, Omega Piezo, 2011], either for the mechanical losses, for the dielectric losses or for electro-mechanical properties. For hard PZTs, the mechanical quality factor is usually above 1000, providing mechanical hysteretic losses lower than 0.1%.

Electrical

On the electrical side, the value usually provided by the manufacturers is the dielectric loss, $\tan\delta$. This value represents the delay between electric field and the polarization of the material. For low electrical fields and hard PZTs, the reported values are within the range 0.16% to 1.6%, being more frequently around 0.4%.

Electromechanical

However, as the piezoelectric materials are couplers between strain and electric field, describing the mechanical and electrical hysteretic losses is not enough to fully describe the hysteresis properties of interest. Even though those values are not reported, it is expected that they are of the order of the sum of the losses on both the mechanical and electrical fields. Thus, for a typical hard PZT, the hysteretic losses should be of the order of 0.5%.

This properties are usually measured taking in account the whole hysteresis cycle, from saturation in one direction until the saturation on the opposite direction. Cycles with smaller amplitudes or biased with a constant value should result in smaller losses.

A.2.3 Aging

Aging is a broad term that describes the gradual change of the piezoelectric properties of a material after a major disturbance, such as a temperature shocks or poling. The variations can be small, with a simple decay, or sudden, with the loss of the piezoelectric properties. This latter one is referred to as depoling. A model of a normal decay and ways of avoiding depoling are discussed next.

Time

The piezoelectric properties, such as the coupling coefficients and the dielectric constant, will decay with time. An exponencial decay is assumed [Morgan ElectroCeramics, 2011] and the decay rate depends on the material composition, on the geometry of the device and on the manufacturing process. An example, with the time stability of planar coupling coefficients for soft and hard PZTs, is presented in fig. A.2.

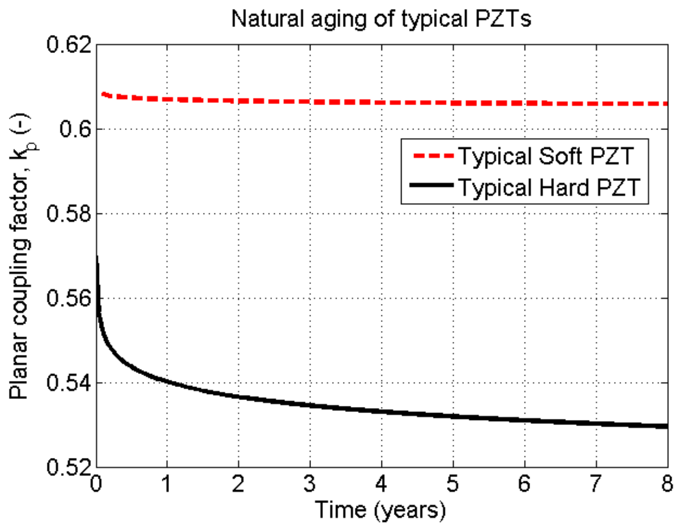

Figure A.2: Time stability of planar coupling factor, for typical hard and soft PZTs

It can be seen that soft PZTs are, in general, more stable than hard PZTs. Thus, for mechanisms designed to last long with a high efficiency, soft PZTs should be preferable than hard PZTs. This normal time decay can be modified under the thermal, electrical and mechanical influences, as discussed next.

Temperature

As mentioned before, there is a critical temperature in which the material undergoes a transformation and looses it piezoelectric properties. Giurgiutiu [Giurgiutiu, 2001] suggests that the operating temperature should remain below $50°C$ of the Curie temperature. This safety margin is there to avoid a series of factors, including the acceleration of aging and creep, the decrease of the maximum safe mechanical stress and the facilitation of depoling. A more conservative margin is suggested by [Morgan ElectroCeramics, 2011], who suggest not to exceeded half the Curie temperature, in degrees Celsius. This is justified as the transition from piezoelectric to paraelectric behaviors is not abrupt for all materials.

The Curie temperatures of comercial materials seldom have values lower than $200°C$. The addition of PT, as in PZT-PT and PMN-PT is typically done to increase the Curie temperature so that the material has stable piezoelectric properties at room temperature.

Voltage

The ceramics can also be depoled if it is subject to a very intense electric field with polarity inverted to the original poling voltage. Typical limits are $500V/m$ for soft PZTs and $1000V/m$ for hard PZTs.

Mechanical stress

Finally, high mechanical stress can also depole a PZT. The limits are specific not only to the specific material used, but are also a function of the duration of the applied stress. Stress applied for a long period of time should have lower magnitudes in order not to cause a decay of the piezoelectric properties.

A.2.4 Other properties

Next are summarized other properties, divided in mechanical, electromagnetic and thermal.

Mechanical

Density, ρ, is a commonly reported property. It provides the volumetric weight of the material.

The modulus of elasticity, Y or E, is obtained from the slope of the elastic model of stress-strain, linear part of the stress-strain curve. The anisotropy of the piezoelectric materials is manifested for this property.

The Poisson's ratio, ν, relates the lateral strain to the axial strain when the material is subject to axial loading.

A non-standard property often reported is the frequency constant, N, with units of $Hz\,m$. It provides an estimation of a resonance frequency, with the dependence of a characteristic dimension. It is sometimes reported with respect to specific directions.

Electromagnetic

An usual electrical property is also relevant here: the resistivity, ρ, which is related to the resistance of a piece of material, subtracted the effect of the size of it.

Finally, the relative permittivity, K or ε_r, which also is reported in accordance to the directions involved. This number is a ratio of the permittivity of the dielectric over the permittivity of free space. The analogous magnetic property is the relative permeability, μ.

Thermal

The specific heat, c, quantifies the amount of energy necessary to increase in $1\,K$ the temperature of one kilogram of a given material.

At last, the thermal conductivity, k or λ, quantifies the rate of heat transfer due to conduction, on steady state, through a material.

A.2.5 Discussion

After defining the material electromechanical conversion phenomena and the typical properties of those materials, it is possible to make a rough comparison among them. The average properties of representative materials for the phenomena are summarized in tab. A.1, compiled from [APC International, Ltd., 2011, Ecertec, 2001, Etrema Products Inc., 2011, Giurgiutiu, 2001, Morgan ElectroCeramics, 2011, Pan et al., 2000, TRS Technologies, 2010b,a]. Data not found is marked with a dash. Piezomagnetic were left aside, given the lack of sources. The properties are, in general, measured with respect to the translation from electrical energy into mechanical, i.e., with the materials behaving as actuators. This implies that the relaxor ferroelectric PMN manifests the electrostrictive behavior, additionally.

Table A.1: Comparison among soft and hard piezoelectrics, electrostrictive and magnetostrictive materials

	Hysteresis	Sensitivity	Coupling factor	Curie temp.
Soft PZT	High	Medium	Medium	Medium
Hard PZT	Medium	Low	Medium-low	High
PMN-PT	Low	High	Medium	Low
PMN-PT monocrystal	Very low	Very high	Very high	Low
Terfenol-D	-	-	Medium-high	Very high

A.3 Common practices

A.3.1 Mechanical bias

Given that PMNs and Terfenol-D are ceramics which are specially brittle [John et al., 2007], it is desirable to prestress the material in order to keep it always working under compression to preserve the integrity of the part. Prestress also changes the maximum obtainable strain (when using the material as actuator) and the hysteretic losses [Pan et al., 2000]. Those properties can increase or decrease, depending on the material specific composition. For PZTs and PMNs, depoling will happen, given a high enough prestress. An example of the dependency of hysteresis and sensitivity with mechanical prestressing is shown in fig. A.3.

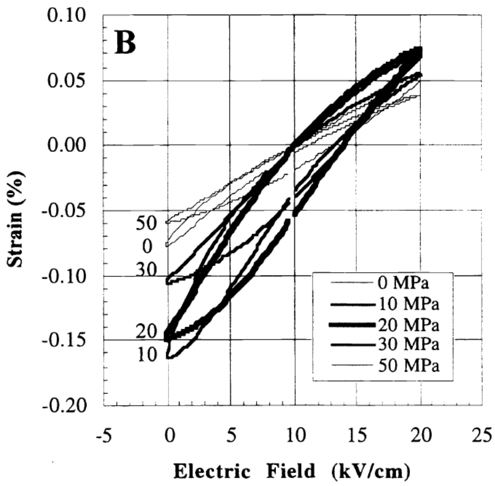

Figure A.3: Influence of compressive prestress on the piezoelectric behavior for a soft PZT, of trade name TRSHK1, extracted from [Pan et al., 2000]

The plot shows a concave variation with prestress for both sensitivity and hysteresis, with a maximum for sensitivity and hysteresis around 10 MPa and 20 MPa, respectively. However, those conclusions are not extensive to other materials. In fact, each material behaves in a unique way, as shown in fig. A.4. Those plots are results of tests imposing an electric field of $\pm 10\,\frac{kV}{cm}$ around a constant electrical field of $10\,\frac{kV}{cm}$. The materials marked with a full marker are hard PZTs and the ones with hollow markers, soft PZTs.

For magnetostrictive materials, prestressing avoids the phenomenon of frequency doubling, which would happen with an unbiased mechanical load as the material would only expand on the direction of the applied magnetic field.

A.3.2 Electrical bias

Electrical bias is also possible, applying a DC signal in addition to the AC variation. Its main advantage is the prevention of depoling, when the electrical field of the DC signal is aligned with the initial polarization of the material. [Pan et al., 2000] report that it can reduce hysteresis and provide a larger strain, while using the material as actuator. Tests for a soft PZT are shown in fig. A.5.

Biasing is necessary also to avoid frequency doubling on electrostrictors.

Bibliography

APC International, Ltd. Piezoelectric constants. Available at http://www.americanpiezo.com, 2002.

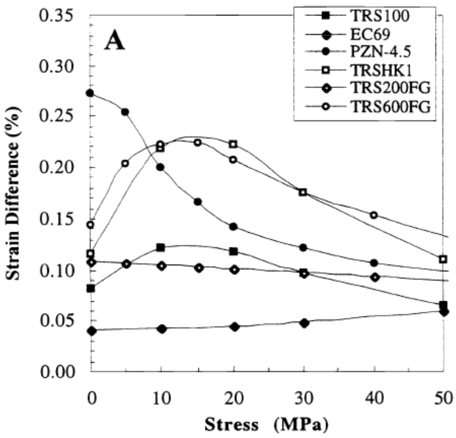

(a)

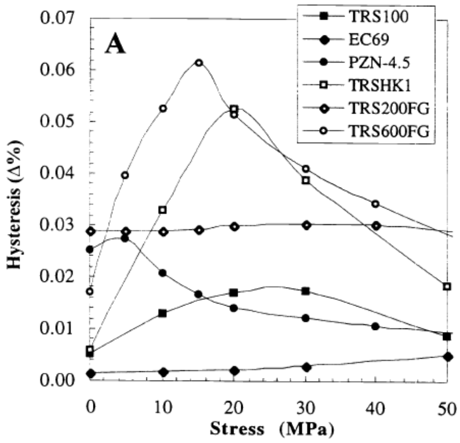

(b)

Figure A.4: Influence of prestressing on (a) sensitivity and (b) hysteresis. Extracted from [Pan et al., 2000]

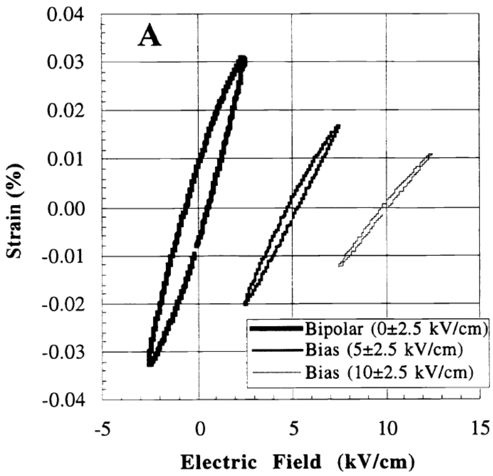

Figure A.5: Influence of a constant electric field on the piezoelectric behavior for a soft PZT, of trade name TRSHK1, extracted from [Pan et al., 2000]

APC International, Ltd. *Physical and piezoelectric properties of APC materials.* Available at http://www.americanpiezo.com, 2011.

M. F. Ashby. *Materials selection in mechanical design.* Butterworth Heinemann. Elsevier Science & Technology, 4th edition, 2010.

M. Brokate, A. Pokrovskii, D. Rachinskii, and O. Rasskazov. *The science of hysteresis*, volume Mathematical modeling and applications, chapter Differential equations with hysteresis via a canonical example, pages 125–292. Elsevier, 2006.

W. D. Callister Jr. *Materials science and engineering: an introduction.* Willey, 7th edition, 2007.

A. A. Cavalheiro. *Influence of potassium and lithium additives on the relaxor ceramic magnesium lead niobate (PMN).* PhD thesis, Instituto de Química de Araraquara da Universidade Estadual Paulista “Júlio de Mesquita Filho”, 2002.

Ecertec. *Ultrax powders & ceramics 2001-2002.* Available at http://www.ecertec.com, 2001.

Etrema Products Inc. *Data sheet terfenol-D*. Available at http://www.etrema-usa.com, 2011.

Á. F. García. Histéresis en un tubo en forma de u que gira alrededor de un eje. Available at http://www.sc.ehu.es/sbweb/fisica, Dec. 2010.

V. Giurgiutiu. Actuators and smart strucutres. In S. G. Braun, editor, *Encyclopedia of vibration*, pages 58–81. Elsevier, Oxford, 2001.

S. John, J. Sirohi, G. Wang, and N. M. Wereley. Comparison of piezoelectric, magnetostrictive, and electrostrictive hybrid hydraulic actuators. *Journal of intelligent material systems and structures*, 18: 1035–1048, 2007.

T. King and M. Pozzi. *Smart technologies*, chapter Piezoelectric Materials, pages 141–170. World Scientific, 2003.

Morgan ElectroCeramics. *Piezoelectric ceramics*. Available at http://www.morganelectroceramics.com/, 2011.

Omega Piezo. *Ceramic components*. Available at http://www.omegapiezo.com, 2011.

Ming-Jen Pan, Paul W. Rehrig, John P. Kucera, Seung Eek E. Park, and Wesley S. Hackenberger. Comparison of actuator properties for piezoelectric and electrostrictive materials. In Christopher S. Lynch, editor, *Smart Structures and Materials 2000: Active Materials: Behavior and Mechanics*, volume 3992, pages 80–90. SPIE, 2000.

V. M. Ristic. *Principles of acoustic devices*. Wiley-Interscience, 1983.

L. Solymar and D. Walsh. *Electrical properties of materials*. Oxford, 7th edition, 2004.

TRS Technologies. *Single crystal piezoelectrics*. Available at http://www.trstechnologies.com, 2010a.

TRS Technologies. *Electrostrictors*. Available at http://www.trstechnologies.com, 2010b.

R. Vepa. *Dynamics of smart structures*. Wiley, 2010.

Appendix B

Comparison among conversion methods

A comparison among the conversion methods accomplished by [Roundy, 2003] is used recurrently in the literature to affirm that electrostatic conversion is capable of handling less power than the others. Roundy's calculations are discussed next and summarized in tab. B.1, where σ_Y is the yield stress, Y is the Young's modulus, k the coupling factor, ε the electric permittivity, E the electric field, B the magnetic B-field and μ the magnetic permeability.

For piezoelectric materials, the energy that the material can handle per unit volume is calculated by the energy stored in the stress-strain field for uniaxial loading up to yield multiplied by the squared coupling coefficient. As the squared coupling coefficient provides a ratio between the electric energy output by the mechanical energy input, the overall formula defines the total electrical energy that the piezoelectric material can provide without leaving its elastic regime.

For electrostatic conversion, a standard formula ([Solymar and Walsh, 2004], for instance) is used to determine the energy that the dielectric is capable of store. The Paschen's curve is used to provide a theoretical maximum, considering air at atmospheric pressure as a dielectric.

For electromagnetic conversion, a magnetic dual of the electric formula is used. However, as much stronger magnetic fields are possible, it results that more energy can be stored in a magnetic field, as compared to electric fields.

Table B.1: Comparison among conversion methods, by [Roundy, 2003].

		Practical maximum	Theoretical maximum
Piezoelectric	$\frac{\sigma_Y^2 k^2}{2Y}$	$17.7 \frac{mJ}{cm^3}$	$335 \frac{mJ}{cm^3}$
Electrostatic	$\frac{\varepsilon E^2}{2}$	$4 \frac{mJ}{cm^3}$	$44 \frac{mJ}{cm^3}$
Electromagnetic	$\frac{B^2}{2\mu}$	$4 \frac{mJ}{cm^3}$	$400 \frac{mJ}{cm^3}$

A possibility not explored is to use a different dielectric material between the capacitor plates. Our literature search pointed a single paper that used a dielectric liquid between the capacitor electrodes [Borca-Tasciuc et al., 2010]. Despite the higher energy density of the dielectric, the fact that they chose a fluid to fill the variable volume between the plates adds inevitably inertia and viscosity (damping) into the system.

A better idea would be to use a solid, coating the electrodes and obtaining a composed dielectric, so that the relative motion between the electrodes is still made possible with the volume filled with air. This would require that the material used for coating has a much higher energy density than air, as composed dielectric arrangement depend on both materials [Feynman et al., 1964]. Fortunately, there are many materials that can cope with this requirements, besides being suited for MEMS fabrication [Maluf and Williams, 2004].

Table B.2: Theoretical maximum for energy density for electric field in selected materials suited for MEMS fabrication.

Material	Energy density
Silicon	$47.4 \frac{mJ}{cm^3}$
GaAs	$92.8 \frac{mJ}{cm^3}$
SiC	$1717.7 \frac{mJ}{cm^3}$
Diamond	$24349.0 \frac{mJ}{cm^3}$
LPCVD*	$26562.6 \frac{mJ}{cm^3}$
Alumina*	$30855.0 \frac{mJ}{cm^3}$

* properties that provide the minimum energy density were used

This observation opens a new avenue of possibilites for the design of electrostatic energy harvesters.

Bibliography

D.-A. Borca-Tasciuc, M.M. Hella, and A. Kempitiya. Micro-power generators for ambient intelligence applications. In *Soft Computing Applications (SOFA), 2010 4th International Workshop on*, pages 19 –24, Jul. 2010.

Richard P. Feynman, Robert B. Leighton, and Matthew Sands. *The Feynman lectures on Physics*, volume II. Addison-Wesley, 1964.

Nadim Maluf and Kirt Williams. *An Introduction to Microelectromechanical Systems Engineering.* Artech House, 2nd edition, 2004.

Shadrach Joseph Roundy. *Energy scavenging for wireless sensor nodes with a focus on vibration to electricity conversion.* PhD thesis, University of California, Berkeley, 2003.

L. Solymar and D. Walsh. *Electrical properties of materials.* Oxford, 7th edition, 2004.

Appendix C

ANSYS code for analysis of statically balanced folded suspension

```
!!!!!!!!!!!!!!!!!!!!!!!!!!!!!!!!!!!!!!!!!!!!!!!!!!!!!!!!!!!!!!!!!!!!!!!!!!!!!!!!!!!!!!!!
!          Buckled beam analysis --- Statically balanced folded suspension         !
!!!!!!!!!!!!!!!!!!!!!!!!!!!!!!!!!!!!!!!!!!!!!!!!!!!!!!!!!!!!!!!!!!!!!!!!!!!!!!!!!!!!!!!!
!                                                                                      !
!     Sergio de Paula Pellegrini                   sergio.pellegrini@gmail.com       !
!                                                                                      !
!     Delft, NL                                    May 2012                          !
!                                                                                      !
!     Special thanks to Toon Lamers, my ANSYS sensei                                 !
!!!!!!!!!!!!!!!!!!!!!!!!!!!!!!!!!!!!!!!!!!!!!!!!!!!!!!!!!!!!!!!!!!!!!!!!!!!!!!!!!!!!!!!!


FINISH
/CLEAR

/FILENAME,buckledbeam,1
/TITLE, non-linear analysis, beam
/UNITS, SI

/CWD,'C:\ANSYS'  ! Specifies folder

!!!!!!!!!!!!!!!!!!!!!!!!!!!!!!!!!!!!!!!!!!!!!!!!!!!!!!!!!!!!!!!!!!!!!!!!!!!!!!!!!!!!!!!!
! Define parameters                                                                    !
!!!!!!!!!!!!!!!!!!!!!!!!!!!!!!!!!!!!!!!!!!!!!!!!!!!!!!!!!!!!!!!!!!!!!!!!!!!!!!!!!!!!!!!!

*SET,b,5e-3
*SET,h1,1e-3
*SET,L,0.04

*SET,E,113.9e9
*SET,v,0.3
*SET,range,L/4   ! Range of motion tested
*SET,preload,294 ! Buckling force
*SET,nrsteps,50  ! Number of steps to apply both the buckling force & the range tested

!!!!!!!!!!!!!!!!!!!!!!!!!!!!!!!!!!!!!!!!!!!!!!!!!!!!!!!!!!!!!!!!!!!!!!!!!!!!!!!!!!!!!!!!
! Define basic geometry tested                                                         !
```

```
!!!!!!!!!!!!!!!!!!!!!!!!!!!!!!!!!!!!!!!!!!!!!!!!!!!!!!!!!!!!!!!!!!!!!!!!!!!!!!!!!!!!!!!

/PREP7
!KEYPOINTS
K, 1 , 0 , 0
K, 2 , 0 , L


!LINES
LSTR, 1 , 2

!!!!!!!!!!!!!!!!!!!!!!!!!!!!!!!!!!!!!!!!!!!!!!!!!!!!!!!!!!!!!!!!!!!!!!!!!!!!!!!!!!!!!!!
! Define element settings                                                             !
!!!!!!!!!!!!!!!!!!!!!!!!!!!!!!!!!!!!!!!!!!!!!!!!!!!!!!!!!!!!!!!!!!!!!!!!!!!!!!!!!!!!!!!


! Element
  ET,1,BEAM3
  R,1,b*h1,b*h1**3/12,h1

! Material properties
  MP,EX,,E
  MP,PRXY,,v

!!!!!!!!!!!!!!!!!!!!!!!!!!!!!!!!!!!!!!!!!!!!!!!!!!!!!!!!!!!!!!!!!!!!!!!!!!!!!!!!!!!!!!!
! Meshing                                                                             !
!!!!!!!!!!!!!!!!!!!!!!!!!!!!!!!!!!!!!!!!!!!!!!!!!!!!!!!!!!!!!!!!!!!!!!!!!!!!!!!!!!!!!!!

TYPE,1
REAL,1
ESIZE,2e-4
LMESH,1

FINISH

!!!!!!!!!!!!!!!!!!!!!!!!!!!!!!!!!!!!!!!!!!!!!!!!!!!!!!!!!!!!!!!!!!!!!!!!!!!!!!!!!!!!!!!
! Solution settings                                                                   !
!!!!!!!!!!!!!!!!!!!!!!!!!!!!!!!!!!!!!!!!!!!!!!!!!!!!!!!!!!!!!!!!!!!!!!!!!!!!!!!!!!!!!!!

/SOLU

!Static analysis
  ANTYPE,STATIC,NEW    ! Static analysis
  NLGEOM,1             ! Include large deflections
  PSTRESS,0
  NSUBST,nrsteps,100,1 ! Number of steps
  OUTRES,ALL,ALL       ! Determine output write all results for all steps
  AUTOTS,0             ! Automatic timestep size

!!!!!!!!!!!!!!!!!!!!!!!!!!!!!!!!!!!!!!!!!!!!!!!!!!!!!!!!!!!!!!!!!!!!!!!!!!!!!!!!!!!!!!!
! Set boundary conditions                                                             !
!!!!!!!!!!!!!!!!!!!!!!!!!!!!!!!!!!!!!!!!!!!!!!!!!!!!!!!!!!!!!!!!!!!!!!!!!!!!!!!!!!!!!!!

! Fixed dof
  DK,1,ALL
  DK,2,UX
```

```
  DK,2, ,0, ,0,ROTZ, , , , , ,

!!!!!!!!!!!!!!!!!!!!!!!!!!!!!!!!!!!!!!!!!!!!!!!!!!!!!!!!!!!!!!!!!!!!!!!!!!!!!!!!!!!!!!!!
! First load case: destabilizing force                                                 !
!!!!!!!!!!!!!!!!!!!!!!!!!!!!!!!!!!!!!!!!!!!!!!!!!!!!!!!!!!!!!!!!!!!!!!!!!!!!!!!!!!!!!!!!

FK,2,FY,-preload  ! Prescribes force

SOLVE

!!!!!!!!!!!!!!!!!!!!!!!!!!!!!!!!!!!!!!!!!!!!!!!!!!!!!!!!!!!!!!!!!!!!!!!!!!!!!!!!!!!!!!!!
! Second load case: cross displacement                                                 !
!!!!!!!!!!!!!!!!!!!!!!!!!!!!!!!!!!!!!!!!!!!!!!!!!!!!!!!!!!!!!!!!!!!!!!!!!!!!!!!!!!!!!!!!

DK,2,UX,range     ! Prescribes displacement

SOLVE


!!!!!!!!!!!!!!!!!!!!!!!!!!!!!!!!!!!!!!!!!!!!!!!!!!!!!!!!!!!!!!!!!!!!!!!!!!!!!!!!!!!!!!!!
! Post processing                                                                      !
!!!!!!!!!!!!!!!!!!!!!!!!!!!!!!!!!!!!!!!!!!!!!!!!!!!!!!!!!!!!!!!!!!!!!!!!!!!!!!!!!!!!!!!!


! Step 1: open the time history post processing

  /POST26            ! Post-processor that deals with time history
  FILE,'buckledbeam','rst','.'
  /UI,COLL,1
  NUMVAR,200        ! Maximum number of allowed variables inside the post-processor
  SOLU,2,NCMIT
  STORE,MERGE
  REALVAR,2,2

! Step 2: select motion of keypoint X

  KSEL,S,KP,,2,
  NSLK
  *SET,node_nr,NDNEXT(0)
  NSOL,2,node_nr,U,X,U_x
  STORE,MERGE
  RFORCE,3,node_nr,F,X,R_x
  STORE,MERGE

!stap 3: Export selected keypoints to txt file

  ! Save time history variables to file exprot.txt
  *CREATE,scratch,gui

  *DEL,_P26_EXPORT
  *DIM,_P26_EXPORT,TABLE,2*nrsteps,3
  VGET,_P26_EXPORT(1,0),1
  VGET,_P26_EXPORT(1,1),2
  VGET,_P26_EXPORT(1,2),3

  /OUTPUT,'export','txt'
```

```
  *VWRITE,'Geometry'
  %14c
  *VWRITE,' ','L',L
  %14c %14c %14.5G
  *VWRITE,' ','b',b
  %14c %14c %14.5G
  *VWRITE,' ','h',h1
  %14c %14c %14.5G

  *VWRITE,'Material'
  %14c
  *VWRITE,' ','E',E
  %14c %14c %14.5G
  *VWRITE,' ','Poisson',v
  %14c %14c %14.5G

  *VWRITE,'Load'
  %14c
  *VWRITE,' ','Buckling',preload
  %14c %14c %14.5G
  *VWRITE,' ','Stroke tested',range
  %14c %14c %14.5G

  *VWRITE,'Numerical'
  %14c
  *VWRITE,' ','Resolution',nrsteps
  %14c %14c %14.5G

  *VWRITE,'LOAD/TIME','U_x','F_X'
  %14C %14C %14C

  *VWRITE,_P26_EXPORT(1,0),_P26_EXPORT(1,1),_P26_EXPORT(1,2)
  %14.5G %14.5G %14.5G


  /OUTPUT,TERM
  *END
  /INPUT,scratch,gui
  ! End of time history save

FINISH
```